# Transcriptome-wide analysis of the function of Ded1 in translation preinitiation complex assembly in a reconstituted in vitro system

Fujun Zhou[1], Julie M. Bocetti[1]*, Meizhen Hou[1]*, Daoming Qin[3]*, Alan G. Hinnebusch[2†] and Jon R. Lorsch[1†]

[1]Section on the Mechanism and Regulation of Protein Synthesis
*Eunice Kennedy Shriver* National Institute of Child Health and Human Development
National Institutes of Health
Bethesda, MD USA

[2]Section on Nutrient Control of Gene Expression
*Eunice Kennedy Shriver* National Institute of Child Health and Human Development
National Institutes of Health
Bethesda, MD USA

*Equal contributions

[†]Corresponding Author

[3]Current address: Steamify LLC, Mclean, VA USA

**ABSTRACT**

We have developed a deep sequencing-based approach, Rec-Seq, that allows simultaneous monitoring of ribosomal 48S pre-initiation complex (PIC) formation on every mRNA in the translatome in an in vitro reconstituted system. Rec-Seq isolates key early steps in translation initiation in the absence of all other cellular components and processes. Using this approach we show that the DEAD-box ATPase Ded1 promotes 48S PIC formation on the start codons of >1000 native mRNAs, most of which have long, structured 5'-untranslated regions (5'UTRs). Remarkably, initiation measured in Rec-Seq was enhanced by Ded1 for most mRNAs previously shown to be highly Ded1-dependent by ribosome profiling of *ded1* mutants in vivo, demonstrating that the core translation functions of the factor are recapitulated in the purified system. Our data do not support a model in which Ded1acts by reducing initiation at start codons in 5'UTRs and instead indicate it functions by directly promoting mRNA recruitment to the 43S PIC and scanning to locate the start codon. We also provide evidence that eIF4A, another essential DEAD-box initiation factor, is required for efficient PIC assembly on almost all mRNAs, regardless of their structural complexity, in contrast to the preferential stimulation by Ded1 of initiation on mRNAs with long, structured 5'UTRs.

41 **INTRODUCTION**

42 Translation initiation in eukaryotes begins with the assembly of the 43S preinitiation
43 complex (PIC), containing the small (40S) ribosomal subunit bound to the eIF2•GTP•Met-
44 $tRNA_i$ ternary complex and several initiation factors (eIFs), including eIF1, eIF1A, eIF5, eIF4B,
45 and eIF3. The 43S PIC binds the 5' end of $m^7G$-capped mRNAs with the assistance of the cap-
46 binding protein complex eIF4F, comprised of cap-binding subunit eIF4E, scaffolding and
47 mRNA-binding subunit eIF4G, and DEAD-box RNA helicase eIF4A. The resulting 43S•mRNA
48 complex, or 48S PIC, scans the 5'-untranslated region (5'UTR) for a suitable start codon, whose
49 selection triggers release of most of the initiation factors. Subsequent joining of the large (60S)
50 ribosomal subunit to the 40S•Met-$tRNA_i$ complex, with the aid of eIF1A and the GTPase factor
51 eIF5B, forms the 80S initiation complex, poised to begin the elongation phase of protein
52 synthesis (Hinnebusch 2014).

53 The efficiency of translation initiation on specific mRNAs is strongly influenced by the
54 secondary structures in the 5'UTR and the length of the 5'UTR (Sonenberg and Hinnebusch
55 2009; Niederer et al. 2022). It is believed that the inhibitory structures in mRNA 5'UTRs are
56 resolved by DEAD/H-box RNA helicases (Hinnebusch 2014). However, we and others have
57 demonstrated that eIF4A is required for the efficient recruitment of a variety of mRNAs tested in
58 vitro regardless of their degrees of structure (Pestova and Kolupaeva 2002; Yourik et al. 2017).
59 Consistent with this, profiling of translating 80S ribosomes in vivo (Ribo-Seq analysis) in an
60 eIF4A temperature-sensitive yeast mutant (*tif1-ts*) revealed that eIF4A inactivation reduced the
61 relative translation efficiencies (Kertesz et al. 2010) of less than 40 mRNAs, despite a strong
62 reduction in bulk polysome assembly (Sen et al. 2015), thus suggesting that the majority of
63 mRNAs have similarly strong requirements for eIF4A in yeast cells. Mammalian eIF4A has been

64 suggested to remodel the 40S subunit to enhance PIC attachment to mRNAs and function beyond
65 its role in RNA unwinding (Sokabe and Fraser 2017) and might facilitate the threading of the 5′-
66 end of mRNA into the 40S entry channel (Kumar et al. 2016). Other evidence suggests that ATP-
67 bound eIF4A stabilizes eIF4F association with mRNA, in a manner reversed by ATP hydrolysis,
68 underlying dynamic eIF4F-mRNA interaction (Izidoro et al. 2022).

69 In contrast to eIF4A, inactivation of yeast DEAD-box helicase Ded1 in a cold-sensitive
70 mutant (*ded1-cs*) was found to reduce the relative TEs of more than 1100 mRNAs in Ribo-Seq
71 experiments (Sen et al. 2015; Sen et al. 2019). These Ded1-hyper-dependent mRNAs displayed a
72 marked tendency for long and structured 5'UTRs (Sen et al. 2015). Profiling of small (40S)
73 ribosomal subunits in the *ded1-cs* mutant provided evidence that Ded1 stimulates the translation
74 of Ded1-hyperdependent mRNAs by promoting attachment of 43S PICs to the mRNA 5'ends or
75 subsequent scanning to the start codon (Sen et al. 2019). Furthermore, in a purified yeast
76 translation initiation system several mRNAs identified as being hyper-dependent on Ded1 in
77 vivo also displayed greater stimulation by Ded1 of 48S PIC assembly than observed for either
78 Ded1-hypodependent mRNAs or variants of the hyper-dependent mRNAs lacking their 5'UTR
79 secondary structures (Gupta et al. 2018). Together, these findings suggest that Ded1 is important
80 particularly for stimulating translation of mRNAs that have long, structured 5'UTRs. Several
81 lines of evidence indicate that Ded1 activity on such mRNAs is enhanced by interaction of its N-
82 terminal domain with eIF4A and eIF4E, and of its C-terminal domain with eIF4G (Gao et al.
83 2016; Gupta et al. 2018; Gulay et al. 2020), indicating functional coupling between eIF4F and
84 Ded1 in 48S PIC assembly. Other evidence suggests that Ded1 broadly promotes scanning
85 through 5'UTRs by blocking initiation at alternative start codons positioned just upstream of

86 secondary structures that are unwound by Ded1 in vivo, thus allowing the scanning PIC to
87 continue downstream to the main start codon of the mRNA (Guenther et al. 2018).
88 It appears that Ded1 can regulate translation of mRNAs in vivo in ways ostensibly
89 distinct from its functions in promoting PIC attachment or scanning on structured mRNAs. There
90 is evidence that Ded1 can repress translation by segregating mRNAs into phase-separated RNA–
91 protein granules, processing bodies (PBs) or stress granules (SGs), during cell stresses. Granule
92 formation in glucose-starved cells is reduced by depletion of Ded1, and is enhanced by Ded1
93 overexpression or impairment of its ATPase activity in non-starved cells in a manner regulated
94 by regions in the Ded1 NTD and CTD (Beckham et al. 2008; Hilliker et al. 2011; Hondele et al.
95 2019). It was suggested that Ded1 initially forms an inactive complex with eIF4F and mRNA
96 that is stalled at a step upstream of 43S PIC joining and subsequently utilizes ATP hydrolysis to
97 allow progression into the initiation pathway (Beckham et al. 2008; Hilliker et al. 2011).
98 Interestingly, purified Ded1 can undergo phase separation into liquid-like droplets in a manner
99 reversed by activation of its ATPase activity by a segment of eIF4G, and there is evidence that it
100 functionally interacts with another DEAD-box helicase required for PB formation, Dhh1, in a
101 progression of translationally inactive mRNAs from PBs to SGs during glucose starvation
102 (Mugler et al. 2016; Hondele et al. 2019).
103 Heat-shock also evokes Ded1 sequestration in SGs in a manner antagonized at low
104 temperatures by a polar intrinsically disordered region (IDR) in the Ded1 NTD. Purified Ded1
105 displayed heat-induced phase separation in vitro in a manner enhanced by mRNA and the Ded1
106 CTD but suppressed by the N-terminal IDR. Interestingly, heat-shock preferentially reduced the
107 TEs of mRNAs with structured 5' UTRs and increased their condensation, in a manner
108 modulated by the N-terminal IDR, leading to the model that condensation of Ded1 and

109 associated mRNAs preferentially reduces the translation of Ded1-hyperdependent mRNAs with
110 structured 5'UTRs during heat-shock(Iserman et al. 2020). Other findings indicate that glucose-
111 starvation or heat-shock leads to widespread dissociation of Ded1, eIF4A and eIF4B from the
112 5'UTRs of mRNAs (Castelli et al. 2011; Bresson et al. 2020), which could underlie reduced
113 translation of Ded1-hyperdependent mRNAs that remain soluble in stressed cells. Examining
114 the TE changes conferred by glucose starvation or heat-shock by ribosome profiling suggested
115 that Ded1-hyperdependent mRNAs vary greatly in their translational suppression during stress,
116 which might involve a combinatorial effect of impairing eIF4A, eIF4B, and Ded1 function on the
117 most affected subsets (Sen et al. 2021).

118 It is possible that Ded1 has additional functions in the nucleus, as it appears to shuttle
119 between nucleus and cytoplasm and interacts both physically and functionally with the nuclear
120 cap-binding proteins (Senissar et al. 2014). Ded1 was also found to co-purify with pre-90S and
121 pre-40S immature ribosomes (Schäfer et al. 2003), and thus might function in ribosome
122 biogenesis.

123 A difficulty with interpreting the previous ribosome profiling experiments with *ded1*
124 mutations is that the inactivated mutant protein could have had dominant effects rather than
125 simply producing a loss of Ded1 function. For example, in view of evidence that inhibition of
126 Ded1 ATPase activity can lead to the formation of translationally inert mRNP granules, it is
127 possible that the *ded1* mutations in the catalytic domain analyzed by ribosome profiling led to
128 impaired translation of many Ded1-hyperdependent mRNAs in non-stressed cells owing to their
129 sequestration with the mutant *ded1* proteins in condensates inaccessible to the initiation
130 machinery. It was also possible that the inactivated mutant proteins bound to mRNAs, the
131 ribosome or other initiation factors in a manner that inhibited translation. The *ded1* mutations

132 could also indirectly impair translation of Ded1-hyperdependent mRNAs by reducing their
133 export from the nucleus, by reducing expression of another protein with a role in production or
134 function of the translation initiation machinery, by activating stress responses that alter the
135 functions of initiation factors, or by eliciting quality control responses that alter the rate of
136 translation elongation. Even wild-type Ded1 could influence translation indirectly by
137 modulating the association of various RNA-binding proteins with mRNAs, a function ascribed to
138 other DEAD-box proteins (Linder and Jankowsky 2011). As noted above, we demonstrated that
139 several mRNAs that were found to be Ded1-hyperdependent in vivo displayed a greater
140 stimulation of 48S PIC assembly by Ded1 compared to several in vivo hypo-dependent mRNAs
141 in a fully purified system, confirming a direct role of Ded1 in stimulating initiation on these few
142 mRNAs in the soluble phase in the absence of any other cellular proteins besides ribosomes and
143 canonical initiation factors. However, it was possible that many other mRNAs found to be
144 hyperdependent on Ded1 in vivo are not stimulated directly by Ded1's ability to resolve
145 secondary structures in 5'UTRs and promote PIC recruitment or scanning to the start codon.
146 We have developed an elaboration of the reconstituted yeast translation initiation system
147 (Acker et al. 2007) that enables examination of 48S PIC assembly on all native yeast mRNAs
148 simultaneously. This approach, dubbed Recruitment-Sequencing (Rec-Seq), allowed us to
149 measure direct effects of Ded1 on PIC attachment to mRNA and scanning to the start codon in
150 reactions containing only 40S ribosomal subunits, methionyl-initiator tRNA (Met-tRNA$_i$),
151 GDPNP and ATP, and the core initiation factors, thus excluding contributions from all other
152 cellular proteins and processes. Rec-Seq also allowed us to isolate the crucial and highly
153 regulated series of events leading up to 48S PIC assembly from all later steps of initiation and
154 elongation. Processes such as mRNA localization and decay and RNA and protein

155 compartmentalization, which can complicate in vivo analyses, likewise do not contribute to the
156 outcome of Rec-Seq experiments. Because we could vary Ded1 concentration in reactions, or
157 leave it out entirely, Rec-Seq allowed us to directly interrogate the factor's role instead of relying
158 on inferences from the effects of *ded1* mutations. Moreover, we could evaluate whether
159 preventing initiation at alternative start codons in 5'UTRs is an important aspect of Ded1
160 enhancement of PIC assembly at the canonical start codons on Ded1-stimulated transcripts.
161 Our studies indicate that in the Rec-Seq system Ded1 stimulates 48S PIC assembly on
162 ~1000 mRNAs. These Ded1-dependent mRNAs include most of the mRNAs previously found to
163 be hyper-dependent on Ded1 in vivo by ribosome profiling of the *ded1-cs* mutant. The fact that
164 addition of Ded1 stimulates 48S PIC assembly on these mRNAs in the reconstituted Rec-Seq
165 system argues against the involvement of other cellular processes or proteins beyond the core
166 initiation machinery in Ded1 function, and the possibility that the in vivo ribosome profiling
167 results were influenced by dominant negative effects of the *ded1-cs* mutation or by altered
168 expression or activity of the translational machinery in the mutant cells. The mRNAs that are
169 strongly dependent on Ded1 in the Rec-Seq system exhibit a high propensity for long and
170 structured 5'UTRs, providing compelling evidence that Ded1 acts directly to stimulate 48S PIC
171 formation by unwinding 5'UTR structures to facilitate mRNA binding to the PIC and scanning to
172 find the start codon. Our results also indicate that alternative initiation at upstream start codons is
173 too infrequent, and the suppression of these events by addition of Ded1 too small, to account for
174 the stimulatory effects of Ded1 on 48S PIC assembly in the reconstituted system. Finally, we
175 show that eIF4A strongly stimulates the formation of 48S PICs on the vast majority of yeast
176 mRNAs, regardless of their 5'UTR length or degree of secondary structure, in contrast to the
177 specificity we observe for Ded1 in stimulating recruitment of mRNAs with long, structured

178 5'UTRs. These data are consistent with the model that eIF4A plays a general role in facilitating
179 binding of all mRNAs to the 43S PIC, whereas Ded1 unwinds inhibitory secondary structures to
180 promote PIC binding and scanning on mRNAs with structured 5'UTRs.
181
182 **RESULTS**
183 **Rec-Seq, an in vitro approach to measure 48S PIC formation transcriptome-wide.** We
184 previously developed a fully reconstituted yeast translation initiation system (Acker et al. 2007)
185 that allows measurement of stable recruitment of mRNAs to 43S pre-initiation complexes
186 (Mitchell et al. 2010) to form 48S PICs using defined concentrations of purified components for
187 individual mRNAs. In addition to purified small (40S) ribosomal subunits, reactions include
188 initiation factors eIF1, eIF1A, eIF5, the eIF2·GTP·Met-tRNA$_i$ ternary complex (TC, assembled
189 using non-hydrolyzable GDPNP), eIF3, the mRNA-recruitment factors eIF4G·eIF4E complex,
190 eIF4A and eIF4B, and ATP. In the initial version of this system, we monitored recruitment of a
191 single capped, radiolabeled, in vitro transcribed mRNA in each reaction. Formation of a stable
192 48S PIC with the anticodon of Met-tRNA$_i$ base paired to the AUG start codon in the mRNA was
193 resolved from free mRNA by native gel electrophoresis and quantified by phosphorimaging of
194 the mRNA. Among other things, this assay has been used to elucidate the molecular roles of eIFs
195 essential for 48S PIC assembly (Hinnebusch 2014); provide evidence that eIF4A is essential for
196 recruitment of various mRNAs to the 43S PIC regardless of the amount of secondary structure in
197 their 5'UTRs (Yourik et al. 2017); and reconstitute the ability of Ded1 to overcome 5'UTR
198 secondary structures found in several Ded1-hyperdependent mRNAs (Gupta et al. 2018). An
199 important limitation of the assay, however, was that only a single mRNA could be examined at a
200 time, and the effects of competition among the many different mRNAs that exist in a cell could

201 not be assessed. In addition, the use of an electrophoretic mobility-shift assay (EMSA) limits the
202 analysis to very short native transcripts, eg. *RPL41A* mRNA, or the use of synthetic constructs
203 truncated at their 3' ends in place of longer, full-length native mRNAs (Gupta et al. 2018). Such
204 constructs might not recapitulate functionally important interactions between the 5'UTR and
205 other parts of the mRNA.

206 To circumvent these limitations, we modified the system to allow 48S PIC formation on
207 all native mRNAs in the standard yeast transcriptome to be monitored simultaneously using an
208 approach we call Rec-Seq for "Recruitment-Sequencing" (Fig. 1A). In place of a single,
209 radiolabeled mRNA we used oligo(dT) affinity-purified total mRNA from wild-type yeast cells
210 grown in nutrient-replete conditions. This total polyA(+) mRNA was incubated for various times
211 with pre-assembled 43S PICs, eIF3, eIF4 factors, ATP and other components (depending on the
212 experiment; Fig. 1-S1). The reactions were then treated with RNase I to digest mRNA regions
213 not protected by the ribosomal complex. For each reaction, 48S PICs were isolated by
214 sedimentation through a sucrose gradient and ribosome-protected fragments (RPFs) were
215 purified by gel electrophoresis and converted to cDNAs by reverse-transcription followed by
216 PCR amplification to generate sequencing libraries. This approach allowed us to monitor PIC
217 assembly on all native yeast mRNAs in parallel.

218 To make results comparable among replicates and across experiments, we used an
219 internal normalization approach in which 48S PICs were assembled on two non-native mRNAs
220 encoding Renilla or firefly luciferase and treated with RNase I. A constant amount of these
221 "spike-in" 48S PICs were added to each experimental reaction prior to sucrose gradient
222 sedimentation (Fig. 1-S2A). RPFs corresponding to both the main AUG (mAUG) and several
223 internal AUGs (iAUGs) were found to be highly reproducible among biological replicates for

224 these spike-in controls (Fig. 1-S2B-D). Normalizing results with these control RPFs allowed us
225 to achieve high reproducibility among triplicate biological replicate experiments (Fig. 1-S3) and
226 also allowed us to measure absolute rather than relative 48S PIC formation efficiencies despite
227 differences in final read depths from reaction to reaction.

228 To assess the function of Ded1 in mRNA recruitment, scanning and start codon
229 recognition, we carried out Rec-Seq experiments on reactions that contained all of the canonical
230 initiation factors shown in Figure 1A (including eIF4A) and either lacked Ded1 or contained 100
231 or 500 nM Ded1. The reactions were initiated by adding total polyA(+) mRNA to the pre-formed
232 43S complexes and other factors, and then quenched rapidly after 15 min by depleting ATP with
233 addition of a "Stop buffer" containing hexokinase and glucose. We chose 15 minutes because
234 recruitment has reached its observed endpoint for nearly all mRNAs at this time. The RPFs thus
235 measured give the final distribution of competitive recruitment efficiencies under these
236 experimental conditions, in which there is a two-fold excess of total mRNA over 43S PICs. After
237 sequencing cDNA libraries prepared from the RNAse I-treated purified 48S PICs and removing
238 sequencing reads mapping to non-coding RNAs, the reads mapping to protein coding sequences
239 were examined.

240 A metagene plot of the number of RPF reads versus position of RPF 5'ends relative to the
241 mAUG codon for each mRNA revealed that the overwhelming majority contain a single peak of
242 RPFs with the bulk of 5' ends located 12 nt upstream of the mAUG codon (Fig. 1B-D). This is
243 the position expected for PICs with the 40S P site containing the AUG start codon base paired
244 with the anticodon of Met-tRNA$_i$ (Ingolia et al. 2009; Archer et al. 2016). A minority of RPFs
245 have 5'ends closer to the AUG codon (Fig. 1B-D), which could result from invasion of RNase I
246 into the 40S exit channel in a minor fraction of PICs positioned at the start codon, or from low-

247 level degradation of purified RPFs during library construction. The two reactions containing
248 Ded1 have a somewhat greater abundance of RPFs at the start codons compared to the reaction
249 lacking Ded1 (Fig. 1-S4A).

250 We examined individual Rec-Seq traces for several mRNAs previously shown through
251 ribosome profiling to be either hyper- or hypo-dependent on Ded1 for translational efficiency
252 and that had also been shown to be similarly dependent on Ded1 for 43S PIC recruitment in vitro
253 in the reconstituted yeast initiation system (Fig. 1E, F; Fig. 1S-4). The Ded1 hyper-dependent
254 mRNAs showed strong Ded1-enhancement of Rec-Seq RPF peaks mapping to the mAUG (Fig.
255 1S-4B-E), as exemplified for *OST3* in Fig. 1E. In contrast, mRNAs previously shown to be
256 hypo-dependent on Ded1 by ribosome profiling, including *HOR7* (Fig. 1F), showed modest
257 stimulation, no enhancement, or even diminished RPF counts at the mAUG in reactions
258 containing 100 or 500 nM Ded1 vs. no Ded1 (Fig. 1S-4F-I).

259 We conducted differential expression analysis using the software DESeq2 (Love et al.
260 2014) to identify mRNAs that exhibit statistically significant changes in normalized RPFs
261 mapping to the main start codon (mRPFs) on addition of Ded1. Groups of ~1000 transcripts
262 among the 3052 for which Rec-Seq data were obtained showed >2-fold increased mRPFs in the
263 presence of 100 or 500 nM Ded1 compared to no added Ded1, whereas only ~100 transcripts
264 showed higher mRPFs at 500 nM versus 100 nM Ded1 (Fig. 2A-C, red dots). Substantially
265 smaller numbers of mRNAs displayed decreased mRPFs as Ded1 concentration was increased
266 (Fig. 2A-C, dark blue dots). Importantly, 87% of mRNAs showing significant increases in
267 mRPFs at 100 nM Ded1 were also increased at 500 nM Ded1 (Fig. 2D), and 68% of the mRNAs
268 with significantly diminished mRPFs at 100 nM Ded1 were also decreased at 500 nM Ded1 (Fig.
269 2E)—both highly significant overlaps. These data indicate consistency in the effects of Ded1

270 observed in different experiments. The 1006 mRNAs with significantly increased mRPFs at 500
271 nM Ded1 had median increases of 3.6-fold and 4.8-fold at 100 nM and 500 nM Ded1,
272 respectively (Fig. 2F, cols. 3-4). Similarly, the 911 mRNAs that had significantly increased
273 mRPFs in 100 nM Ded1 had median increases of 4.1-fold and 5.2-fold at 100 nM and 500 nM
274 Ded1, respectively, and the 793 mRNAs common to both sets had median increases of 4.7-fold
275 and 6.1-fold (Fig. 2F, cols. 5-8). Although the greater median stimulation at 500 nM vs. 100 nM
276 Ded1 is significant for all three mRNA groups, these results indicate that 100 nM Ded1 is nearly
277 saturating for enhancement of 48S PIC assembly for the majority of Ded1-stimulated mRNAs in
278 the in vitro system.

279 The set of mRNAs displaying diminished mRPFs at 500 nM Ded1 showed substantially
280 smaller reductions at 100 nM (Fig. 2F, cols. 9-10), indicating that the inhibitory effect of Ded1
281 on these mRNAs is not saturated at the lower concentration. For the remaining two groups that
282 showed Ded1 suppression of mRPFs at 100 nM or both 100nM and 500 nM Ded1, the median
283 degree of Ded1 inhibition did not differ significantly between the two concentrations (Fig. 2F,
284 cols. 11-14), indicating that inhibition by Ded1 was saturated at 100 nM.

285 The mRPF reads for each gene were normalized to the total RNA reads across the coding
286 sequences (CDS) of the mRNA (normalized for CDS length)—a measure of transcript
287 abundance—to calculate the recruitment efficiency (RE) of each transcript. The RE is analogous
288 to translational efficiency (TE) determined by in vivo Ribo-Seq experiments. We examined
289 changes in RE between experiments containing different concentrations of Ded1 by ordering
290 mRNAs according to the change in RE between 0 and 100 nM Ded1 and then using this ordering
291 to generate a heat-map depiction of ΔRE values for all 3052 transcripts observed by Rec-Seq
292 between 0 and 100 nM Ded1, 0 and 500 nM Ded1, and 100 and 500 nM Ded1 (Fig. 2G).

293 Consistent with Figures 2D and E, the results indicate that most mRNAs with increased REs on
294 addition of 100 nM Ded1 also have increased RE at 500 nM Ded1 (compare red lines in cols. 1-
295 2), which for certain mRNAs is of greater magnitude at 500 nM (relatively darker red bars in col.
296 2). The decrease in RE observed for a smaller number of mRNAs upon Ded1 addition (Fig. 2G,
297 blue lines) generally appears to be greater at 500 nM versus 100 nM Ded1 (cf. blue lines in cols.
298 1-2), which is also consistent with the results in Figs. 2E and F.

299 Examining the distributions of all mRNAs across 10 bins of increasing RE values at each
300 concentration of Ded1 revealed an obvious shift of mRNAs from bins of lowest RE to bins of
301 higher RE when Ded1 was included in the Rec-Seq reactions (Fig. 2H, cf. orange vs. blue and
302 magenta bars, particularly in the first three bins on the left). The similar distributions observed
303 for the 100 nM and 500 nM Ded1 data are consistent with results in Figs. 2F-G indicating that
304 stimulation by Ded1 is nearly saturated at 100 nM. These data suggest that Ded1 confers
305 relatively greater stimulation for mRNAs that are recruited by 43S PICs poorly in the absence of
306 Ded1. Supporting this conclusion, the increase in RE between reactions with 500 nM vs. no
307 Ded1 was greatest for the subset of mRNAs of lowest RE and least for the mRNAs with highest
308 RE in reactions without Ded1 (Fig. 2I). This finding recapitulates and extends previous results on
309 several individual mRNAs wherein Ded1 strongly stimulated 43S PIC recruitment of Ded1
310 hyper-dependent transcripts exhibiting poor recruitment in reactions lacking Ded1, while more
311 weakly stimulating Ded1 hypo-dependent mRNAs that could be recruited efficiently without
312 Ded1 (Gupta et al. 2018).

313 In summary, the Rec-Seq results are highly consistent among biological replicates and
314 reproducibly identify a subset of ~1000 of the 3052 mRNAs detected in the analysis for which
315 assembly of 48S PICs is strongly stimulated by Ded1, with a marked tendency for greater

316 stimulation for mRNAs that recruit PICs poorly in Ded1's absence. These data support previous
317 conclusions from in vivo ribosome profiling analysis of a *ded1-cs* mutant that a significant
318 number (~600 to ~1100) of yeast mRNAs exhibit heightened dependence on Ded1 relative to the
319 average mRNA (Ded1-hyperdependent transcripts) (Sen et al. 2015; Sen et al. 2019). The
320 previous ribosome profiling studies also identified transcripts exhibiting increased relative TEs
321 in *ded1* mutant cells deficient in Ded1 activity (Ded1-hypodependent transcripts), consistent with
322 translational repression by wild-type Ded1. It was unclear, however, whether the translational
323 efficiencies of these last mRNAs were truly elevated in *ded1* cells or merely reduced by a
324 smaller amount than the average transcript to yield an increase in relative TE. Owing to the
325 spike-in normalization employed here, it is clear that the absolute occupancies of 48S PICs at
326 mAUGs on mRNAs showing reduced REs on Ded1 addition are indeed diminished by Ded1,
327 although it remains unclear whether the repression is direct or results indirectly from increased
328 competition for limiting PICs conferred by enhanced PIC recruitment on the Ded1-stimulated
329 mRNAs. We examine this question further below.
330
331 **Transcripts showing strong Ded1 stimulation of 48S PIC assembly in Rec-Seq have long**
332 **and structured 5'UTRs.** The mRNAs judged to be hyper-dependent on Ded1 from Ribo-Seq
333 experiments on *ded1* mutants are enriched for transcripts with longer than average 5'UTRs with
334 a heightened propensity for forming secondary structures (Sen et al. 2015). To examine these
335 trends in our in vitro system, we divided the subset of all transcripts analyzed by Rec-Seq with
336 annotated lengths for their predominant 5'UTRs (N = 2804, (Pelechano et al. 2013)) into six bins
337 of equal size and plotted their average REs in the presence or absence of Ded1. In the absence of
338 Ded1, the average RE values for these bins is roughly constant for the first four 5'UTR length

339 bins and then decreases markedly in the fifth and sixth bins (Fig. 3A, orange). The addition of
340 Ded1 differentially enhanced RE values depending on 5'UTR length, conferring the largest
341 increase for transcripts with the longest 5'UTRs (bin 6), smaller increases for bins 3-5 having the
342 next longest 5'UTRs, and little or no increase for the mRNAs in bins 1-2 with the shortest
343 5'UTRs (Fig. 3A, cyan & purple vs. orange). The 5'UTR length trends were confirmed by
344 plotting median RE changes conferred by 100 nM or 500 nM Ded1 versus no Ded1 for all six
345 bins (Fig. 3B-C) which showed little or no stimulation in bins 1-2 and progressively larger
346 increases in bins 3 to 6. Consistent with this, comparing 500 nm to 100 nm Ded1 (Fig. 3D)
347 revealed that the higher concentration of Ded1 actually reduced the median REs of the mRNAs
348 with shortest 5'UTRs in bins 1-2, while increasing it for the transcripts with longest 5'UTRs in
349 bins 5-6.

350 To examine the correlation between 5'UTR secondary structure and the effects of Ded1 on
351 RE values, we used a compilation of propensities for secondary structure in the yeast
352 transcriptome (Kertesz et al. 2010) in which each nucleotide in 3000 different yeast transcripts
353 was assigned a "parallel analysis of RNA structure" (PARS) score based on its susceptibility to
354 digestion with single- or double-stranded specific nucleases in yeast mRNA reannealed in vitro.
355 In this analysis a higher PARS score denotes a higher probability of double-stranded
356 conformation. We calculated various cumulative PARS scores for 5'UTRs, including the sum of
357 scores for (i) all 5'UTR nucleotides (Total PARS); (ii) the 30 nt surrounding the start codon
358 (Start30 PARS; for mRNAs with a 5'UTR ≥15 nt); (iii) the highest cumulative score in any 30 nt
359 window (Max30 PARS). For each sequence interval, the 1874 transcripts observed in Rec-Seq
360 with available PARS data were divided into 6 bins of increasing PARS scores and examined for
361 RE changes conferred by Ded1 in Rec-Seq.

362 The average REs of mRNAs binned according to the 5'UTR Max30 PARS scores decline
363 steadily with increasing PARS scores in Rec-Seq reactions lacking Ded1 (Fig. 3E, orange).
364 Importantly, the negative effect of increasing Max30 PARS scores was essentially eliminated by
365 addition of 100 nM or 500 nM Ded1 (Fig. 3E, purple and cyan). Consistent with this, addition of
366 100 nM or 500 nM Ded1 confers significant increases in median RE that get progressively larger
367 with increasing Max30 PARS scores (Fig. 3F,G). Increasing Ded1 from 100 to 500 nM modestly
368 increased the median RE for mRNAs in the two highest Max30 PARS score bins (Fig. 3H).
369 Similar effects on average RE values were observed for 5'UTR Total PARS and Start30 PARS
370 scores (Fig. 3S-1A-D), with relatively greater Ded1 stimulation for the mRNAs with larger
371 scores for both parameters (Fig. 3-S1C-D). Coding sequence (CDS) length also correlated with
372 diminished average RE values (Fig. 3I), and this effect was reversed by Ded1 for the mRNAs
373 with longest CDS lengths in the last two or three bins at both 100 and 500 nM Ded1 (Fig, 3I-L).
374 The correlation between CDS length and RE could be indirect because CDS length also
375 correlates with 5'UTR length such that mRNAs with longer CDSs also tend to have longer
376 5'UTRs (Fig. 3S1-E,F). Overall, the Rec-Seq results suggest that Ded1 efficiently overcomes the
377 impediment to 48S PIC assembly posed by structures within 5'UTRs, which are cumulative in
378 longer 5'UTRs. This agrees with the conclusion reached from Ribo-Seq analysis of *ded1* mutants
379 in which Ded1-hyperdependent mRNAs were found to have significantly higher median PARS
380 scores for all 5'UTR intervals tested as well as longer than average 5'UTR lengths (Sen et al.
381 2015).
382 We next examined the dependence of Ded1 enhancement of 48S PIC assembly on the
383 sequences surrounding the start codon. The context scores of AUGs, $AUG_{CAI}$, quantify the
384 similarity between the -6 to +3 positions surrounding a given AUG to the start codons of the 2%

385 most highly translated yeast mRNAs (Zur and Tuller 2013). These context scores range from
386 ~0.16 (poorest) to ~0.97 (best) among all yeast mAUG codons. Binning mRNAs by context
387 score reveals a steady increase in RE with increasing context scores in Rec-Seq reactions lacking
388 Ded1 (Fig. 3-S2A, orange), indicating that good sequence context around the AUG codon
389 promotes 48S PIC formation. However, inclusion of 100 or 500 nM Ded1 increases the average
390 and median RE values similarly for all bins of context scores (Fig. 3-S2A, cyan and purple; Fig.
391 3-S2B, C). We conclude that the stimulatory effects of Ded1 on 48S PIC formation are
392 independent of the sequence context surrounding the AUG codon. Thus, Ded1 preferentially
393 stimulates recruitment of mRNAs burdened with structured 5'UTRs but not with poor AUG
394 sequence context.
395
396 **Transcripts showing Ded1 stimulation of 48S PIC assembly in Rec-Seq include the**
397 **majority of Ded1-hyperdependent mRNAs identified by Ribo-Seq analysis of a *ded1***
398 **mutant.**
399 We next asked whether mRNAs exhibiting stimulation of 48S PIC assembly by Ded1 in
400 Rec-Seq include those judged to be hyper-dependent on Ded1 in vivo by Ribo-Seq analysis of
401 the *ded1-cs* mutant (Sen et al. 2015). First, to assess the similarity between the sets of mRNAs
402 examined in our Rec-Seq experiments and in previous Ribo-Seq experiments, we plotted RNA-
403 Seq reads for all mRNAs observed in Rec-Seq versus those from WT or *ded1-cs* yeast strains in
404 the Ribo-Seq experiments and found that they were very strongly linearly correlated with
405 Spearman coefficients (ρ) of 0.90 and 0.88, respectively (Fig. 4A, B). The mRNAs from the WT
406 and *ded1-cs* strains identified in Ribo-Seq experiments were also well correlated (ρ = 0.97) (Fig.
407 4C). Thus, despite having been prepared using somewhat different methods, the total mRNA

408 used in our Rec-Seq experiments was very similar in sequence abundance to that observed in
409 previous in vivo ribosome profiling experiments.

410 Importantly, we observed a highly significant correlation ($\rho = 0.60$, $P = 4.2 \times 10^{-300}$)
411 between the mRPFs from Rec-Seq reactions lacking Ded1 and 80S RPFs from Ribo-Seq
412 experiments with the *ded1-cs* mutant at the non-permissive temperature where Ded1 function is
413 impaired (Fig. 4D). We saw similar correlations between mRPFs from Rec-Seq reactions
414 containing 100 nM or 500 nM Ded1 and 80S RPFs from Ribo-Seq experiments on the WT
415 *DED1* strain (Figs. 4E-F; $\rho = 0.53$ and $\rho = 0.54$, respectively). A total of 3035 mRNAs were
416 detected in common across all these experiments. Thus, a marked correlation exists between the
417 amounts of translation on each mRNA observed in vivo (80S RPFs) measured in Ribo-Seq
418 experiments and 48S PIC formation measured in our in vitro Rec-Seq experiments, and this
419 holds at different levels of Ded1 activity.

420 We also observed significant correlations between ΔRE values measured in Rec-Seq for
421 reactions containing no Ded1 versus 100 nM or 500 nM Ded1 and changes in translational
422 efficiencies (ΔTE values) measured in Ribo-Seq for *ded1-cs* versus WT *DED1* cells at the non-
423 permissive temperature (Fig. 4G, H). Consistent with this, the mRNAs exhibiting increased REs
424 on addition of either concentration of Ded1 and the mRNAs showing decreased TEs in *ded1-cs*
425 versus *DED1* cells in Ribo-Seq all have significantly higher median 5'UTR lengths, Max30
426 PARS scores, or Total PARS scores compared to all observed mRNAs and to the mRNAs that
427 behave oppositely in Rec-Seq or Ribo-Seq (Fig. 4I-K). Strikingly, 80-90% of the mRNAs
428 showing significantly decreased TEs conferred by *ded1-cs* in Ribo-Seq displayed significantly
429 increased REs on addition of 100 nM or 500 nM Ded1 in Rec-Seq reactions (Fig. 4L, M).

430 Despite the significant correlations shown in Fig. 4A-H, it should be noted that 11% of
431 the Ded1-hyperdependent mRNAs showing TE reductions in *ded1-cs* cells in Ribo-Seq did not
432 exhibit significant stimulation of 48S PIC assembly by Ded1 in our Rec-Seq experiments (Fig.
433 4L, set of 39 mRNAs). Such mRNAs might be stimulated by Ded1 at a step following 48S PIC
434 assembly that is not monitored by Rec-Seq or they might require additional factors for Ded1
435 stimulation of 48S PIC assembly that are lacking in our Rec-Seq experiments. It is also evident
436 that the majority of mRNAs stimulated by 500 nM Ded1 in our Rec-Seq experiments were not
437 judged to be Ded1-hyperdependent in Ribo-Seq analysis of the *ded1-cs* mutant (Fig. 4L, set of
438 683 mRNAs; "Group Y"). This could be explained by the fact that TEs in the Ribo-Seq analysis
439 of the *ded1-cs* mutant were measured relative to the average transcript (Sen et al. 2015) and thus
440 both Ded1 hyper- and hypo-dependent transcripts could have decreased translation in the Ded1-
441 deficient mutant at the non-permissive temperature relative to WT cells, but with the former
442 decreased more than the average transcript and the latter decreased similar to or less than the
443 average. Consistent with this interpretation, bulk polysome assembly is dramatically reduced
444 only minutes after shifting the *ded1-cs* mutant to the non-permissive temperature, indicating a
445 reduction in translation initiation on a large fraction of mRNAs (Sen et al. 2015). Because the
446 Rec-Seq method employs an internal standard, the measured REs are absolute rather than relative
447 and thus lead to a larger set of mRNAs with increased RE upon Ded1 addition than that for the
448 relative TE reductions in the *ded1-cs* mutant at the non-permissive temperature in the Ribo-Seq
449 experiments. Consistent with this explanation, the 683 Group Y mRNAs that were significantly
450 stimulated in Rec-Seq by 500 nM Ded1 but not classified as Ded1-hyperdependent in Ribo-Seq,
451 displayed a smaller, albeit still significant, median increase in RE upon addition of 500 nM Ded1
452 than did the 319 mRNAs ("Group X") that were classified as Ded1 hyper-dependent in the

453 Ribo-Seq experiments (Fig. 4N). Moreover, the Group Y mRNAs had a substantially smaller
454 median decrease in relative TE between the *ded1-cs* mutant and WT cells than did the Ded1
455 hyper-dependent Group X mRNAs (Fig. 4O). The median TE change of Group Y mRNAs was
456 less than 2-fold and thus would not have met the criteria used for significance in the Ribo-Seq
457 experiments. Thus, normalization of TE changes to the average mRNA in Ribo-Seq undoubtedly
458 obscured the Ded1-dependence in vivo of many of the mRNAs stimulated by Ded1 in Rec-Seq
459 reactions.

460 Together, our findings suggest that despite the much greater complexity of the system in
461 vivo in terms of both components and processes, the effects of Ded1 on the translation of many
462 mRNAs in cells is similar to what we see in the reconstituted Rec-Seq system that contains only
463 a core set of translation components and is not influenced by processes such as mRNA transport,
464 decay and compartmentalization/phase separation. This seems a remarkable result given the
465 number of in vivo roles that have been ascribed to Ded1 beyond simply promoting mRNA
466 recruitment and scanning. The significant correlation between the effects of adding Ded1 to Rec-
467 Seq experiments in vitro and of inactivating Ded1 in Ribo-Seq in vivo leads to the important
468 insight that 48S PIC formation is frequently the rate limiting step for translation initiation that is
469 stimulated by Ded1 in vivo.

470

471 **Evidence that Ded1 can promote leaky scanning of canonical AUG start codons.**

472 In Rec-Seq reactions lacking Ded1, RPFs at internal AUG start codons (iAUGs) located
473 within CDSs (iRPFs) occur at 3.0% of all RPFs found anywhere in the CDS (at either the main
474 or internal start sites, cdsRPFs), but this proportion increases to 4.2% and 7.8% on addition of
475 100 or 500 nM Ded1 to the reactions (Fig. 5A). The increase in iRPFs as Ded1 concentration

476 increases is shown clearly by metagene plots for all transcripts (Fig. 5B-D) and for four specific
477 genes in Fig. 5E-H, three of which also illustrate that Ded1 can increase iRPFs at genes where
478 48S PIC assembly at the mAUG is not stimulated or even reduced by Ded1 (Fig. 5E-G). DESeq2
479 analysis reveals that Ded1 elicits >2-fold increases in iRPFs for 590 and 1586 mRNAs at 100 or
480 500 nM Ded1, respectively, whereas only 1 or 2 transcripts showed reduced iRPFs on addition of
481 Ded1, out of all 3052 transcripts detected (Fig. 5I-J). Thus, induction of iRPFs by Ded1 is
482 widespread in Rec-Seq.

483 A hallmark of increased leaky scanning in an mRNA would be a reciprocal decrease in
484 mRPF when an increase in iRPF occurs (Fig. 5S-1A). This situation, particularly well-illustrated
485 for *ETT1* and *DBP5* in Fig. 5E-F, is consistent with Ded1-stimulated read-through of the mAUG
486 codon leading to PICs continuing to scan downstream and initiating at iAUGs instead.
487 Importantly, a reciprocal reduction in mRPFs and increase in iRPFs of comparable magnitude on
488 Ded1 addition is evident for the group of 182 mRNAs identified above (Fig. 2B) showing >2-
489 fold reduction of mRPFs at 500 nM Ded1 (Fig. 5K). Moreover, 125 (69%) of these 182
490 transcripts belong to the group of 1586 mRNAs identified in Fig. 5J displaying >2-fold increases
491 in iRPFs at 500 nM Ded1 (Fig. 5L, green/red intersection). These 125 transcripts are shown as
492 black dots in the scatterplot of changes in mRPFs at 500 nM vs. 0 nM Ded1 in Fig. 5M. To apply
493 a stringent criteria for leaky scanning, we identified the mRNAs among this last group of 125
494 mRNAs for which the increase in iRPFs is comparable in magnitude (>50%) to the decrease in
495 mRPFs in the manner expected if iRPFs arise from PICs that scan past the mAUG and initiate
496 internally instead (highlighted with yellow circles in Fig. 5M). This analysis reveals that leaky
497 scanning of the mAUG could account for at least 46% (84/182) of all mRNAs showing
498 decreased mRPFs on addition of 500 nM Ded1. Many of the remaining 56% could arise from

499 increased competition for 43S PICs caused by Ded1 stimulation of PIC formation on other
500 mRNAs with long, structured 5'UTRs, which are poorly recruited in the absence of Ded1 but
501 begin competing for PICs when Ded1 is added to the system.

502 Considering that Ded1 inhibits 48S PIC assembly at the mAUG codons of so few
503 mRNAs (only 182 out of 3052 tested), and that translation initiation continues on at least 46% of
504 these transcripts and merely shifts to iAUGs, our data do not support a model in which a high
505 concentration of Ded1 leads to widespread translational repression by causing mRNAs to
506 undergo phase-transitions into translationally silenced states. If this is a significant repressive
507 function of Ded1 in vivo, it likely requires even higher concentrations of Ded1, modification of
508 Ded1, or additional factors not present in the Rec-Seq system.

509 Among the 1586 transcripts showing significantly increased initiation at iAUGs at 500
510 nM Ded1, roughly ~1/3$^{rd}$ (508) exhibit increased rather than decreased mRPFs on Ded1 addition
511 (Fig. 5L, red/blue intersection). In fact, this trend is evident for the entire group of 1006 mRNAs
512 showing increased PIC assembly at the mAUGs at 500 nM Ded1 (Fig. 5N), although the median
513 increase in iRPFs conferred by 500 nM Ded1 (23.2 iRPFs) is smaller for this group than that
514 observed for the mRNAs described above where PIC assembly at the mAUG is repressed by
515 Ded1 (86 iRPFs, Fig. 5K). One possibility is that a high concentration of Ded1 increases
516 readthrough of mAUGs on a large fraction of mRNAs but that in most cases this low-level leaky
517 scanning is offset by larger increases in PIC attachment to mRNAs to yield a net increase in
518 mRPFs despite enhanced mAUG readthrough. Consistent with this proposal, box plots of RE
519 values show that the mRNAs with mRPFs increased by Ded1 are initiated inefficiently in the
520 absence of Ded1, whereas the mRNAs that display decreased mRPFs in the presence of Ded1
521 tend to be initiated very efficiently in Ded1's absence (Fig. 5S-1B). Presumably, because the

522 latter mRNAs do not exhibit significantly increased recruitment of 43S PICs when Ded1 is
523 added, the increased leaky scanning of their mAUGs induced by Ded1 is not offset by increased
524 overall recruitment of PICs, resulting in a net decrease in PIC assembly at the mAUGs.

525 To assess whether the sequence context around the mAUG influences its susceptibility to
526 Ded1-induced leaky scanning, we examined the average fraction of all coding sequence RPFs
527 (cdsRPF) that are iRPFs, a ratio we refer to as Relative Ribosome Occupancy ($RRO_{iRPF/cdsRPF}$), as
528 a function of the context score for the bases surrounding the mAUG. As shown in Fig. 5O, with
529 both 0 and 500 nM Ded1 the average $RRO_{iRPF/cdsRPF}$ decreases as the context scores around the
530 mAUGs increase (cyan and purple lines), consistent with the idea that the better the context the
531 more stably the PIC is bound and the less likely leaky scanning through the mAUG is. Plotting
532 the ratio of RRO values at 500 nM to 0 nM Ded1 yields a flat line with $\log_2\Delta RRO$ values of
533 ~0.75 for all bins (Fig. 5O, orange line). These last results suggest that addition of 500 nM Ded1
534 increases the frequency of leaky scanning by ~1.7-fold regardless of mAUG context. This in
535 turn implies that Ded1 does not inspect the context sequence but rather promotes scanning to
536 reduce the dwell-time of the PIC at the AUG similarly for both weak and strong contexts.

537 Rather than invoking leaky scanning, it could be proposed that the RPFs formed at iAUGs
538 originate from a small fraction of mRNA isoforms with transcription initiation sites within the
539 CDSs (Arribere and Gilbert 2013; Lu and Lin 2019) that contain the internal initiation sites as
540 the first AUGs encountered on scanning from the cap. Alternatively, the iRPFs could be formed
541 on uncapped mRNAs cleaved at the 5' end in cells or in vitro, which would require cap-
542 independent initiation. In either case, Ded1 could stimulate PIC assembly at the iAUGs by the
543 same mechanism identified above for canonical mAUGs. Several lines of evidence argue against
544 this possibility and instead favor the Ded1-induced leaky scanning model proposed above. First,

545 the level of iAUG initiation relative to mAUG initiation (RRO) depends strongly on the
546 sequence context surrounding the mAUG (Fig. 5O), as expected for the leaky scanning model
547 but inconsistent with a model in which iAUG occupancy arises from 5'-truncated mRNA
548 isoforms or fragments. In addition, mRNAs that have a high level of iAUG occupancy relative to
549 mAUG occupancy (RRO $\geqslant$ 0.5) tend to have less secondary structure in the 5'-ends of their
550 coding sequences than do mRNAs with less iAUG occupancy (Fig. 5P, cols. 3-8, compare blue
551 and orange boxes), consistent with a model in which secondary structures just downstream of the
552 mAUG inhibit further scanning and diminish mAUG readthrough. This result is not predicted by
553 the truncated mRNA isoform/fragment model. Finally, it is difficult to account for the reciprocal
554 effects of Ded1 in repressing mRPFs while inducing iRPFs by comparable amounts for the same
555 genes (Fig. 5K) if the events occur independently on different transcript isoforms.
556 Overall, these data suggest that a high Ded1 concentration increases leaky scanning of the
557 mAUG for approximately half (1586/3052; Fig. 5J) of the mRNAs in the yeast translatome that
558 were observed in this study. In some cases this leads to a decrease in mRPFs, and may account
559 for nearly 50% of the mRNAs for which Ded1 suppresses 48S PIC assembly at the mAUG,
560 while in others the overall enhancement of PIC loading on the mRNA induced by Ded1 likely
561 offsets the increased leaky scanning for a net stimulation of 48S PIC assembly at the mAUG.
562 The inhibitory effect of Ded1 on proper initiation at mAUGs for the subsets of mRNAs
563 described above for which mRPFs are significantly decreased by 500 nM Ded1 in the Rec-Seq
564 experiments also appears to be operative in vivo as the median TEs of these sets of mRNAs are
565 increased in *ded1-cs* cells at the non-permissive temperature relative to WT cells (Fig. 5-S2),
566 signifying Ded1-hypodependence. These data are consistent with Ded1 activity diminishing the

567 relative translation levels of these mRNAs in WT cells, in alignment with our observations in the
568 Rec-Seq experiments.
569
570 **Ded1 does not increase initiation at canonical AUG codons in Rec-Seq by suppressing**
571 **alternative initiation events in 5'UTRs.**
572 It has been proposed that a key function of Ded1 is to increase the fidelity of start codon
573 selection by promoting readthrough of upstream AUG (uAUG) and near-cognate codons to boost
574 the fraction of scanning PICs that initiate at the mAUG codon (Guenther et al. 2018). To
575 determine whether this mechanism operates in the reconstituted system, we analyzed the effect
576 of Ded1 in Rec-Seq reactions on the total RPFs mapping to the 5'-UTRs of mRNAs (uRPFs).
577 We observed that 40 – 60% of all uRPFs detected when Ded1 is present in the reaction mapped
578 to the *GCN4* 5'UTR (Fig. 6-S1), and we therefore excluded *GCN4* mRNA in calculating the
579 [total uRPF]/[total mRPF] ratio in order to measure effects on the overall translatome. In the
580 absence of Ded1, the ratio of total uRPFs to mRPFs was 0.0021 (Fig. 6A, col. 1). Addition of
581 100 nM Ded1 decreased the ratio to 0.0017 and increasing the concentration to 500 nM
582 decreased it further only slightly, to 0.0016 (Fig. 6A, cols. 2-3). A decreased uRPF/mRPF ratio
583 on addition of Ded1 is expected if Ded1 suppresses PIC assembly at upstream start codons as
584 proposed in the aforementioned model. However, even in the absence of Ded1, uRPFs represent
585 a very small fraction of all RPFs and this fraction is decreased by only ~30% upon addition of
586 Ded1.
587 We next visualized the effects of Ded1 on upstream initiation in individual mRNAs by
588 plotting the uRPFs in the absence of Ded1 vs. the presence of 100 or 500 nM Ded1 (Fig. 6B and
589 C, respectively). Going from 0 to 100 nM Ded1 led to a significant reduction (ΔRPFs < 0.5, FDR

590 < 0.05) in uRPFs for only 9 mRNAs (Fig. 6B, dark blue dots). Moreover, only one mRNA
591 (*SXM1*) showed a decrease in uRPFs comparable in magnitude (>50%) to the corresponding
592 increase in mRPFs in the manner expected if Ded1-stimulated leaky scanning of uAUGs
593 stimulates PIC assembly at the mAUG (Fig. 6B, yellow circle). In contrast, uRPFs for 14
594 mRNAs were significantly increased (ΔRPFs > 2, FDR < 0.05), presumably due to enhanced PIC
595 attachment to these mRNAs caused by addition of Ded1. Similar results were obtained in going
596 from 0 to 500 nM Ded1, which resulted in only 25 mRNAs with significantly decreased uRPFs,
597 and only two showing reductions >50% of the magnitude of the observed increase in mRPFs for
598 the mRNA (*MSC7* and *UIP5*), whereas 30 mRNAs showed significant increases in uRPFs (Fig.
599 6C). Taken together, these results indicate that in the in vitro Rec-Seq system Ded1 produces
600 significant decreases in upstream initiation on only a small fraction of all mRNAs, and that the
601 decreases in uRPFs are large enough to explain the increased initiation at the mAUG codon for
602 only one or two such mRNAs. In addition, there are at least as many cases in which upstream
603 initiation is increased rather than decreased, most likely due to overall enhancement of PIC
604 attachment to these mRNAs by Ded1. These data do not support the model that Ded1 enhances
605 translation initiation at mAUG codons primarily by promoting leaky scanning of uAUG codons.
606 Additional evidence supporting our conclusion came from comparing the magnitude of
607 changes in uRPFs versus mRPFs conferred by Ded1 for a group of 257 mRNAs containing RPFs
608 in both 5'UTRs and at mAUG codons exceeding a minimum threshold read abundance. Overall,
609 the mRPFs are an order of magnitude higher than uRPFs in the absence or presence of Ded1 at
610 either concentration (Fig. 6D, see median values below each column). Addition of 100 nM Ded1
611 decreases the median uRPFs by 2, from 10 to 8, but increases mRPFs by 80, from 65 to 145.
612 Likewise, with 500 nM Ded1 relative to no Ded1, uRPFs decrease by 4, whereas mRPFs

613 increase by 109. Thus, the magnitude of the RPF decreases in 5'UTRs are much too small to
614 account for the increases in RPFs at mAUG codons elicited by addition of Ded1. Taken together,
615 our data indicate that, at least in the reconstituted in vitro system, Ded1 functions by directly
616 increasing PIC attachment to mRNAs and scanning to the main start codons rather than by
617 diminishing inhibitory initiation in 5'UTRs.
618
619 **eIF4A plays a distinct role from Ded1 and stimulates recruitment of most mRNAs**
620 **regardless of their 5'UTR lengths or structures.**
621 Previous work in vitro and in vivo has indicated that eIF4A and Ded1 play distinct roles
622 in promoting translation initiation. In the reconstituted system, no assembly of 48S PICs was
623 observed for a variety of individual mRNAs in the absence of eIF4A but presence of Ded1,
624 indicating that Ded1 cannot take the place of eIF4A (Gupta et al. 2018). In contrast, 48S PIC
625 formation occurred efficiently on many mRNAs in vitro in the presence of eIF4A but absence of
626 Ded1, and all mRNAs studied required eIF4A for PIC assembly, regardless of their degree of
627 secondary structure (Pestova and Kolupaeva 2002; Yourik et al. 2017; Gupta et al. 2018). In vivo
628 ribosome profiling studies also led to the conclusion that eIF4A is universally required for
629 translation of most mRNAs, whereas Ded1 preferentially stimulates translation of mRNAs with
630 long, structured 5'UTRs (Sen et al. 2015).
631 Our results here strongly support the previous conclusions that Ded1 functions by
632 alleviating structural impediments to PIC loading and scanning in the 5'UTRs of particular
633 mRNAs burdened by these features. To probe further functional differences between Ded1 and
634 eIF4A, we performed Rec-Seq reactions in the absence of Ded1 and presence of either 5000 nM
635 (1X) or 500 nM (0.1X) eIF4A. It was not possible to do the experiment in the absence of eIF4A

636 because the factor is essential for 48S PIC formation on most, if not all, mRNAs. A scatterplot of
637 mRPFs at 5000 versus 500 nM eIF4A shows that PIC assembly at the mAUGs of most mRNAs
638 increases when the concentration of eIF4A is raised 10-fold (Fig. 7A, light blue density above
639 the diagonal). Of 2809 mRNAs observed in these experiments, 782 reached the level of
640 significance in DEseq2 analysis of $\geqslant$ 2-fold change in mRPFs and FDR < 0.05. Only one
641 mRNA (*SCW10*) met the criteria for significantly decreased mRPFs (Fig. 7A, dark blue dot).
642 Consistent with these results, increasing the eIF4A concentration from 500 to 5000 nM increased
643 the REs of almost all mRNAs, with a median change of ~5.7-fold (Fig. 7B, col. 1). By
644 comparison, addition of either 100 or 500 nM Ded1 in a background of 5000 nM eIF4A
645 increased the median RE by only 1.3-fold, with RE for many mRNAs not changing (Fig. 7B,
646 cols. 2-3). Rather, a large number of outliers are increased dramatically more than the median
647 ΔRE value when Ded1 is added to the reactions, consistent with the preferential stimulation of
648 48S PIC assembly by Ded1 for mRNAs with long, structured 5'UTRs shown above (Fig. 3). In
649 our previous Ribo-Seq experiments on an eIF4A mutant, where changes in TE were determined
650 relative to the effect on the average mRNA, the vast majority of mRNAs displayed no change in
651 relative TE despite a strong reduction in bulk translation, implying TE reductions of similar
652 magnitude for nearly all mRNAs (Sen et al. 2015).
653 To examine whether length or structure of 5'UTRs influences the stimulatory effects of
654 eIF4A in Rec-Seq, we plotted ΔRE values between 500 and 5000 nM eIF4A as a function of
655 5'UTR length or Max30 PARS values. Importantly, the median ΔRE values remain constant
656 across the first five bins of 5'UTR lengths and four bins of Max30 PARS scores and actually
657 decrease significantly in the sixth bins (Fig. 7C, D). This behavior contrasts with that described
658 above for addition of Ded1 to Rec-Seq reactions, which showed progressively greater

659 enhancement of RE as 5'UTR length and Max30 PARS scores increased (Fig. 3B, C, F and G).
660 The distinct effects of increasing eIF4A concentration versus addition of Ded1 on mRNAs
661 binned according to 5'UTR length, 5'UTR Max30 PARS, or 5'UTR Total PARS values are
662 depicted in Figs. 7E-G. Consistent with these results, inspection of RPF traces for individual
663 mRNAs reveals that eIF4A enhances 48S PIC assembly on mRNAs judged to be either hypo- or
664 hyper-dependent on Ded1 in Ribo-Seq experiments (Sen et al. 2015) (Fig. 7H-K). Overall, these
665 results are consistent with previous conclusions that eIF4A stimulates recruitment of all mRNAs,
666 regardless of their degree of secondary structure, whereas Ded1 specifically acts on mRNAs with
667 long, structured 5'UTRs. Our data are also in line with previous work indicating that Ded1 has
668 much stronger helicase activity than eIF4A (Rogers et al. 1999; Yang et al. 2007; Rajagopal et
669 al. 2012) and thus the former is likely to play a role in unwinding stable secondary structures
670 whereas the latter mediates engagement of mRNAs with the 43S PIC by resolving ensembles of
671 weaker interactions within mRNAs or by modulating the structure of the mRNA channel of the
672 40S ribosomal subunit (Sokabe and Fraser 2017; Yourik et al. 2017).
673

674 **DISCUSSION**

675 We have developed a deep sequencing-based approach, "Rec-Seq," for measuring the
676 efficiency with which 48S PICs form on each mRNA in the yeast transcriptome in a
677 reconstituted in vitro system. Using this approach, we have provided evidence that the DEAD-
678 box translation initiation factor Ded1 specifically stimulates 48S PIC formation on mRNAs with
679 long, structured 5'UTRs, which supports the model that the factor generally acts by unwinding
680 secondary structures in 5'UTRs to promote 43S PIC binding and scanning to locate the start
681 (Berthelot et al. 2004; Sen et al. 2015; Guenther et al. 2018; Gupta et al. 2018; Sen et al. 2019;

682 Sen et al. 2021). We showed that 48S PIC formation on a set of ~1000 mRNAs is significantly
683 less efficient in the absence of Ded1 than in its presence, demonstrating a positive function for
684 the factor on these mRNAs. It is striking that the Ded1-stimulated mRNAs identified in our in
685 vitro system include the great majority of mRNAs identified as being hyperdependent on Ded1
686 in vivo by ribosome profiling of a *ded1-cs* mutant. This concordance argues that the mRNAs
687 showing the strongest dependence on Ded1 for efficient translation in vivo are stimulated by the
688 factor at the stage of 48S PIC assembly. It further argues against the possibility that the TE
689 reductions observed for Ded1 hyperdependent mRNAs in *ded1-cs* cells frequently result from
690 dominant inhibitory properties of the mutant *ded1* proteins. Ded1 also stimulated 48S PIC
691 assembly in Rec-Seq for many mRNAs not classified as Ded1-hyperdependent by Ribo-Seq.
692 However, as explained above, translation of these mRNAs was likely impaired by the *ded1-cs*
693 mutation but to a degree that was less than the 2-fold cutoff required for statistical significance,
694 or that was less than the effect on the average mRNA and thus yielded a positive change in the
695 relative TE values determined in the Ribo-Seq analysis.
696 Compared to the sizeable group of >1000 mRNAs for which 500 nM Ded1 stimulated 48S
697 PIC assembly, we identified a much smaller set of only 182 mRNAs for which 48S PIC
698 assembly was significantly repressed by Ded1 in Rec-Seq experiments. We obtained evidence
699 that at least 84 of these transcripts were repressed owing to Ded1-stimulated leaky scanning of
700 the mAUG codon rather than by Ded1 blocking PIC attachment or scanning. As a group, the
701 mRNAs exhibiting Ded1 repression in Rec-Seq show increased relative TE in Ribo-Seq analysis
702 of the *ded1-cs* mutant, regardless of whether they display evidence of Ded1-enhanced leaky
703 scanning of the mAUG codons in Rec-Seq (Fig. 5-S2). This behavior is consistent with loss of
704 Ded1 repression or with smaller than average reductions in TE in *ded1-cs* vs. WT cells. The

705 latter possibility is consistent with our finding that the 182 mRNAs inhibited by 500 nM Ded1 in
706 Rec-Seq assemble 48S PICs very efficiently without Ded1 (Fig. 5-S1). Being relatively
707 independent of Ded1 for PIC assembly, these mRNAs should experience a smaller than average
708 reduction in translation in *ded1-cs* cells owing to reduced competition for limiting 43S PICs with
709 the Ded1-dependent mRNAs that should be strongly impaired for PIC assembly. We argued
710 above that a similar mechanism can also explain the repression of RE by Ded1 in Rec-Seq
711 experiments for the subset of 98 mRNAs without evidence of appreciable leaky scanning of the
712 mAUG codon, owing to increased competition for 43S PICs with the Ded1-stimulated
713 transcripts. It remains to be seen whether Ded1 acts directly to repress 48S PIC assembly on any
714 individual mRNAs in yeast. It is possible that at higher concentrations of Ded1 than were
715 achievable in these in vitro experiments or in the presence of additional factors that modify
716 Ded1's ATPase or RNA binding activities the factor could directly inhibit a subset of mRNAs,
717 by acting as an mRNA clamp that impedes scanning by the PIC, or by sequestering the mRNAs
718 in insoluble condensates. It might be interesting in the future to test candidate factors in Rec-Seq
719 to determine if they switch Ded1 from being a stimulatory helicase to an inhibitory mRNA
720 clamp that removes transcripts from the soluble phase.

721 We found that the presence of 500 nM Ded1 in Rec-Seq reactions increased 48S PIC
722 assembly at internal AUG codons on ~50% of all detected transcripts. In ~1/3$^{rd}$ of these 1586
723 transcripts, there is a parallel increase in RPFs at the mAUG codons, suggesting that Ded1
724 stimulates 43S PIC attachment at the 5' ends of these transcripts to increase initiation
725 proportionately at all AUGs in the mRNA. As mentioned, in ~5% of the mRNAs (84/1586), the
726 increased internal initiation may result from leaky scanning of the mAUG codons, as we found a
727 comparable reduction in initiation at the mAUG. In this view, Ded1 might resolve secondary

728 structures positioned just downstream of the mAUG codon that increase the dwell-time of the
729 PIC and increase the probability of PIC assembly versus continued scanning downstream that
730 leads to initiation on iAUG codons, in the manner first described for mammals by Kozak (Kozak
731 1990). Interestingly, Ded1 enhanced this apparent mAUG read-through to similar extents
732 regardless of the mAUG context, which would imply that Ded1 promotes scanning of the PIC
733 past the mAUG without inspecting the context nucleotides surrounding it.

734 Ded1 also significantly reduced RPFs at upstream AUG and near-cognate start codons in the
735 5'UTRs of a small number of transcripts (25 mRNAs at 500 nM Ded1), possibly by the same
736 mechanism mentioned above involving unwinding of downstream secondary structures.
737 However, this reduction was associated with a comparable increase in RPFs at the mAUG for
738 only two of these mRNAs. Our findings that PIC assembly at uAUGs in the absence of Ded1 is
739 rare, and that suppression of these rare occurrences by Ded1 cannot explain the much larger
740 increases in initiation at the mAUGs conferred by Ded1, argue that, at least in this in vitro
741 system, Ded1 does not stimulate initiation primarily by promoting leaky scanning of upstream
742 start codons to enable PIC assembly at the mAUGs in the manner proposed for Ded1 function in
743 vivo (Guenther et al. 2018).

744 Finally, our data show that Ded1 and eIF4A, another essential DEAD-box translation
745 initiation factor, have distinct functions. Unlike Ded1, which has pronounced specificity for
746 activating initiation on mRNAs with long, structured 5'UTRs, eIF4A strongly promotes
747 initiation on nearly all mRNAs, regardless of the length or degree of structure of their 5' leaders.
748 Because our system employs internal "spike-in" standards, we were able to measure the absolute
749 enhancement provided by eIF4A for mRNA recruitment upon increasing its concentration from
750 500 to 5000 nM, a 5.7-fold increase in median RE (Fig. 7B). In contrast, addition of Ded1 to the

751 system produced a much smaller change in median RE, of only 1.3-fold, while conferring much
752 larger effects, >10-fold, on many mRNAs with long, structured 5'-UTRs. These findings support
753 our previous conclusions from Ribo-Seq analysis of Ded1 and eIF4A mutants that Ded1
754 preferentially stimulates translation of mRNAs burdened with structured 5'UTRs while eIF4A
755 enhances the translation of nearly all mRNAs equally (Sen et al. 2015).
756 Our data provide information on the intrinsic efficiency of 48S PIC formation on cellular
757 mRNAs in the yeast translatome. In the presence of 500 nM Ded1, RE values follow a roughly
758 normal distribution spanning a 1000-fold range (Fig. 2H), indicating that even in the presence of
759 Ded1, there are still large differences in the intrinsic efficiencies with which mRNAs are
760 recruited to the 43S PIC and scanned to locate the start codon. In the presence of Ded1, there is
761 little dependence of RE on 5'UTR structure or length (Fig. 3A,E) and thus other mRNA
762 characteristics must set the 48S PIC formation efficiencies. The strength of sequence context
763 around the start codon has a modest (~2-fold) effect (Fig. 3S-2A), but not nearly enough to
764 explain the range of REs observed. The 1000-fold range we observe here is strikingly similar to
765 the range reported in a systematic study of 5'UTR variants in a yeast lysate-based translation
766 system (Niederer et al. 2022). In that work, the authors provided evidence that a variety of
767 sequence elements in 5'UTRs can enhance or inhibit translation initiation through a range of
768 mechanisms. Thus, it is likely that in the presence of Ded1, no single mRNA feature sets the
769 efficiency of 48S complex assembly and instead a multitude of effects and interactions are
770 involved, possibly including specific interactions between mRNA elements and initiation factors
771 or the ribosome (Niederer et al. 2022). In addition, mRNA elements outside of the 5'UTR,
772 including the poly(A) tail and its interaction with PABP, might influence the efficiency of 48S

773 PIC formation. Further studies will be required to elucidate fundamental principles and specific
774 cases of how mRNA sequences dictate translational efficiency.
775

776 **MATERIALS AND METHODS**

777 **Purification of yeast total mRNA**

778 WT *Saccharomyces cerevisiae* strain F729/BY4741 (*MATa his3Δ1 leu2Δ0 met15Δ0*
779 *ura3Δ0)* (Winzeler et al. 1999) was cultured in Yeast Extract–Peptone–Dextrose (YPD) medium
780 to $OD_{600}$ of ~1. Harvested cells were washed once with cold water and stored in -80°C before
781 use. The frozen cell pellet from a 500 ml culture was thawed on ice and mechanically disrupted
782 by vortexing with glass beads three times for 2 min each at maximum speed in a cold room (4°C)
783 in 2 ml of buffer RL (provided in the kit), 3 ml phenol:chloroform:isoamyl alcohol 25:24:1 (pH
784 5.2) and 3 ml ice cold glass beads. Following 5 min centrifugation at 14000 rpm in a Sorvall
785 LYNX 6000 Superspeed centrifuge using a Fiberlite F14-14 x 50cy rotor, the supernatant was
786 transferred to a fresh tube and total RNA was prepared using a GenElute total RNA purification
787 Maxi kit (Sigma-Aldrich; RNB200) following the manufacturer's protocol. 400 µg total RNA in
788 250 µl water was applied to a GeneElute mRNA miniprep kit (Sigma-Aldrich; MRN70-1KT),
789 following the manufacturer's protocol. The purified total mRNA was treated by 5'-Phosphate-
790 Dependent Exonuclease (Lucigen, TER51020) to degrade RNAs with 5' monophosphates, such
791 as 18S and 25S ribosomal RNAs, at 0.3 µg/µl mRNA in 1X buffer A (provided in the kit), 1U/µl
792 RiboGuard RNase Inhibitor (Lucigen; RG90925), 0.1 U/µl 5'-Phosphate-Dependent
793 Exonuclease. Following a 1 h incubation at 30°C, the total mRNA was extracted using
794 phenol:chloroform:isoamyl alcohol 25:24:1 (pH 5.2), ethanol precipitated, resuspended in 10
795 mM Tris (pH 8.0) and stored in -80 °C.

796

797 **Purification of 40S ribosome subunits and translation initiation factors**

798 Eukaryotic initiation factors eIF1, eIF1A, eIF2, eIF3, eIF4A, eIF4B, eIF4G·4E and eIF5
799 were expressed and purified as described previously (Acker et al. 2007; Mitchell et al. 2010;
800 Rajagopal et al. 2012; Gupta et al. 2018). 40S ribosomal subunits were prepared as described in
801 Munoz et al. (2017). Ded1 protein (N-terminal His6-tag, pET22b vector) was purified as
802 described previously (Gupta et al. 2018).

803

804 **Preparation of spike-in mRNAs and charged initiator tRNA**

805 The templates for *in vitro* transcription of the 5' fragments of *FLUC* and *RLUC* genes
806 were amplified by PCR from plasmid FJZ1061 (Zhou et al. 2020) using primers T7-FLUC and
807 FLUC-R for *FLUC*, T7-RLUC and RLUC-R for *RLUC* (Table S1). The mRNAs and initiator
808 tRNA were transcribed by run-off transcription using T7 RNA polymerase and gel purified as
809 described previously (Acker et al. 2007; Mitchell et al. 2010). mRNAs were capped (m7GpppG)
810 using GTP and vaccinia virus capping enzyme (Mitchell et al. 2010). Initiator tRNA was
811 methionylated *in vitro* using methionine and *E. coli* methionyl-tRNA synthetase as previously
812 described (Walker and Fredrick 2008; Yourik et al. 2017).

813

814 **mRNA recruitment assays on spike-in mRNAs and total mRNA**

815 48S PICs were assembled on pre-mixed spike-in mRNAs (molar ratio FLUC/RLUC ~
816 1:10) as described previously (Mitchell et al. 2010; Yourik et al. 2017) in 1X Recon buffer (30
817 mM HEPES-KOH, pH 7.4, 100 mM KOAc, 3 mM Mg(OAc)2, and 2 mM DTT) containing 300
818 nM eIF2, 0.5 mM GDPNP·$Mg^{2+}$, 200 nM Met-$tRNA_i$Met, 1 μM eIF1, 1 μM eIF1A, 300 nM

819 eIF5, 300 nM eIF4B, 300 nM eIF3, 30 nM 40S subunits, 5 μM eIF4A, 30 nM eIF4E·eIFG, 5 μM
820 Ded1 and 15 nM mRNA. The reaction was incubated at 26°C for 20 min before being rapidly
821 quenched by adding stop buffer (1X Recon buffer, 37.5 mM glucose and 0.04 U/μl Hexokinase
822 (Roche Diagnostics, REF:11426362001)) in a 3:10 v/v ratio. RPFs of 48S PICs were generated
823 by incubating the reaction with RNase I (Thermo Fisher; AM2295) at a final concentration 2.5
824 U/μl, followed by adding SUPERaseIN RNase inhibitor (Thermo Fisher; AM2696) at a final
825 concentration 1.2 U/μl. Recruitment reactions using purified yeast total mRNA with different
826 Ded1 concentrations were performed similarly as for spike-in mRNAs, but incubated at 22°C for
827 15 min, with all of the same initiation factor concentrations except 60 nM input total mRNA and
828 three different Ded1 concentrations (0 nM, 100 nM and 500 nM), with 3 replicates for each
829 condition. The recruitment reactions were rapidly quenched by stop buffer and incubated with
830 RNase I to generate RPFs from 48S PICs as described above. Aliquots (4.5 μl) of spike-in RPFs
831 were mixed with the experimental sample RPFs and resolved on a 5-25% sucrose gradient by
832 ultracentrifugation for 3 h at 38,000 rpm and 4°C in an SW41Ti rotor in a Beckman Coulter
833 Optima XPN80 centrifuge. Fractions 6-13 of 20 total fractions were collected from the bottom of
834 each tube, extracted using phenol:chloroform:isoamyl alcohol 25:24:1 (pH 5.2), ethanol
835 precipitated, resuspended in 10 mM Tris (pH 8.0) and stored in -80 °C.
836

837 **Sequencing library construction**

838 RecSeq sequencing library construction was conducted according to a previously
839 described protocol (McGlincy and Ingolia 2017), with modifications, using identical barcoded
840 linkers (NI-810 to NI-815), RT primer (NI-802) and PCR primers (NI-798, NI-799, NI-822 to
841 NI-824). The RNA fragments purified from 48S PIC RPFs were dephosphorylated using T4

842 Polynucleotide Kinase (PNK) (NEB; M0201L) and ligated to pre-adenylated linkers (NI-810 to
843 NI-815) containing 5 nt sample barcodes unique for each sample using truncated T4 RNA ligase
844 2 (K227Q) (NEB; M0351L). Ligated fragments were separated from free linkers on a 15%
845 polyacrylamide TBE-Urea gel and then pooled and purified for reverse transcription using RT
846 primer NI-802 and ProtoScript II Reverse Transcriptase (NEB; M0368S). The ~105 nt cDNAs
847 were separated from free RT primers on a 15% TBE-Urea gel and circularized using
848 CircLigaseII ssDNA Ligase (Biosearch Technologies; CL9021K). PCR was carried out using
849 forward primer NI-798, and reverse primers (NI-799, NI-822 to 824) as already described
850 (McGlincy and Ingolia 2017) .
851 RNA-Seq for input total mRNA was performed as previously described (Ingolia et al.
852 2009; Ingolia 2010). Briefly, total mRNA was randomly fragmented at 70°C for 8 min in
853 fragmentation reagent (Thermo Fisher; AM8740) and size-selected for 50-90 nt fragments for
854 constructing a sequencing library using Universal miRNA Cloning Linker (NEB; S1315S) and
855 the RNA-Seq library construction procedures described above. Sequencing was done on an
856 Illumina NovaSeq 6000 system at the NHLBI DNA Sequencing and Genomics Core at NIH
857 (Bethesda, MD).
858
859 **Deep sequencing data processing and downstream analysis**
860 The constant linker sequence (AGATCGGAAGAGCAC) in barcoded linkers was
861 removed from Illumina NovaSeq reads using Cutadapt 4.0, and the mixed sample sequences
862 were separated by the sample barcodes and aligned to the *S. cerevisiae* non-coding RNA genome
863 using STAR 2.7.9a (Dobin et. al, 2013) to remove non-coding RNA reads. The remaining RNA
864 reads were then mapped to the reference genome (R64-1-1 S288C Sac cer3 Genome Assembly)

865 and spike-in "genome" using STAR 2.7.9a. Reads unaligned to the yeast genome were then
866 mapped to the spike-in genome to obtain spike-in RPF counts. Similarly, reads unaligned to the
867 spike-in genome were aligned to the yeast genome for genomic mRNA RPF counts. Size factors
868 for each sample were calculated using the geometric means of the numbers of 25-34 nt reads
869 mapping to both the mAUG and the many internal AUGs of the spike-in mRNAs, *FLUC* and
870 *RLUC*. Consistent with previous reports (Vandesompele et al. 2002), it was essential to use the
871 geometric mean rather than arithmetic mean for the spike-in normalizations, presumably because
872 of the exponential nature of the PCR amplification step of library construction. All samples were
873 normalized to the sample with highest spike-in geometric mean among 9 samples (3 replicates
874 each for 0 nm, 100 nm and 500 nm Ded1). Size-factor normalized wiggle tracks for each
875 replicate or average of replicates were produced from the alignment file, one each for genes on
876 the Watson or Crick strand. The sequences for the input total mRNA were processed similarly:
877 after trimming NEB universal linker sequences and removing non-coding RNAs, the remaining
878 reads were mapped to the yeast genome. Wiggle tracks were produced by assigning reads to the
879 position of their 5'ends. Two-dimensional metagene plots were produced by aligning all
880 genomic mRNAs to their mAUGs and plotting the density of all RPFs based on foot-print
881 lengths and the positions of their 5'ends map using a custom python script
882 (https://github.com/zhoufj/Metagene_plot).
883 For counting RPFs on mRNAs, all 25-34 nt Rec-Seq reads were assigned to their predicted
884 P-site mapped on the mRNA. The reads mapped between the -3 and +6 of the mAUG were
885 counted as main RPFs (mRPFs), the reads counted between the mAUG and the stop codon of the
886 CDS were counted as CDS RPFs (cdsRPFs), and the reads from the +9 position of the mAUG to
887 the stop codon counted as internal RPFs (iRPFs). mRNA read counts were determined for all

888 codons of the main CDS. DESeq2 (Love et al. 2014) was employed for differential expression
889 analysis of changes in RPF, recruitment efficiency (RE), or relative ribosome occupancy (RRO)
890 values, and to impose cutoffs for minimum read numbers (as indicated in figure legends) and
891 remove outliers. Size-factors calculated from spike-in RPFs were applied in DESeq2 analysis as
892 customized size-factors.
893
894 **Main AUG Context scores**
895 The AUG context adaptation index (context score) (Miyasaka 1999) for all mAUGs with
896 annotated 5'UTRs > 5 nt were previously calculated (Martin-Marcos et al. 2017).
897
898 **PARS scores**
899 The PARS scores, including Total, Max30, Start30, Plus15, Plus30 and Plus45 PARS were
900 caculated as previously described (Sen et al. 2015) using the same data set (Kertesz et al. 2010).
901
902 **Recruitment efficiency (RE) calculations**
903 Reads of input RNA-Seq were counted from the main start codon to the stop codon and
904 normalized to CDS length to calculate mRNA density. The recruitment efficiencies (REs) for
905 each mRNA in each codition were calculated as the ratio between the nomalized mRPF value
906 and mRNA density.

907 ACCESSION NUMBER

908 Sequencing data from this study have been submitted to the NCBI Gene Expression Omnibus
909 (GEO; http://www.ncbi.nlm.nih.gov/geo/) under the accession number GSE244093.

**ACKNOWLEDGMENTS**

This work was supported by the Intramural Research Program of the *Eunice Kennedy Shriver* National Institute of Child Health and Human Development. We thank other members of our laboratories and those of Tom Dever and Nick Guydosh for many helpful suggestions. We thank Ryan K Dale in NICHD/NIH Bioinformatics and Scientific Programming Core and Byung-sik Shin for their helps in sequencing data processing.

918 **Figure Legend:**

919 **Figure 1. Recruitment Sequencing (Rec-Seq) allows transcriptome-wide analysis of early**
920 **steps of translation initiation in a purified system.**

921 (**A**) Overview of steps in the Rec-Seq method. 48S ribosomal pre-initiation complexes (PICs)
922 are assembled in vitro from purified *S. cerevisiae* components. 48S PICs are treated with RNase
923 I to digest unprotected mRNA and then isolated using sucrose density gradient
924 ultracentrifugation. Ribosome-protected mRNA fragments (RPFs) are used to construct a
925 sequencing library. **(B-D)** Metagene plots of RPF distributions over 150 nt windows (-50 to +100
926 nt) on all mRNAs aligned to their main AUG start codons for no Ded1 (B); 100 nM Ded1 (C), or
927 500 nM Ded1 (D). RPF lengths are shown on the Y axis and the position of the 5'ends of the
928 RPFs relative to the main start codon are shown on the X axis. A 5'end located 12 nt from the
929 start codon is expected for 48S PICs with the AUG in the P site of the 40S subunit (Wagner et al.
930 2020). The color scale shows RPF density. All reads for 3 replicates for each condition were
931 combined. **(E, F)** RPFs for the 0, 100 and 500 nM Ded1 experiments for previously identified
932 Ded1 hypo-dependent (*OST3,* E) and hyper-dependent (*HOR7,* F) mRNAs. The position of the
933 main CDS is shown in cyan and the −3 to −1 and +4 context nucleotides surrounding the main
934 AUG are shown in brick red text. mRNA sequencing reads are also shown below each set of
935 tracks (gray). The Integrated Genome Viewer (IGV, Broad Institute) was used to display RPF
936 and mRNA reads, with RPF and nucleotide (nt) scales indicated on top of each panel. For these
937 and all other gene browser views, the RPFs are plotted to their predicted P-site positions, and the
938 mRNA reads are plotted to their first position from their transcript 5'ends.

939

940 **Figure 1-S1. A schematic diagram of mRNA recruitment in translation initiation.** The cap-
941 binding protein complex eIF4F, consisting of eIF4E, eIF4G and eIF4A subunits attaches to the
942 cap at the mRNA 5' end. The 43S PIC, which includes the 40S ribosomal subunit, eIFs 1, 1A, 3
943 and 5 and the eIF2•GTP•Met-tRNA$_i$ ternary complex, binds to the 5' end of mRNA with the aid
944 of the eIF4F complex and eIF4B and scans downstream in search of the start codon. A stable
945 48S-PIC is formed when a start codon is recognized.
946
947 **Figure 1-S2. Internal spike-in normalization controls using preformed 48S PICs on non-**
948 **native mRNAs**. **(A)** Steps in applying 48S-PIC spike-in controls for data normalization. Firefly
949 and Renilla luciferase mRNAs (*FLUC* and *RLUC)* were in vitro transcribed from PCR-amplified
950 gene templates containing T7 promoters and enzymatically capped using previously described
951 protocols (Acker et al. 2007). The 48S PICs formed on the spike-in mRNAs were prepared
952 separately from the testing samples in a recruitment reaction followed by RNase I treatment to
953 digest unprotected mRNA. A constant amount of spike-in 48S PICs were resolved by
954 sedimentation through the same sucrose gradients containing the experimental samples. The
955 RPFs from these spike-in PICs served as internal controls for losses occurring during library
956 construction and allowed data normalization across experimental samples. For deep sequencing
957 data processing, non-coding RNA reads were removed and the remaining RPFs were aligned to
958 spike-in mRNA sequences for calculating sample size factors and also aligned to the yeast
959 genome to produce RPF counts on all yeast mRNAs. The RPF counts for all mRNAs in the
960 genome were applied to DESeq2 using sample size factors calculated from the geometric means
961 of spike-in mRNA RPFs mapped to *FLUC*/*RLUC* main AUGs and a number of internal AUGs.
962 Recruitment efficiency (RE) values were calculated by normalizing the size-factor corrected

963 RPFs to input mRNA densities. **(B-D)** Scatterplots of *FLUC* and *RLUC* RPF reads at the main
964 and internal AUGs, in the first two of three replicate samples for each condition. The green
965 diagonal line is for 1:1 ratio and the Spearman correlation coefficients (r) were calculated using
966 "cor.test" function in R using option "method = spearman."
967
968 **Figure 1-S3. Transcriptome-wide reproducibility of RPFs among replicates**
969 **(A-I)** Scatterplots of log2 main AUG ribosome occupancies (normalized by the geometric means
970 of RPF reads on *FLUC* and *RLUC* spike-in mRNAs) for comparing each of two of the three
971 replicates in different conditions, 0 nM Ded1 (A, D and G), 100 nM Ded1 (B, E and H) and 500
972 nM Ded1 (C, F and I) for all mRNAs with ⩾ 90 total RPF reads in the 9 samples combined.
973 Spearman correlation coefficients (r) were calculated as in Fig. 1-S2B-D.
974
975 **Figure 1-S4. RPFs on main AUGs are consistent among replicates.**
976 **(A)** Box plot analysis of normalized RPF reads for 3052 mRNAs with > 90 total reads in 9
977 samples (each of 3 replicates for 0, 100 and 500 nM Ded1). **(B-I)** 48S PIC-protected fragments
978 (RPFs) and input mRNA reads for 3 replicates of each of the 3 conditions (0, 100 and 500 nM
979 Ded1) on 8 example mRNAs across 3' portions of the 5'UTR and 5' portions of the CDS regions
980 flanking the main AUGs. RPF and nt scales are shown in the top right corner of each panel. The
981 position of the main CDS and the −3 to −1 and +4 context nucleotides surrounding the main
982 AUG are labeled as in Fig. 1E-F. mRNAs shown are (B) *NPT1*; (C) *PMA1*; (D) *SFT2*; (E) *ICE2*;
983 (F) *AIM41*; (G) *RCP10*; (H) *RPL41A;* and (I) *RPL16A*.
984
985 **Figure 2. Ded1 promotes the recruitment of a group of 1000 mRNAs.**

986 **(A-C)** Scatterplots of normalized read densities on the main start codons of mRNAs (mRPF,
987 number of RPFs mapping to the main AUG normalized by the geometric means of the spike-in
988 internal control RPFs) for 3052 mRNAs with > 90 total reads in 9 samples (3 replicates each for
989 0, 100 and 500 nM Ded1) for 100 versus 0 nM Ded1 (A), 500 versus 0 nM Ded1 (B), or 500
990 versus 100 nM Ded1 (C). mRNAs with significantly changed recruitment were defined as those
991 with false discovery rates (FDR) < 0.05 and RPF changes (ΔRPF) of > 2 for increased or < 0.5
992 for decreased are indicated in red or dark blue, respectively. The number of significantly changed
993 mRNAs are indicated in red (increased) and blue (decreased). (**D and E**) Overlaps between the
994 mRNAs displaying significantly increased (D) or significantly reduced (E) mRPFs between 100
995 and 500 nM Ded1 conditions. P-values for the overlap between each group were calculated using
996 an online tool (http://nemates.org/MA/progs/overlap_stats.html). **(F)** Box plot analysis of the
997 distribution and median of log2 change in mRPF between 0 and 100 nM Ded1 ($\Delta mRPF_{100/0\ nM\ Ded1}$,
998 orange) or 0 and 500 nM Ded1 ($\Delta mRPF_{500/0\ nM\ Ded1}$, cyan) for all 3052 mRNAs (cols. 1-2),
999 and for the following 6 groups of mRNAs: 1006 or 911 for which mRPFs were significantly up
1000 in 500 or 100 nM Ded1, respectively, relative to no Ded1 (cols. 3-6, for red dots in B and A);
1001 793 mRNAs for which mRPFs were significantly up with both 100 and 500 nM Ded1 (cols. 7-8,
1002 for the overlapping mRNAs in D); 182 and 71 mRNAs for which mRPFs were significantly
1003 down in 500 or 100 nM Ded1 relative to no Ded1 (cols. 9-12, blue dots in B and A); and 48
1004 mRNAs for which mRPFs were significantly down with both 100 and 500 nM Ded1 (cols.13-14,
1005 for the overlaps in E). The blue horizontal line shows no change in mRPFs (ΔmRPF = 1). **(G)**
1006 Heat-map analysis of the recruitment efficiency changes $\Delta RE_{100/0\ nM\ Ded1}$, $\Delta RE_{500/0\ nM\ Ded1}$ and
1007 $\Delta RE_{500/100\ nM\ Ded1}$ for the 3052 mRNAs described in A-C, ordered by rank of $\Delta RE_{100/0\ nM\ Ded1}$
1008 from most increased (top) to most decreased (bottom) using the R heatmap.2 function. (**H**) The

1009 distributions of all observed mRNAs across 10 bins of increasing RE values at each
1010 concentration of Ded1 (0, 100, 500 nM). **(I)** Boxplot analysis of $\Delta RE_{500/0\ nM\ Ded1}$ for all 3052
1011 observed mRNAs binned by RE in the absence of Ded1 ($RE_{-Ded1}$) from the lowest to the highest.
1012
1013 **Figure 3. Ded1 promotes the recruitment of mRNAs with long or structured 5'UTRs.**
1014 **(A)** Line plot analysis of average recruitment efficiency (RE) for the 2804 mRNAs observed in
1015 the RecSeq experiments that have annotated 5'UTRs binned by 5'UTR length at 0, 100 and 500
1016 nM Ded1. Average RE values were determined from the RE values of all mRNAs in each bin.
1017 **(B-D)** Box plot analyses of the recruitment efficiency changes (ΔRE) between each of two
1018 different conditions for the same mRNA bins as in (A) for $\Delta RE_{100/0nM_Ded1}$ (B), $\Delta RE_{500/0nM_Ded1}$
1019 (C), or $\Delta RE_{500/100nM_Ded1}$ (D). **(E)** Line plot analysis of average RE values for the 1874 mRNAs
1020 observed in the RecSeq experiments with reported PARS scores binned according to Max30
1021 PARS scores from the lowest to highest. PARS scores were determined by Kertesz et al. (2010)
1022 and Max30 and other PARS score intervals were calculated as described in Sen et al. (2015). **(F-**
1023 **H)** Box plot analyses for the same mRNA bins as in (E) for $\Delta RE_{100/0nM_Ded1}$ (F), $\Delta RE_{500/0nM_Ded1}$
1024 (G), or $\Delta RE_{500/100nM_Ded1}$ (H). **(I)** Line plot analysis of average REs for all 3052 mRNAs divided
1025 into six equal-sized bins according to CDS lengths from the shortest to the longest for 0, 100 and
1026 500 nM Ded1. **(J-L)** Box plot analysis for the same mRNA bins as in (I) for $\Delta RE_{100/0nM_Ded1}$ (J),
1027 $\Delta RE_{500/0nM_Ded1}$ (K), or $\Delta RE_{500/100nM_Ded1}$ (L). All bins contain an equal number of mRNAs.
1028
1029 **Figure 3-S1. Ded1 preferentially stimulates 48S PIC formation on structured mRNAs. (A,**
1030 **B)** Line plot analysis of log2 average REs at 0, 100 and 500 nM Ded1for mRNAs binned
1031 according to total PARS scores (A) or the sum of PARS scores of the 30 nucleotides surrounding

1032 the start codon (for mRNAs with a 5'UTR of ⩾15 nt) (Start30 PARS, B). **(C, D)** Line plot
1033 analysis of log2 average ΔREs for 100/0 nM, 500/0 nM and 500/100 nM Ded1 for the 2035
1034 mRNAs observed in RecSeq that have annotated PARS scores binned according to Total PARS
1035 (C) or Start30 PARS (D) scores from the lowest to highest. **(E-F)** Box plots comparing 5'UTR
1036 or CDS lengths for the 4694 yeast mRNAs that have annotated 5'UTRs (Pelechano et al. 2013)
1037 for CDS lengths plotted for mRNAs binned by 5'UTR length from the shortest to the longest (E),
1038 or 5'UTR lengths plotted for mRNAs binned by CDS lengths from shortest to longest (F). All
1039 bins contain equal numbers of mRNAs.
1040
1041 **Figure 3-S2. Ded1 has little effect on discriminating main AUG context scores. (A)** Line plot
1042 analysis of average REs for the 2768 observed in RecSeq that have annotated 5'UTR lengths >5
1043 nt, divided into six equal-sized bins according to context scores from lowest to the highest at 0,
1044 100 and 500 nM Ded1. **(B-C)** Box-plot analyses of $\Delta RE_{100/0nM\ Ded1}$ (B) and $\Delta RE_{500/0nM\ Ded1}$ (C)
1045 values for the same mRNA bins as in (A).
1046
1047 **Figure 4. Ded1 dependencies observed in Rec-Seq experiments correlate strongly with in**
1048 **vivo results from previous ribosome profiling of the *ded1-cs* mutant.**
1049 **(A-B)** Scatterplots comparing Rec-Seq input RNA reads and ribosome profiling mRNA reads of
1050 WT (A) or *ded1-cs* (B) strains. (**C**) Scatterplot comparing ribosome profiling mRNA reads
1051 between WT and *ded1-cs* strains. **(D-F)** Scatterplots comparing 48S PIC RPFs from Rec-Seq to
1052 80S RPFs from ribosome profiling for the 3035 mRNAs that passed the significance cutoffs in
1053 both experiments for Rec-Seq at 0 nM Ded1 versus ribosome profiling of the *ded1-cs* mutant (D)
1054 or Rec-Seq at 100 nM (E) or 500 nM (F) Ded1 versus ribosome profiling of the WT strain. **(G-**

1055 **H)** Scatterplots comparing changes in translational efficiency (ΔTE) from ribosome profiling of
1056 the *ded1-cs* mutant versus WT to $\Delta RE_{0/100nM_Ded1}$ (G) or $\Delta RE_{0/500nM\ Ded1}$ (H) values from Rec-Seq.
1057 **(I-K)** Boxplot analysis of 5'UTR lengths (I), Max30 PARS (J), or Total PARS (K) for mRNAs
1058 with annotated 5'UTR lengths or PARS scores that showed significantly decreased (Down) or
1059 increased (Up) REs in 100 nM or 500 nM Ded1 versus no Ded1, or significantly increased (Up)
1060 or decreased (Down) TEs in the *ded1-cs* mutant versus WT. **(L-M)** Overlaps between mRNAs
1061 identified by Rec-Seq at 100 nM Ded1 (L) or 500 nM Ded1 (M) with significantly increased REs
1062 versus no Ded1 in Rec-Seq and mRNAs with significantly increased TEs in ribosome profiling
1063 of the *ded1-cs* mutant versus WT. P-values for the overlaps were calculated as described in Fig.
1064 2D-E**.** Group X and Y mRNAs in (L) are those in common between the two groups being
1065 compared (X) or those found exclusively in the set of 1002 mRNAs with significantly increased
1066 RE in 500 nM Ded1 versus no Ded1 in Rec-Seq (Y). **(N-O)** Boxplot analysis of log2
1067 $\Delta RE_{500/0nM_Ded1}$ (N) or log2 $\Delta TE_{ded1\text{-}ts\text{-}}$ (O) values for all 3035 mRNAs observed in both Rec-Seq
1068 and ribosome profiling, the 1002 mRNAs with significantly increased recruitment with 500 nM
1069 Ded1 versus no Ded1 (of L), the 319 mRNAs in group X (of L), and the 683 mRNAs in group Y
1070 (of L).
1071
1072 **Figure 5. Ded1 increases leaky scanning of main start codons**
1073 (**A**) The ratio of the total RPFs internal to the CDS in mRNAs, excluding the main start codon, to
1074 the total RPFs for the full CDS including the main start codon (iRPF/cdsRPF ratio) for each of
1075 the three replicates at 0, 100 and 500 nM Ded1. iRPFs were counted from the +9 position of the
1076 main AUG to the stop codon, while the cdsRPFs were counted from the start codon to the stop
1077 codon of the CDS. The average of the three replicates is indicated by the colored bars (red,

1078 green and blue for 0, 100 and 500 nM Ded1, respectively). **(B-D)** Metagene plots showing RPF
1079 density distribution on all mRNAs aligned to their main AUGs as in Fig. 1B-D for 0 (B), 100 (C)
1080 and 500 nM Ded1 (D), with color scales adjusted to show internal RPFs (iRPFs). **(E-H)** 48S PIC
1081 RPFs and input mRNA reads on four selected mRNAs that showed elevated internal ribosome
1082 occupancies in 100 and 500 nM Ded1 conditions. The -3 to -1 and +4 context nucleotides
1083 surrounding the main AUG, iAUG or upstream AUG (uAUG) are indicated in brick red text. **(I-**
1084 **J)** Scatterplots comparing log2 iRPF between 100 (I) or 500 nM Ded1 (J) to 0 nM Ded1 as
1085 described in Fig. 2A-B for the same group of 3052 mRNAs. Red dots show mRNAs that meet
1086 the significance cutoff for increases in iRPF (FDR < 0.05, >2-fold increase in iRPFs) and blue
1087 dots show mRNAs that meet the significance cutoff for decreases in iRPF (FDR < 0.05, <0.5-
1088 fold decrease in iRPFs). **(K)** Box plot comparing mRPFs and iRPFs between 500 and 0 nM
1089 Ded1 for the 182 mRNAs that showed significantly reduced mRPFs with 500 nM Ded1 versus
1090 no Ded1. **(L)** Overlaps between mRNAs with significantly elevated iRPFs (orange), significantly
1091 reduced mRPFs (green) or significantly increased mRPFs (blue) with 500 nM Ded1 relative to 0
1092 nM Ded1. The Venn diagram was generated and p-values calculated as in Fig. 2D. **(M)** Scatter
1093 plot comparing mRPFs with 500 nM versus 0 nM Ded1. The 125 mRNAs that showed
1094 significantly increased iRPFs and significantly decreased mRPFs in 500 nM Ded1 relative to 0
1095 nM Ded1 are labeled by black dots. Among this set, the mRNAs for which the iRPFs increase by
1096 at least 50% of the decrease in mRPFs are labeled by yellow circles, to indicate the 84 mRNAs
1097 for which the decrease in mRPFs could be responsible for the increase in iRPFs. **(N)** Boxplot
1098 comparing mRPFs and iRPFs between 500 nM and 0 nM Ded1 for the 1006 mRNAs that
1099 showed significantly increased mRPFs. **(O)** Line plot analysis of average RRO (relative
1100 ribosome occupancy; iRPF/cdsRPF ratio; left axis) and $\Delta RRO_{500/0\ nM\ Ded1}$ (right axis) for 2441 of

1101 3052 mRNAs in J with 5'UTR length >5 nt binned by main AUG context scores from lowest to
1102 highest. **(P)** Boxplot analysis of Start30, Plus15, Plus30 and Plus45 PARS scores for mRNAs
1103 with $RRO_{iRPF/cdsRPF} < 0.5$ (orange) or $\geqslant 0.5$ with 500 nM Ded1.

1104

1105 **Figure 5-S1. Supporting evidence that Ded1 promotes leaky scanning of the main start**
1106 **codon. (A)** Schematic of a 43S PIC leaky scanning through the main AUG and assembling at an
1107 internal AUG in the presence of Ded1. **(B)** Evidence that mRNAs whose recruitment is inhibited
1108 by 500 nM Ded1 in Rec-Seq assays generally assemble 48S PICs very efficiently without Ded1**.**
1109 Boxplot analysis of REs of groups of mRNAs at 0 nM (cyan) or 500 nM (yellow) Ded1 for all
1110 3052 mRNAs observed in Rec-Seq, the 1006 mRNAs with significantly increased mRPFs at 500
1111 nM Ded1 versus no Ded1 (Fig. 2B, red dots); and the 182 mRNAs with significantly decreased
1112 mRPFs with 500 nM Ded1 versus no Ded1 (Fig. 2B, blue dots).

1113

1114 **Figure 5-S2. mRNAs with reduced RE at 500 nM Ded1 versus no Ded1 in Rec-Seq assays**
1115 **tend to show increased relative TE in the *ded1-cs* mutant versus WT in ribosome profiling**
1116 **experiments.** Boxplot analysis of $\Delta TE_{ded1\text{-}cs}$ for the groups of mRNAs described in Figure 5L-M:
1117 The 182 mRNAs with mRPFs significantly reduced at 500 nM Ded1 versus no Ded1 (cyan); the
1118 125 mRNAs with significantly decreased mRPFs and increased iRPFs with 500 nM Ded1 versus
1119 no Ded1 (magenta); the 84 mRNAs from the previous set that had an increase in iRPFs that was
1120 at least 50% the of the decrease in mRPFs (yellow circles in Fig. 5M; orange).

1121

1122 **Figure 6. Ded1 modestly promotes readthrough of start codons in 5' UTRs of mRNAs.**

1123 **(A)** The ratios of RPFs in 5'UTRs to RPFs on main start codons (uRPF/mRPF ratios) for each of
1124 the three replicates with 0 (blue), 100 (magenta) or 500 (green) nM Ded1. The 5'UTR RPFs
1125 (uRPFs) were counted from the 5'end of the mRNA to the -5 position relative to the main AUG.
1126 The mean of the three replicates is indicated by the colored bars. uRPFs on *GCN4* mRNA were
1127 analyzed separately (Fig. 6-S1), because 42% and 57% of all uRPFs were mapped to the *GCN4*
1128 5'UTR in assays with 100 and 500 nM Ded1, respectively. **(B-C)** Scatterplots comparing uRPFs
1129 in the presence of either 100 nM (B) or 500 nM (C) Ded1 versus 0 nM Ded1. mRNAs with
1130 significantly increased or decreased uRPFs in the presence of Ded1 are indicated in red or dark
1131 blue dots, respectively. The criteria used for significance were FDR < 0.05 and a greater than 2-
1132 fold increase or decrease. Yellow circles denote the very few mRNAs whose uRPF read number
1133 decreases by more than 50% of the increases in their mRPF reads, indicating a clear reciprocal
1134 relationship between the decrease in uRPFs and the increase in mRPFs. (**D**) Box plot analysis of
1135 mRPF and uRPF read numbers for the 257 mRNAs that had both uRPFs and mRPFs ⩾ 2 reads
1136 averaged over all assays conducted at 0, 100 and 500 nM Ded1 concentrations. Unlogged median
1137 RPF numbers are labeled under each box.
1138
1139 **Figure 6-S1. Approximately half of all uRPFs map to the *GCN4* 5'UTR.** Percentages of all
1140 uRPFs mapped to the *GCN4* 5'UTR for each of the three replicates with 0 (blue), 100 (magenta),
1141 or 500 (green) nM Ded1 concentrations. Colored bars indicate the means of the replicates.
1142
1143 **Figure 7. eIF4A enhances the recruitment of almost all mRNAs**
1144 **(A)** Scatterplots of normalized read densities mapped to main AUGs (mRPFs) with 5000 nM
1145 versus 500 nM eIF4A for the 2809 mRNAs with ⩾ 8 total reads in 4 samples (2 replicates each

1146 for 5000 and 500 nM eIF4A). Red and blue dots show mRNAs with mRPFs significantly
1147 increased or decreased, respectively, at 5000 versus 500 nM eIF4A. The criteria for significance
1148 were FDR < 0.05 and a > 2-fold change in RPFs. **(B)** Boxplot comparing $\Delta RE_{5000/500\ nM\ eIF4A}$
1149 (grey) to $\Delta RE_{100/0\ nM\ Ded1}$ and $\Delta RE_{500/0\ nM\ Ded1}$ (cyan) for the 2698 mRNAs that passed the cutoff
1150 mentioned in (A) in both experiments. **(C)** Boxplot of $\Delta RE_{5000/500\ nM\ eIF4A}$ for the 2538 of all 2809
1151 mRNAs in (A) that have annotated 5'UTRs, divided into six equal sized bins according to
1152 5'UTR lengths from the shortest to the longest. (**D)** Similar to (C), but for the 1708 of all 2809
1153 mRNAs in (A) with annotated PARS scores, binned by Max30 PARS from lowest to highest. **(E-**
1154 **G)** Line plots of mean $\log_2$ RE changes, $\Delta RE_{5000/500\ nM\ eIF4A}$ (green), $\Delta RE_{100/0\ nM\ Ded1}$ (magenta),
1155 and $\Delta RE_{500/0\ nM\ Ded1}$ (blue), for mRNAs divided into six equal sized bins according to the specific
1156 mRNA features of 5'UTR length (E), Max30 PARS score (F), or Total PARS score (G). **(H-K)**
1157 RPFs assembled with 500 or 5000 nM eIF4A and input mRNA reads for mRNAs shown
1158 previously to be hypo-dependent on Ded1 (*RPC10*, *RPL41A*, *HOR7*) or hyper-dependent on
1159 Ded1(*PMA1*) by in vivo ribosome profiling experiments in the *ded1-cs* mutant.
1160
1161

1162 REFERENCES


1163 Acker MG, Kolitz SE, Mitchell SF, Nanda JS, Lorsch JR. 2007. Reconstitution of yeast
1164 translation initiation. Methods Enzymol 430: 111-145.
1165 Archer SK, Shirokikh NE, Beilharz TH, Preiss T. 2016. Dynamics of ribosome scanning and
1166 recycling revealed by translation complex profiling. Nature 535: 570-574.
1167 Arribere JA, Gilbert WV. 2013. Roles for transcript leaders in translation and mRNA decay
1168 revealed by transcript leader sequencing. Genome Res 23: 977-987.
1169 Beckham C, Hilliker A, Cziko AM, Noueiry A, Ramaswami M, Parker R. 2008. The DEAD-box
1170 RNA helicase Ded1p affects and accumulates in Saccharomyces cerevisiae P-bodies. Mol
1171 Biol Cell 19: 984-993.
1172 Berthelot K, Muldoon M, Rajkowitsch L, Hughes J, McCarthy JE. 2004. Dynamics and
1173 processivity of 40S ribosome scanning on mRNA in yeast. Mol Microbiol 51: 987-1001.
1174 Bresson S, Shchepachev V, Spanos C, Turowski TW, Rappsilber J, Tollervey D. 2020. Stress-
1175 Induced Translation Inhibition through Rapid Displacement of Scanning Initiation
1176 Factors. Mol Cell 80: 470-484.e478.
1177 Castelli LM, Lui J, Campbell SG, Rowe W, Zeef LA, Holmes LE, Hoyle NP, Bone J, Selley JN,
1178 Sims PF et al. 2011. Glucose depletion inhibits translation initiation via eIF4A loss and
1179 subsequent 48S preinitiation complex accumulation, while the pentose phosphate
1180 pathway is coordinately up-regulated. Mol Biol Cell 22: 3379-3393.
1181 Gao Z, Putnam AA, Bowers HA, Guenther UP, Ye X, Kindsfather A, Hilliker AK, Jankowsky E.
1182 2016. Coupling between the DEAD-box RNA helicases Ded1p and eIF4A. Elife 5.
1183 Guenther UP, Weinberg DE, Zubradt MM, Tedeschi FA, Stawicki BN, Zagore LL, Brar GA,
1184 Licatalosi DD, Bartel DP, Weissman JS et al. 2018. The helicase Ded1p controls use of
1185 near-cognate translation initiation codons in 5' UTRs. Nature 559: 130-134.
1186 Gulay S, Gupta N, Lorsch JR, Hinnebusch AG. 2020. Distinct interactions of eIF4A and eIF4E
1187 with RNA helicase Ded1 stimulate translation in vivo. Elife 9.
1188 Gupta N, Lorsch JR, Hinnebusch AG. 2018. Yeast Ded1 promotes 48S translation pre-initiation
1189 complex assembly in an mRNA-specific and eIF4F-dependent manner. Elife 7.
1190 Hilliker A, Gao Z, Jankowsky E, Parker R. 2011. The DEAD-box protein Ded1 modulates
1191 translation by the formation and resolution of an eIF4F-mRNA complex. Mol Cell 43:
1192 962-972.
1193 Hinnebusch AG. 2014. The scanning mechanism of eukaryotic translation initiation. Annu Rev
1194 Biochem 83: 779-812.
1195 Hondele M, Sachdev R, Heinrich S, Wang J, Vallotton P, Fontoura BMA, Weis K. 2019.
1196 DEAD-box ATPases are global regulators of phase-separated organelles. Nature 573:
1197 144-148.
1198 Ingolia NT, Ghaemmaghami S, Newman JR, Weissman JS. 2009. Genome-wide analysis in vivo
1199 of translation with nucleotide resolution using ribosome profiling. Science 324: 218-223.
1200 Iserman C, Desroches Altamirano C, Jegers C, Friedrich U, Zarin T, Fritsch AW, Mittasch M,
1201 Domingues A, Hersemann L, Jahnel M et al. 2020. Condensation of Ded1p Promotes a
1202 Translational Switch from Housekeeping to Stress Protein Production. Cell 181: 818-
1203 831.e819.
1204 Izidoro MS, Sokabe M, Villa N, Merrick WC, Fraser CS. 2022. Human eukaryotic initiation
1205 factor 4E (eIF4E) and the nucleotide-bound state of eIF4A regulate eIF4F binding to
1206 RNA. J Biol Chem 298: 102368.

1207 Kertesz M, Wan Y, Mazor E, Rinn JL, Nutter RC, Chang HY, Segal E. 2010. Genome-wide
1208 measurement of RNA secondary structure in yeast. Nature 467: 103-107.
1209 Kozak M. 1990. Downstream secondary structure facilitates recognition of initiator codons by
1210 eukaryotic ribosomes. Proc Natl Acad Sci U S A 87: 8301-8305.
1211 Kumar P, Hellen CU, Pestova TV. 2016. Toward the mechanism of eIF4F-mediated ribosomal
1212 attachment to mammalian capped mRNAs. Genes Dev 30: 1573-1588.
1213 Linder P, Jankowsky E. 2011. From unwinding to clamping - the DEAD box RNA helicase
1214 family. Nat Rev Mol Cell Biol 12: 505-516.
1215 Love MI, Huber W, Anders S. 2014. Moderated estimation of fold change and dispersion for
1216 RNA-seq data with DESeq2. Genome Biol 15: 550.
1217 Lu Z, Lin Z. 2019. Pervasive and dynamic transcription initiation in Saccharomyces cerevisiae.
1218 Genome Res 29: 1198-1210.
1219 Martin-Marcos P, Zhou F, Karunasiri C, Zhang F, Dong J, Nanda J, Kulkarni SD, Sen ND,
1220 Tamame M, Zeschnigk M et al. 2017. eIF1A residues implicated in cancer stabilize
1221 translation preinitiation complexes and favor suboptimal initiation sites in yeast. Elife 6.
1222 McGlincy NJ, Ingolia NT. 2017. Transcriptome-wide measurement of translation by ribosome
1223 profiling. Methods 126: 112-129.
1224 Mitchell SF, Walker SE, Algire MA, Park EH, Hinnebusch AG, Lorsch JR. 2010. The 5'-7-
1225 methylguanosine cap on eukaryotic mRNAs serves both to stimulate canonical translation
1226 initiation and to block an alternative pathway. Mol Cell 39: 950-962.
1227 Miyasaka H. 1999. The positive relationship between codon usage bias and translation initiation
1228 AUG context in Saccharomyces cerevisiae. Yeast 15: 633-637.
1229 Mugler CF, Hondele M, Heinrich S, Sachdev R, Vallotton P, Koek AY, Chan LY, Weis K. 2016.
1230 ATPase activity of the DEAD-box protein Dhh1 controls processing body formation.
1231 Elife 5.
1232 Munoz AM, Yourik P, Rajagopal V, Nanda JS, Lorsch JR, Walker SE. 2017. Active yeast
1233 ribosome preparation using monolithic anion exchange chromatography. RNA Biol 14:
1234 188-196.
1235 Niederer RO, Rojas-Duran MF, Zinshteyn B, Gilbert WV. 2022. Direct analysis of ribosome
1236 targeting illuminates thousand-fold regulation of translation initiation. Cell Systems 13:
1237 256-264.e253.
1238 Pelechano V, Wei W, Steinmetz LM. 2013. Extensive transcriptional heterogeneity revealed by
1239 isoform profiling. Nature 497: 127-131.
1240 Pestova TV, Kolupaeva VG. 2002. The roles of individual eukaryotic translation initiation
1241 factors in ribosomal scanning and initiation codon selection. Genes Dev 16: 2906-2922.
1242 Rajagopal V, Park EH, Hinnebusch AG, Lorsch JR. 2012. Specific domains in yeast translation
1243 initiation factor eIF4G strongly bias RNA unwinding activity of the eIF4F complex
1244 toward duplexes with 5'-overhangs. J Biol Chem 287: 20301-20312.
1245 Rogers GW, Jr., Richter NJ, Merrick WC. 1999. Biochemical and kinetic characterization of the
1246 RNA helicase activity of eukaryotic initiation factor 4A. J Biol Chem 274: 12236-12244.
1247 Schäfer T, Strauss D, Petfalski E, Tollervey D, Hurt E. 2003. The path from nucleolar 90S to
1248 cytoplasmic 40S pre-ribosomes. Embo j 22: 1370-1380.
1249 Sen ND, Gupta N, S KA, Preiss T, Lorsch JR, Hinnebusch AG. 2019. Functional interplay
1250 between DEAD-box RNA helicases Ded1 and Dbp1 in preinitiation complex attachment
1251 and scanning on structured mRNAs in vivo. Nucleic Acids Res 47: 8785-8806.

1252 Sen ND, Zhang H, Hinnebusch AG. 2021. Down-Regulation of Yeast Helicase Ded1 by Glucose
1253 Starvation or Heat-Shock Differentially Impairs Translation of Ded1-Dependent mRNAs.
1254 Microorganisms 9.
1255 Sen ND, Zhou F, Ingolia NT, Hinnebusch AG. 2015. Genome-wide analysis of translational
1256 efficiency reveals distinct but overlapping functions of yeast DEAD-box RNA helicases
1257 Ded1 and eIF4A. Genome Res 25: 1196-1205.
1258 Senissar M, Le Saux A, Belgareh-Touze N, Adam C, Banroques J, Tanner NK. 2014. The
1259 DEAD-box helicase Ded1 from yeast is an mRNP cap-associated protein that shuttles
1260 between the cytoplasm and nucleus. Nucleic Acids Res 42: 10005-10022.
1261 Sokabe M, Fraser CS. 2017. A helicase-independent activity of eIF4A in promoting mRNA
1262 recruitment to the human ribosome. Proc Natl Acad Sci U S A 114: 6304-6309.
1263 Sonenberg N, Hinnebusch AG. 2009. Regulation of Translation Initiation in Eukaryotes:
1264 Mechanisms and Biological Targets. Cell 136: 731-745.
1265 Vandesompele J, De Preter K, Pattyn F, Poppe B, Van Roy N, De Paepe A, Speleman F. 2002.
1266 Accurate normalization of real-time quantitative RT-PCR data by geometric averaging of
1267 multiple internal control genes. Genome Biol 3: Research0034.
1268 Wagner S, Herrmannová A, Hronová V, Gunišová S, Sen ND, Hannan RD, Hinnebusch AG,
1269 Shirokikh NE, Preiss T, Valášek LS. 2020. Selective Translation Complex Profiling
1270 Reveals Staged Initiation and Co-translational Assembly of Initiation Factor Complexes.
1271 Mol Cell 79: 546-560.e547.
1272 Walker SE, Fredrick K. 2008. Preparation and evaluation of acylated tRNAs. Methods 44: 81-86.
1273 Winzeler EA, Shoemaker DD, Astromoff A, Liang H, Anderson K, Andre B, Bangham R,
1274 Benito R, Boeke JD, Bussey H et al. 1999. Functional characterization of the S.
1275 cerevisiae genome by gene deletion and parallel analysis. Science 285: 901-906.
1276 Yang Q, Del Campo M, Lambowitz AM, Jankowsky E. 2007. DEAD-box proteins unwind
1277 duplexes by local strand separation. Mol Cell 28: 253-263.
1278 Yourik P, Aitken CE, Zhou F, Gupta N, Hinnebusch AG, Lorsch JR. 2017. Yeast eIF4A
1279 enhances recruitment of mRNAs regardless of their structural complexity. Elife 6.
1280 Zhou F, Zhang H, Kulkarni SD, Lorsch JR, Hinnebusch AG. 2020. eIF1 discriminates against
1281 suboptimal initiation sites to prevent excessive uORF translation genome-wide. Rna 26:
1282 419-438.
1283 Zur H, Tuller T. 2013. New universal rules of eukaryotic translation initiation fidelity. PLoS
1284 Comput Biol 9: e1003136.
1285

1286

1287

1288 Table S1: Oligonucleotides used for Spike-in mRNA template amplification

| **Primer name** | **Sequence (5' – 3')** |
|---|---|
| T7-FLUC | AAGGAATTCATCTTAACTTT**TAATACGACTCACTATAG**GGCAAAC AAACAAACCAAAACCAAAACCACA***ATG***GAAGACGCCAAAAACATA |
| T7-RLUC | AAGGAATTCATCTTAACTTT**TAATACGACTCACTATAG**GGCAAAC AAACAAACCAAAACCAAAACCACC***ATG***ACTTGCAAAGTTTATGAT |
| FLUC-R | GTCGACGAGGAATTCATTATCAGTGC |
| RLUC-R | GTCGACTTCTCCTTCTTCAGATTTGATC |

1289 Note: T7 promoter sequences are in boldface and underlined; mAUGs are in boldface and italicized

1290

1291

1292

1293

# Figure 1

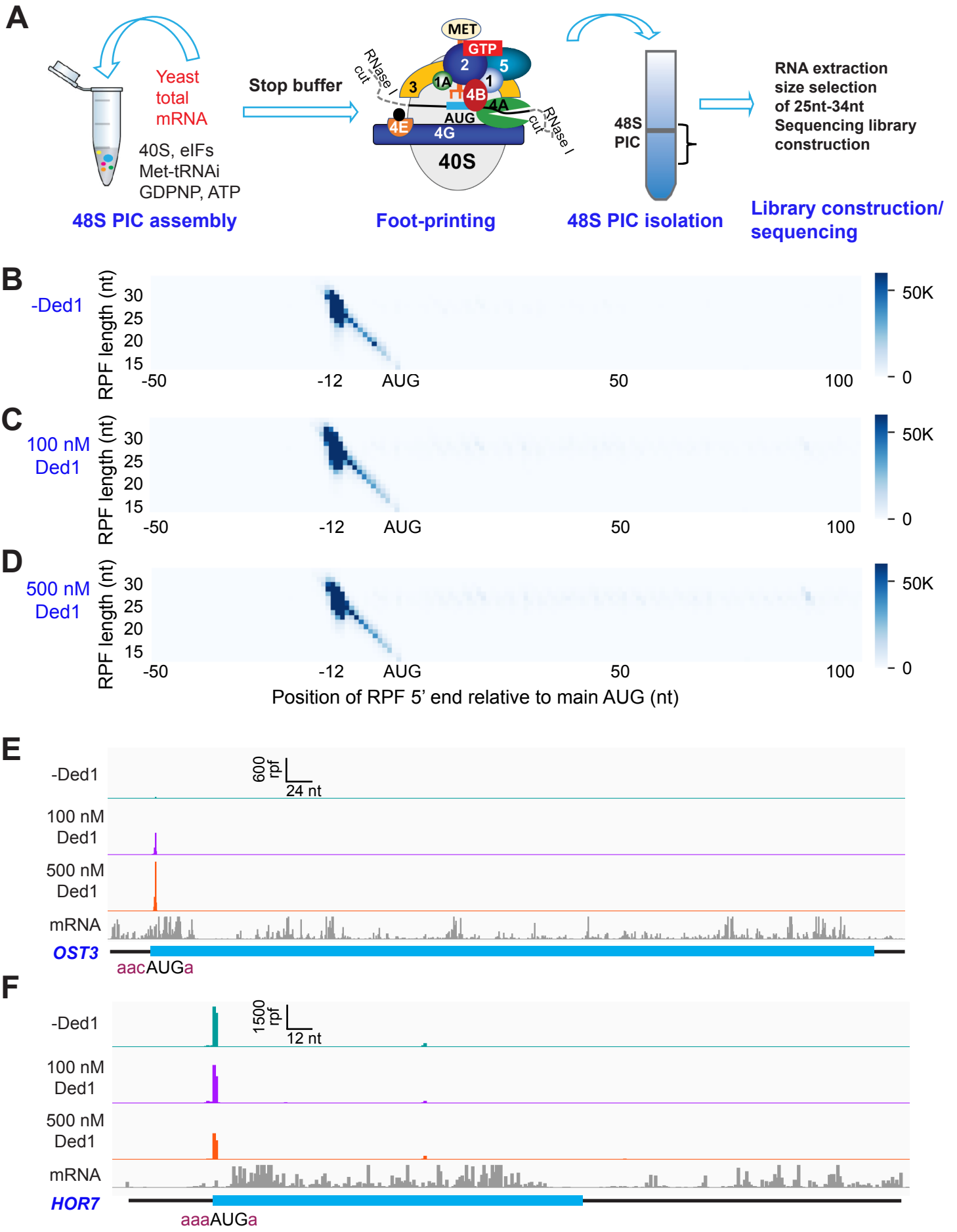
A
Yeast total mRNA
40S, eIFs
Met-tRNAi
GDPNP, ATP
48S PIC assembly
Stop buffer
MET
GTP
2
5
3
1A
1
4B
4A
AUG
4E
4G
40S
RNase I cut
RNase I cut
Foot-printing
48S PIC
48S PIC isolation
RNA extraction
size selection
of 25nt-34nt
Sequencing library
construction
Library construction/ sequencing
B
-Ded1
C
100 nM Ded1
D
500 nM Ded1
RPF length (nt)
30
25
20
15
-50
-12
AUG
50
100
50K
0
Position of RPF 5' end relative to main AUG (nt)
E
-Ded1
600 rpf
24 nt
100 nM Ded1
500 nM Ded1
mRNA
OST3
aacAUGa
F
-Ded1
1500 rpf
12 nt
100 nM Ded1
500 nM Ded1
mRNA
HOR7
aaaAUGa

**Figure 1. Recruitment Sequencing (Rec-Seq) allows transcriptome-wide analysis of early steps of translation initiation in a purified system.**

**(A)** Overview of steps in the Rec-Seq method. 48S ribosomal pre-initiation complexes (PICs) are assembled in vitro from purified *S. cerevisiae* components. 48S PICs are treated with RNase I to digest unprotected mRNA and then isolated using sucrose density gradient ultracentrifugation. Ribosome-protected mRNA fragments (RPFs) are used to construct a sequencing library. **(B-D)** Metagene plots of RPF distributions over 150 nt windows (-50 to +100 nt) on all mRNAs aligned to their main AUG start codons for no Ded1 (B); 100 nM Ded1 (C), or 500 nM Ded1 (D). RPF lengths are shown on the Y axis and the position of the 5'ends of the RPFs relative to the main start codon are shown on the X axis. A 5'end located 12 nt from the start codon is expected for 48S PICs with the AUG in the P site of the 40S subunit (Wagner et al. 2020). The color scale shows RPF density. All reads for 3 replicates for each condition were combined. **(E, F)** RPFs for the 0, 100 and 500 nM Ded1 experiments for previously identified Ded1 hypo-dependent (*OST3,* E) and hyper-dependent (*HOR7,* F) mRNAs. The position of the main CDS is shown in cyan and the −3 to −1 and +4 context nucleotides surrounding the main AUG are shown in brick red text. mRNA sequencing reads are also shown below each set of tracks (gray). The Integrated Genome Viewer (IGV, Broad Institute) was used to display RPF and mRNA reads, with RPF and nucleotide (nt) scales indicated on top of each panel. For these and all other gene browser views, the RPFs are plotted to their predicted P-site positions, and the mRNA reads are plotted to their first position from their transcript 5'ends.

# Figure 2

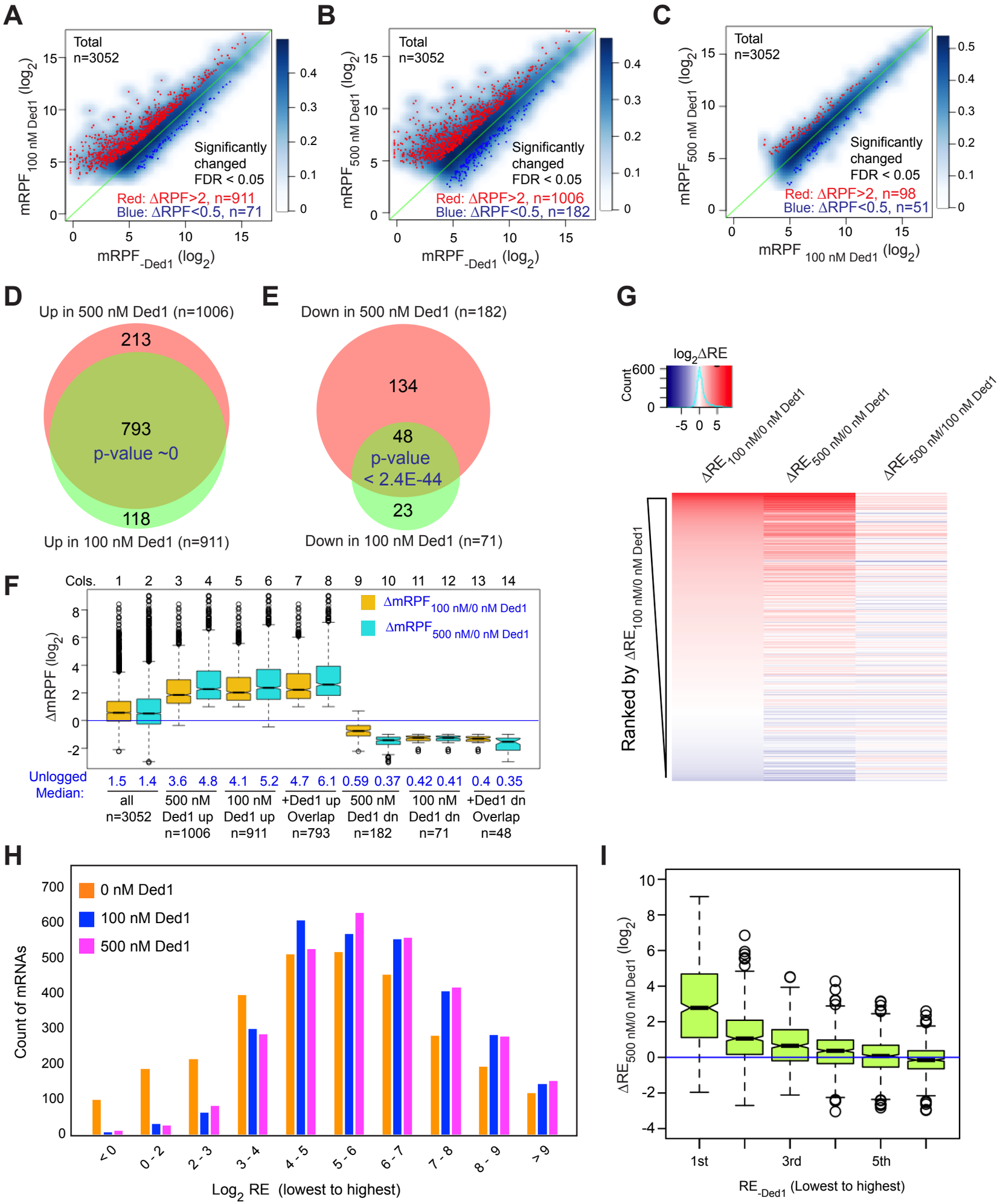
A
Total
n=3052
Significantly changed FDR < 0.05
Red: ΔRPF>2, n=911
Blue: ΔRPF<0.5, n=71
mRPF 100 nM Ded1 (log2)
mRPF -Ded1 (log2)
B
Total
n=3052
Significantly changed FDR < 0.05
Red: ΔRPF>2, n=1006
Blue: ΔRPF<0.5, n=182
mRPF 500 nM Ded1 (log2)
mRPF -Ded1 (log2)
C
Total
n=3052
Significantly changed FDR < 0.05
Red: ΔRPF>2, n=98
Blue: ΔRPF<0.5, n=51
mRPF 500 nM Ded1 (log2)
mRPF 100 nM Ded1 (log2)
D
Up in 500 nM Ded1 (n=1006)
213
793
p-value ~0
118
Up in 100 nM Ded1 (n=911)
E
Down in 500 nM Ded1 (n=182)
134
48
p-value
< 2.4E-44
23
Down in 100 nM Ded1 (n=71)
G
log2ΔRE
Count
600
0
-5 0 5
ΔRE 100 nM/0 nM Ded1
ΔRE 500 nM/0 nM Ded1
ΔRE 500 nM/100 nM Ded1
Ranked by ΔRE 100 nM/0 nM Ded1
F
Cols. 1 2 3 4 5 6 7 8 9 10 11 12 13 14
ΔmRPF 100 nM/0 nM Ded1
ΔmRPF 500 nM/0 nM Ded1
ΔmRPF (log2)
Unlogged Median:
1.5 1.4 3.6 4.8 4.1 5.2 4.7 6.1 0.59 0.37 0.42 0.41 0.4 0.35
all n=3052
500 nM Ded1 up n=1006
100 nM Ded1 up n=911
+Ded1 up Overlap n=793
500 nM Ded1 dn n=182
100 nM Ded1 dn n=71
+Ded1 dn Overlap n=48
H
0 nM Ded1
100 nM Ded1
500 nM Ded1
Count of mRNAs
<0
0-2
2-3
3-4
4-5
5-6
6-7
7-8
8-9
>9
Log2 RE (lowest to highest)
I
ΔRE 500 nM/0 nM Ded1 (log2)
1st
3rd
5th
RE -Ded1 (Lowest to highest)

**Figure 2. Ded1 promotes the recruitment of a group of 1000 mRNAs.**
**(A-C)** Scatterplots of normalized read densities on the main start codons of mRNAs (mRPF, number of RPFs mapping to the main AUG normalized by the geometric means of the spike-in internal control RPFs) for 3052 mRNAs with > 90 total reads in 9 samples (3 replicates each for 0, 100 and 500 nM Ded1) for 100 versus 0 nM Ded1 (A), 500 versus 0 nM Ded1 (B), or 500 versus 100 nM Ded1 (C). mRNAs with significantly changed recruitment were defined as those with false discovery rates (FDR) < 0.05 and RPF changes (ΔRPF) of > 2 for increased or < 0.5 for decreased are indicated in red or dark blue, respectively. The number of significantly changed mRNAs are indicated in red (increased) and blue (decreased). (**D and E**) Overlaps between the mRNAs displaying significantly increased (D) or significantly reduced (E) mRPFs between 100 and 500 nM Ded1 conditions. P-values for the overlap between each group were calculated using an online tool (http://nemates.org/MA/progs/overlap_stats.html). **(F)** Box plot analysis of the distribution and median of log2 change in mRPF between 0 and 100 nM Ded1 ($\Delta mRPF_{100/0\ nM\ Ded1}$, orange) or 0 and 500 nM Ded1 ($\Delta mRPF_{500/0\ nM\ Ded1}$, cyan) for all 3052 mRNAs (cols. 1-2), and for the following 6 groups of mRNAs: 1006 or 911 for which mRPFs were significantly up in 500 or 100 nM Ded1, respectively, relative to no Ded1 (cols. 3-6, for red dots in B and A); 793 mRNAs for which mRPFs were significantly up with both 100 and 500 nM Ded1 (cols. 7-8, for the overlapping mRNAs in D); 182 and 71 mRNAs for which mRPFs were significantly down in 500 or 100 nM Ded1 relative to no Ded1 (cols. 9-12, blue dots in B and A); and 48 mRNAs for which mRPFs were significantly down with both 100 and 500 nM Ded1 (cols.13-14, for the overlaps in E). The blue horizontal line shows no change in mRPFs (ΔmRPF = 1). **(G)** Heat-map analysis of the recruitment efficiency changes $\Delta RE_{100/0\ nM\ Ded1}$, $\Delta RE_{500/0\ nM\ Ded1}$ and $\Delta RE_{500/100\ nM\ Ded1}$ for the 3052 mRNAs described in A-C, ordered by rank of $\Delta RE_{100/0\ nM\ Ded1}$ from most increased (top) to most decreased (bottom) using the R heatmap.2 function. (**H**) The distributions of all observed mRNAs across 10 bins of increasing RE values at each concentration of Ded1 (0, 100, 500 nM). **(I)** Boxplot analysis of $\Delta RE_{500/0\ nM\ Ded1}$ for all 3052 observed mRNAs binned by RE in the absence of Ded1 ($RE_{-Ded1}$) from the lowest to the highest.

# Figure 3

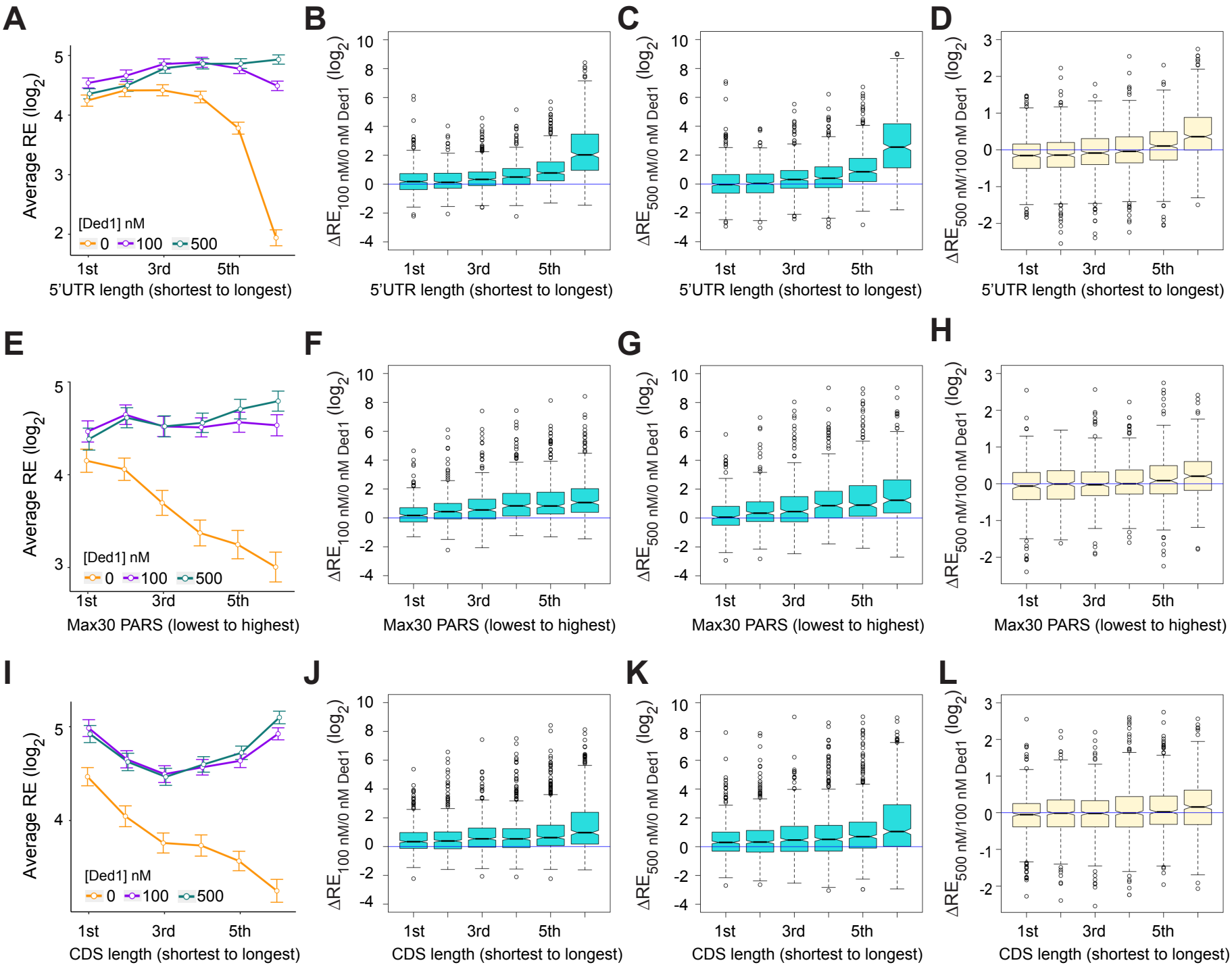
A
B
C
D
E
F
G
H
I
J
K
L
Average RE (log2)
[Ded1] nM
0
100
500
ΔRE100 nM/0 nM Ded1 (log2)
ΔRE500 nM/0 nM Ded1 (log2)
ΔRE500 nM/100 nM Ded1 (log2)
1st
3rd
5th
5'UTR length (shortest to longest)
Max30 PARS (lowest to highest)
CDS length (shortest to longest)

**Figure 3. Ded1 promotes the recruitment of mRNAs with long or structured 5'UTRs.**
**(A)** Line plot analysis of average recruitment efficiency (RE) for the 2804 mRNAs observed in the RecSeq experiments that have annotated 5'UTRs binned by 5'UTR length at 0, 100 and 500 nM Ded1. Average RE values were determined from the RE values of all mRNAs in each bin. **(B-D)** Box plot analyses of the recruitment efficiency changes (ΔRE) between each of two different conditions for the same mRNA bins as in (A) for $\Delta RE_{100/0nM_Ded1}$ (B), $\Delta RE_{500/0nM_Ded1}$ (C), or $\Delta RE_{500/100nM_Ded1}$ (D). **(E)** Line plot analysis of average RE values for the 1874 mRNAs observed in the RecSeq experiments with reported PARS scores binned according to Max30 PARS scores from the lowest to highest. PARS scores were determined by Kertesz et al. (2010) and Max30 and other PARS score intervals were calculated as described in Sen et al. (2015). **(F-H)** Box plot analyses for the same mRNA bins as in (E) for $\Delta RE_{100/0nM_Ded1}$ (F), $\Delta RE_{500/0nM_Ded1}$ (G), or $\Delta RE_{500/100nM_Ded1}$ (H). **(I)** Line plot analysis of average REs for all 3052 mRNAs divided into six equal-sized bins according to CDS lengths from the shortest to the longest for 0, 100 and 500 nM Ded1. **(J-L)** Box plot analysis for the same mRNA bins as in (I) for $\Delta RE_{100/0nM_Ded1}$ (J), $\Delta RE_{500/0nM_Ded1}$ (K), or $\Delta RE_{500/100nM_Ded1}$ (L). All bins contain an equal number of mRNAs.

# Figure 4

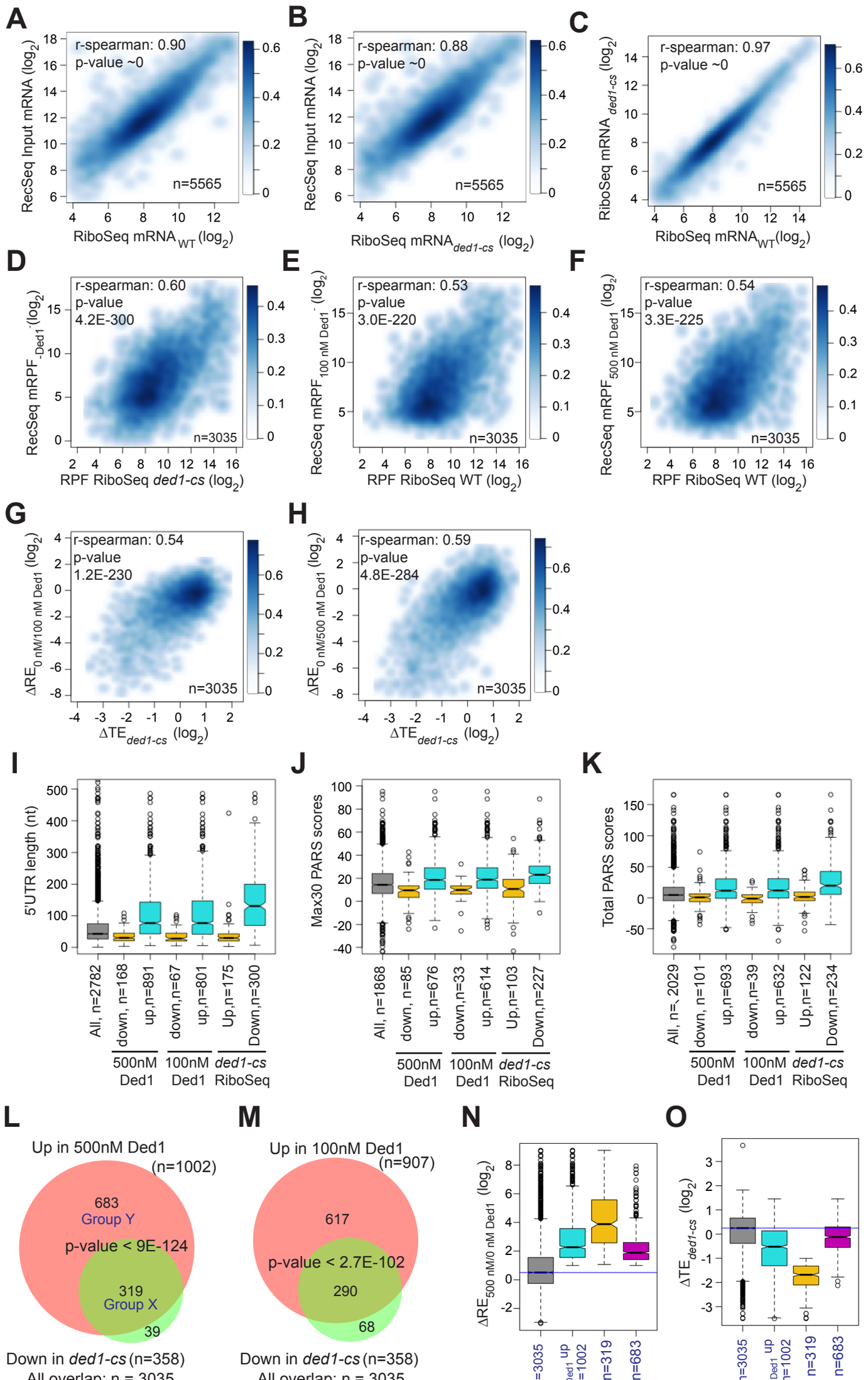
A
r-spearman: 0.90
p-value ~0
n=5565
RecSeq Input mRNA (log2)
RiboSeq mRNA WT (log2)
B
r-spearman: 0.88
p-value ~0
n=5565
RecSeq Input mRNA (log2)
RiboSeq mRNA ded1-cs (log2)
C
r-spearman: 0.97
p-value ~0
n=5565
RiboSeq mRNA ded1-cs (log2)
RiboSeq mRNA WT (log2)
D
r-spearman: 0.60
p-value
4.2E-300
n=3035
RecSeq mRPF -Ded1 (log2)
RPF RiboSeq ded1-cs (log2)
E
r-spearman: 0.53
p-value
3.0E-220
n=3035
RecSeq mRPF 100 nM Ded1 (log2)
RPF RiboSeq WT (log2)
F
r-spearman: 0.54
p-value
3.3E-225
n=3035
RecSeq mRPF 500 nM Ded1 (log2)
RPF RiboSeq WT (log2)
G
r-spearman: 0.54
p-value
1.2E-230
n=3035
ΔRE 0 nM/100 nM Ded1 (log2)
ΔTE ded1-cs (log2)
H
r-spearman: 0.59
p-value
4.8E-284
n=3035
ΔRE 0 nM/500 nM Ded1 (log2)
ΔTE ded1-cs (log2)
I
5'UTR length (nt)
All, n=2782
down, n=168
up,n=891
down,n=67
up,n=801
Up,n=175
Down,n=300
500nM Ded1
100nM Ded1
ded1-cs RiboSeq
J
Max30 PARS scores
All, n=1868
down, n=85
up,n=676
down,n=33
up,n=614
Up,n=103
Down,n=227
500nM Ded1
100nM Ded1
ded1-cs RiboSeq
K
Total PARS scores
All, n=2029
down, n=101
up,n=693
down,n=39
up,n=632
Up,n=122
Down,n=234
500nM Ded1
100nM Ded1
ded1-cs RiboSeq
L
Up in 500nM Ded1
(n=1002)
683
Group Y
p-value < 9E-124
319
Group X
39
Down in ded1-cs (n=358)
All overlap: n = 3035
M
Up in 100nM Ded1
(n=907)
617
p-value < 2.7E-102
290
68
Down in ded1-cs (n=358)
All overlap: n = 3035
N
ΔRE 500 nM/0 nM Ded1 (log2)
all mRNA n=3035
all RE 500nM Ded1 up n=1002
Group X, n=319
Group Y, n=683
O
ΔTE ded1-cs (log2)
all mRNA n=3035
all RE 500nM Ded1 up n=1002
Group X, n=319
Group Y, n=683

**Figure 4. Ded1 dependencies observed in Rec-Seq experiments correlate strongly with in vivo results from previous ribosome profiling of the *ded1-cs* mutant.**
**(A-B)** Scatterplots comparing Rec-Seq input RNA reads and ribosome profiling mRNA reads of WT (A) or *ded1-cs* (B) strains. **(C)** Scatterplot comparing ribosome profiling mRNA reads between WT and *ded1-cs* strains. **(D-F)** Scatterplots comparing 48S PIC RPFs from Rec-Seq to 80S RPFs from ribosome profiling for the 3035 mRNAs that passed the significance cutoffs in both experiments for Rec-Seq at 0 nM Ded1 versus ribosome profiling of the *ded1-cs* mutant (D) or Rec-Seq at 100 nM (E) or 500 nM (F) Ded1 versus ribosome profiling of the WT strain. **(G-H)** Scatterplots comparing changes in translational efficiency (ΔTE) from ribosome profiling of the *ded1-cs* mutant versus WT to $\Delta RE_{0/100nM_Ded1}$ (G) or $\Delta RE_{0/500nM\ Ded1}$ (H) values from Rec-Seq. **(I-K)** Boxplot analysis of 5'UTR lengths (I), Max30 PARS (J), or Total PARS (K) for mRNAs with annotated 5'UTR lengths or PARS scores that showed significantly decreased (Down) or increased (Up) REs in 100 nM or 500 nM Ded1 versus no Ded1, or significantly increased (Up) or decreased (Down) TEs in the *ded1-cs* mutant versus WT. **(L-M)** Overlaps between mRNAs identified by Rec-Seq at 100 nM Ded1 (L) or 500 nM Ded1 (M) with significantly increased REs versus no Ded1 in Rec-Seq and mRNAs with significantly increased TEs in ribosome profiling of the *ded1-cs* mutant versus WT. P-values for the overlaps were calculated as described in Fig. 2D-E**.** Group X and Y mRNAs in (L) are those in common between the two groups being compared (X) or those found exclusively in the set of 1002 mRNAs with significantly increased RE in 500 nM Ded1 versus no Ded1 in Rec-Seq (Y). **(N-O)** Boxplot analysis of log2 $\Delta RE_{500/0nM_Ded1}$ (N) or log2 $\Delta TE_{ded1\text{-}ts\text{-}}$ (O) values for all 3035 mRNAs observed in both Rec-Seq and ribosome profiling, the 1002 mRNAs with significantly increased recruitment with 500 nM Ded1 versus no Ded1 (of L), the 319 mRNAs in group X (of L), and the 683 mRNAs in group Y (of L).

# Figure 5

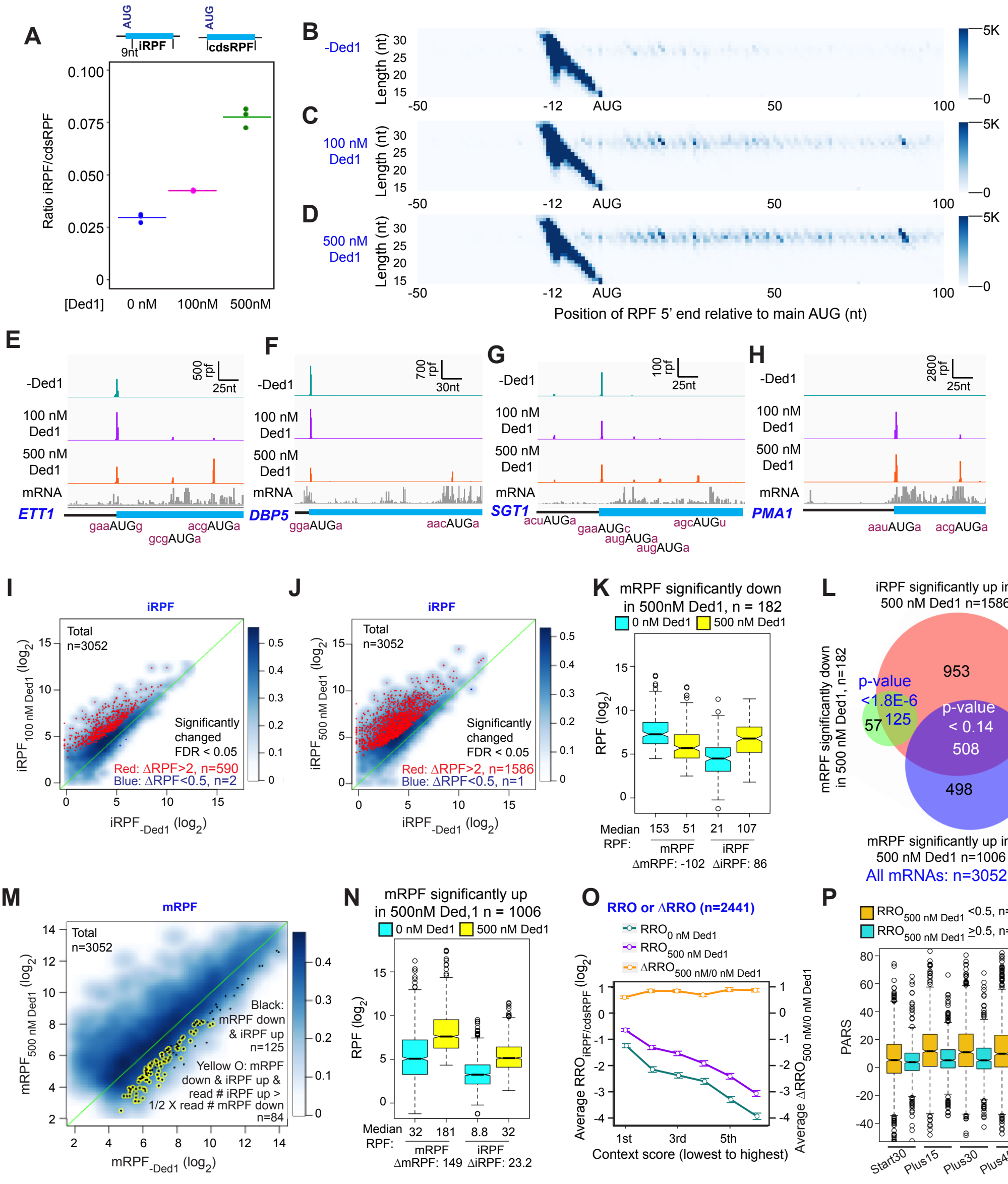
A
AUG
9nt
iRPF
AUG
cdsRPF
Ratio iRPF/cdsRPF
0.100
0.075
0.050
0.025
0
[Ded1]
0 nM
100nM
500nM
B
-Ded1
C
100 nM Ded1
D
500 nM Ded1
Length (nt)
-50
-12
AUG
50
100
5K
0
Position of RPF 5' end relative to main AUG (nt)
E
-Ded1
100 nM Ded1
500 nM Ded1
mRNA
500 rpf
25nt
ETT1
gaaAUGg
gcgAUGa
acgAUGa
F
700 rpf
30nt
DBP5
ggaAUGa
aacAUGa
G
100 rpf
25nt
SGT1
acuAUGa
gaaAUGc
augAUGa
augAUGa
agcAUGu
H
2800 rpf
25nt
PMA1
aauAUGa
acgAUGa
I
iRPF
Total n=3052
Significantly changed FDR < 0.05
Red: ΔRPF>2, n=590
Blue: ΔRPF<0.5, n=2
iRPF100 nM Ded1 (log2)
iRPF-Ded1 (log2)
J
iRPF
Total n=3052
Significantly changed FDR < 0.05
Red: ΔRPF>2, n=1586
Blue: ΔRPF<0.5, n=1
iRPF500 nM Ded1 (log2)
iRPF-Ded1 (log2)
K
mRPF significantly down in 500nM Ded1, n = 182
0 nM Ded1
500 nM Ded1
RPF (log2)
Median RPF:
153
51
21
107
mRPF
iRPF
ΔmRPF: -102
ΔiRPF: 86
L
iRPF significantly up in 500 nM Ded1 n=1586
mRPF significantly down in 500 nM Ded1, n=182
953
p-value <1.8E-6
57
125
p-value < 0.14
508
498
mRPF significantly up in 500 nM Ded1 n=1006
All mRNAs: n=3052
M
mRPF
Total n=3052
Black: mRPF down & iRPF up n=125
Yellow O: mRPF down & iRPF up & read # iRPF up > 1/2 X read # mRPF down n=84
mRPF500 nM Ded1 (log2)
mRPF-Ded1 (log2)
N
mRPF significantly up in 500nM Ded,1 n = 1006
0 nM Ded1
500 nM Ded1
RPF (log2)
Median RPF:
32
181
8.8
32
mRPF
iRPF
ΔmRPF: 149
ΔiRPF: 23.2
O
RRO or ΔRRO (n=2441)
RRO0 nM Ded1
RRO500 nM Ded1
ΔRRO500 nM/0 nM Ded1
Average RROiRPF/cdsRPF (log2)
Average ΔRRO500 nM/0 nM Ded1
1st
3rd
5th
Context score (lowest to highest)
P
RRO500 nM Ded1 <0.5, n=1054
RRO500 nM Ded1 ≥0.5, n=715
PARS
Start30
Plus15
Plus30
Plus45

**Figure 5. Ded1 increases leaky scanning of main start codons**

(**A**) The ratio of the total RPFs internal to the CDS in mRNAs, excluding the main start codon, to the total RPFs for the full CDS including the main start codon (iRPF/cdsRPF ratio) for each of the three replicates at 0, 100 and 500 nM Ded1. iRPFs were counted from the +9 position of the main AUG to the stop codon, while the cdsRPFs were counted from the start codon to the stop codon of the CDS. The average of the three replicates is indicated by the colored bars (red, green and blue for 0, 100 and 500 nM Ded1, respectively). **(B-D)** Metagene plots showing RPF density distribution on all mRNAs aligned to their main AUGs as in Fig. 1B-D for 0 (B), 100 (C) and 500 nM Ded1 (D), with color scales adjusted to show internal RPFs (iRPFs). **(E-H)** 48S PIC RPFs and input mRNA reads on four selected mRNAs that showed elevated internal ribosome occupancies in 100 and 500 nM Ded1 conditions. The -3 to -1 and +4 context nucleotides surrounding the main AUG, iAUG or upstream AUG (uAUG) are indicated in brick red text. **(I-J)** Scatterplots comparing log2 iRPF between 100 (I) or 500 nM Ded1 (J) to 0 nM Ded1 as described in Fig. 2A-B for the same group of 3052 mRNAs. Red dots show mRNAs that meet the significance cutoff for increases in iRPF (FDR < 0.05, >2-fold increase in iRPFs) and blue dots show mRNAs that meet the significance cutoff for decreases in iRPF (FDR < 0.05, <0.5-fold decrease in iRPFs). **(K)** Box plot comparing mRPFs and iRPFs between 500 and 0 nM Ded1 for the 182 mRNAs that showed significantly reduced mRPFs with 500 nM Ded1 versus no Ded1. **(L)** Overlaps between mRNAs with significantly elevated iRPFs (orange), significantly reduced mRPFs (green) or significantly increased mRPFs (blue) with 500 nM Ded1 relative to 0 nM Ded1. The Venn diagram was generated and p-values calculated as in Fig. 2D. **(M)** Scatter plot comparing mRPFs with 500 nM versus 0 nM Ded1. The 125 mRNAs that showed significantly increased iRPFs and significantly decreased mRPFs in 500 nM Ded1 relative to 0 nM Ded1 are labeled by black dots. Among this set, the mRNAs for which the iRPFs increase by at least 50% of the decrease in mRPFs are labeled by yellow circles, to indicate the 84 mRNAs for which the decrease in mRPFs could be responsible for the increase in iRPFs. **(N)** Boxplot comparing mRPFs and iRPFs between 500 nM and 0 nM Ded1 for the 1006 mRNAs that showed significantly increased mRPFs. **(O)** Line plot analysis of average RRO (relative ribosome occupancy; iRPF/cdsRPF ratio; left axis) and $\Delta RRO_{500/0\ nM\ Ded1}$ (right axis) for 2441 of 3052 mRNAs in J with 5'UTR length >5 nt binned by main AUG context scores from lowest to highest. **(P)** Boxplot analysis of Start30, Plus15, Plus30 and Plus45 PARS scores for mRNAs with $RRO_{iRPF/cdsRPF} < 0.5$ (orange) or $\geqslant 0.5$ with 500 nM Ded1.

# Figure 6

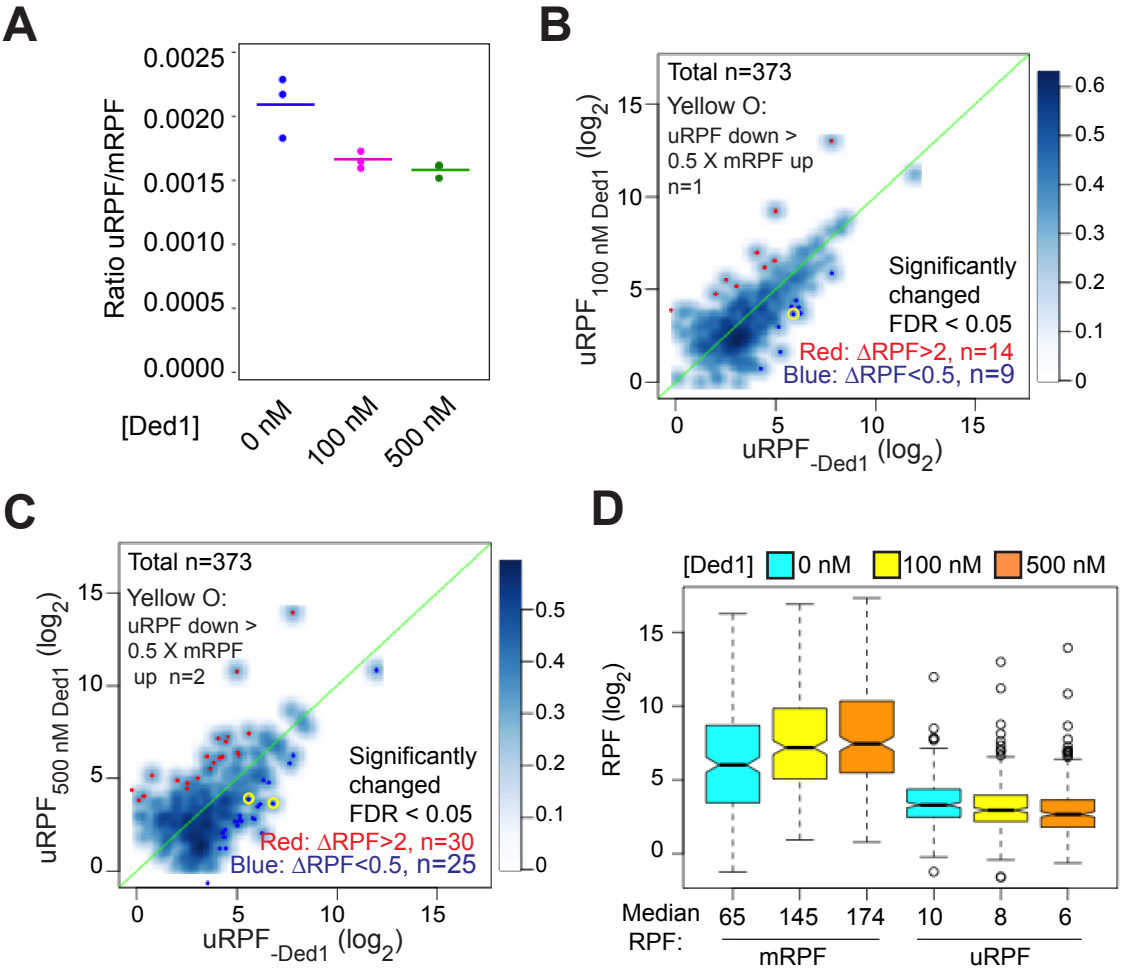
A
Ratio uRPF/mRPF
0.0025
0.0020
0.0015
0.0010
0.0005
0.0000
[Ded1]
0 nM
100 nM
500 nM
B
Total n=373
Yellow O:
uRPF down >
0.5 X mRPF up
n=1
Significantly
changed
FDR < 0.05
Red: ΔRPF>2, n=14
Blue: ΔRPF<0.5, n=9
uRPF 100 nM Ded1 (log2)
uRPF -Ded1 (log2)
C
Total n=373
Yellow O:
uRPF down >
0.5 X mRPF
up n=2
Significantly
changed
FDR < 0.05
Red: ΔRPF>2, n=30
Blue: ΔRPF<0.5, n=25
uRPF 500 nM Ded1 (log2)
uRPF -Ded1 (log2)
D
[Ded1] 0 nM 100 nM 500 nM
RPF (log2)
Median
RPF:
65 145 174 10 8 6
mRPF
uRPF

**Figure 6. Ded1 modestly promotes readthrough of start codons in 5' UTRs of mRNAs.** **(A)** The ratios of RPFs in 5'UTRs to RPFs on main start codons (uRPF/mRPF ratios) for each of the three replicates with 0 (blue), 100 (magenta) or 500 (green) nM Ded1. The 5'UTR RPFs (uRPFs) were counted from the 5'end of the mRNA to the -5 position relative to the main AUG. The mean of the three replicates is indicated by the colored bars. uRPFs on *GCN4* mRNA were analyzed separately (Fig. 6-S1), because 42% and 57% of all uRPFs were mapped to the *GCN4* 5'UTR in assays with 100 and 500 nM Ded1, respectively. **(B-C)** Scatterplots comparing uRPFs in the presence of either 100 nM (B) or 500 nM (C) Ded1 versus 0 nM Ded1. mRNAs with significantly increased or decreased uRPFs in the presence of Ded1 are indicated in red or dark blue dots, respectively. The criteria used for significance were FDR < 0.05 and a greater than 2-fold increase or decrease. Yellow circles denote the very few mRNAs whose uRPF read number decreases by more than 50% of the increases in their mRPF reads, indicating a clear reciprocal relationship between the decrease in uRPFs and the increase in mRPFs. (**D**) Box plot analysis of mRPF and uRPF read numbers for the 257 mRNAs that had both uRPFs and mRPFs ⩾ 2 reads averaged over all assays conducted at 0, 100 and 500 nM Ded1 concentrations. Unlogged median RPF numbers are labeled under each box.

# Figure 7

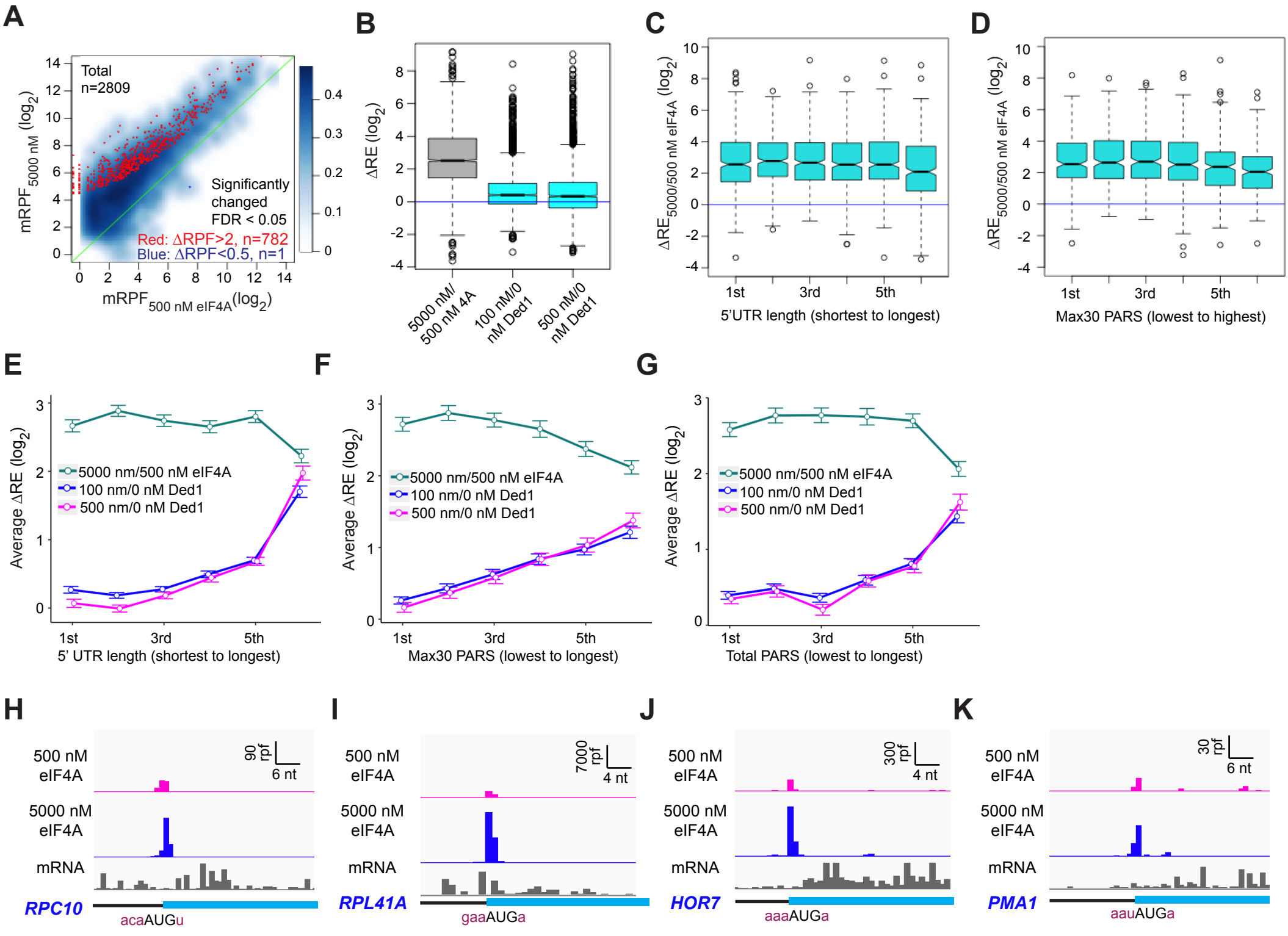
A
Total
n=2809
Significantly
changed
FDR < 0.05
Red: ΔRPF>2, n=782
Blue: ΔRPF<0.5, n=1
mRPF 5000 nM (log2)
mRPF 500 nM eIF4A (log2)
B
ΔRE (log2)
5000 nM/
500 nM 4A
100 nM/0
nM Ded1
500 nM/0
nM Ded1
C
ΔRE 5000/500 nM eIF4A (log2)
1st
3rd
5th
5'UTR length (shortest to longest)
D
ΔRE 5000/500 nM eIF4A (log2)
1st
3rd
5th
Max30 PARS (lowest to highest)
E
Average ΔRE (log2)
5000 nm/500 nM eIF4A
100 nm/0 nM Ded1
500 nm/0 nM Ded1
1st
3rd
5th
5' UTR length (shortest to longest)
F
Average ΔRE (log2)
5000 nm/500 nM eIF4A
100 nm/0 nM Ded1
500 nm/0 nM Ded1
1st
3rd
5th
Max30 PARS (lowest to longest)
G
Average ΔRE (log2)
5000 nm/500 nM eIF4A
100 nm/0 nM Ded1
500 nm/0 nM Ded1
1st
3rd
5th
Total PARS (lowest to longest)
H
500 nM
eIF4A
90
rpf
6 nt
5000 nM
eIF4A
mRNA
RPC10
acaAUGu
I
500 nM
eIF4A
7000
rpf
4 nt
5000 nM
eIF4A
mRNA
RPL41A
gaaAUGa
J
500 nM
eIF4A
300
rpf
4 nt
5000 nM
eIF4A
mRNA
HOR7
aaaAUGa
K
500 nM
eIF4A
30
rpf
6 nt
5000 nM
eIF4A
mRNA
PMA1
aauAUGa

**Figure 7. eIF4A enhances the recruitment of almost all mRNAs**

**(A)** Scatterplots of normalized read densities mapped to main AUGs (mRPFs) with 5000 nM versus 500 nM eIF4A for the 2809 mRNAs with ⩾ 8 total reads in 4 samples (2 replicates each for 5000 and 500 nM eIF4A). Red and blue dots show mRNAs with mRPFs significantly increased or decreased, respectively, at 5000 versus 500 nM eIF4A. The criteria for significance were FDR < 0.05 and a > 2-fold change in RPFs. **(B)** Boxplot comparing $\Delta RE_{5000/500\ nM\ eIF4A}$ (grey) to $\Delta RE_{100/0\ nM\ Ded1}$ and $\Delta RE_{500/0\ nM\ Ded1}$ (cyan) for the 2698 mRNAs that passed the cutoff mentioned in (A) in both experiments. **(C)** Boxplot of $\Delta RE_{5000/500\ nM\ eIF4A}$ for the 2538 of all 2809 mRNAs in (A) that have annotated 5'UTRs, divided into six equal sized bins according to 5'UTR lengths from the shortest to the longest. **(D)** Similar to (C), but for the 1708 of all 2809 mRNAs in (A) with annotated PARS scores, binned by Max30 PARS from lowest to highest. **(E-G)** Line plots of mean $\log_2$ RE changes, $\Delta RE_{5000/500\ nM\ eIF4A}$ (green), $\Delta RE_{100/0\ nM\ Ded1}$ (magenta), and $\Delta RE_{500/0\ nM\ Ded1}$ (blue), for mRNAs divided into six equal sized bins according to the specific mRNA features of 5'UTR length (E), Max30 PARS score (F), or Total PARS score (G). **(H-K)** RPFs assembled with 500 or 5000 nM eIF4A and input mRNA reads for mRNAs shown previously to be hypo-dependent on Ded1 (*RPC10*, *RPL41A*, *HOR7*) or hyper-dependent on Ded1(*PMA1*) by in vivo ribosome profiling experiments in the *ded1-cs* mutant.

# Figure 1-S1

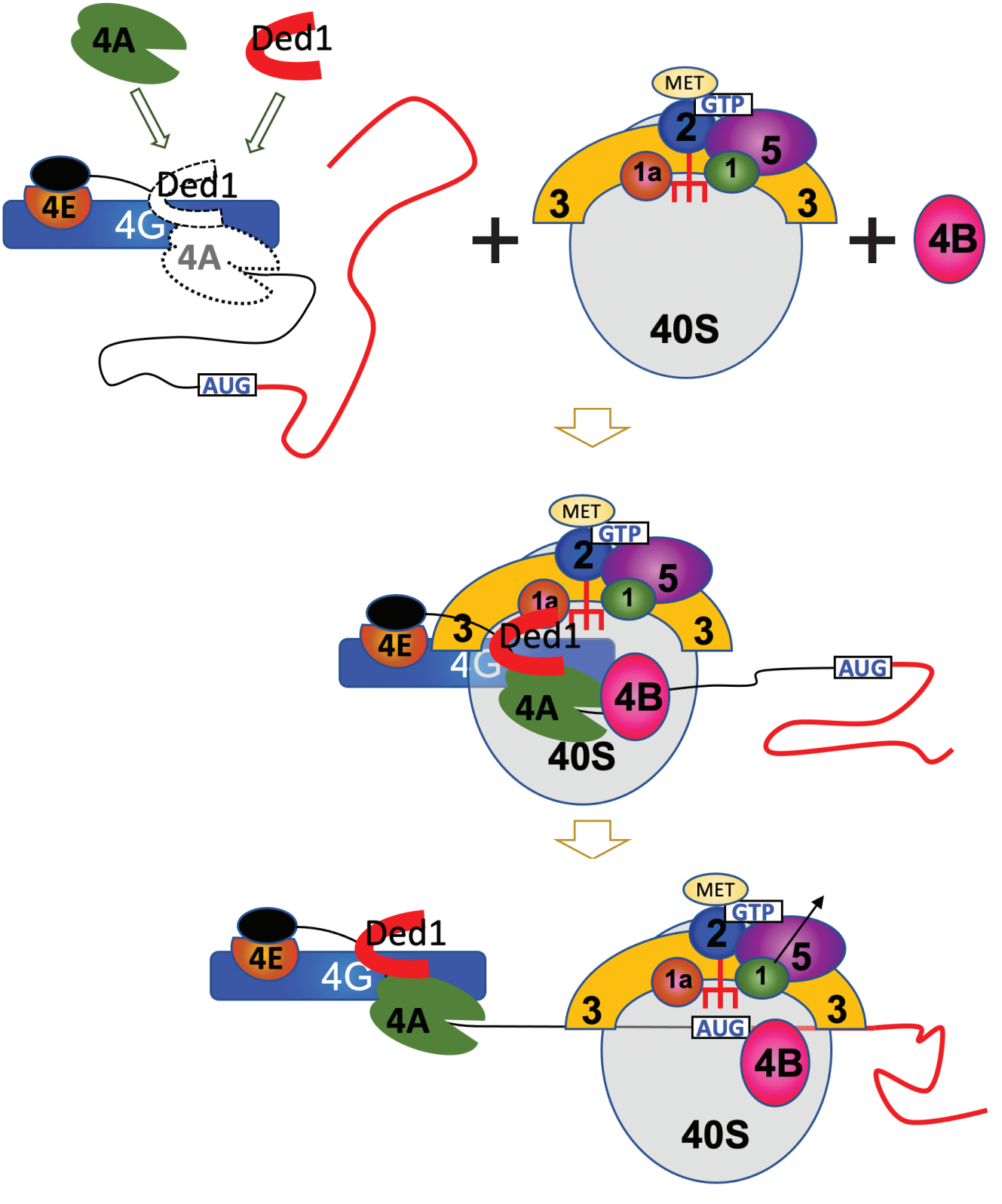
4A
Ded1
4E
4G
Ded1
4A
AUG
MET
GTP
2
5
1a
1
3
3
40S
4B
MET
GTP
2
5
1a
1
3
3
4E
Ded1
4G
4A
4B
AUG
40S
MET
GTP
2
5
1a
1
3
3
4E
Ded1
4G
4A
AUG
4B
40S

**Figure 1-S1. A schematic diagram of mRNA recruitment in translation initiation.** The cap-binding protein complex eIF4F, consisting of eIF4E, eIF4G and eIF4A subunits attaches to the cap at the mRNA 5' end. The 43S PIC, which includes the 40S ribosomal subunit, eIFs 1, 1A, 3 and 5 and the eIF2•GTP•Met-tRNA$_i$ ternary complex, binds to the 5' end of mRNA with the aid of the eIF4F complex and eIF4B and scans downstream in search of the start codon. A stable 48S-PIC is formed when a start codon is recognized.

# Figure 1-S2

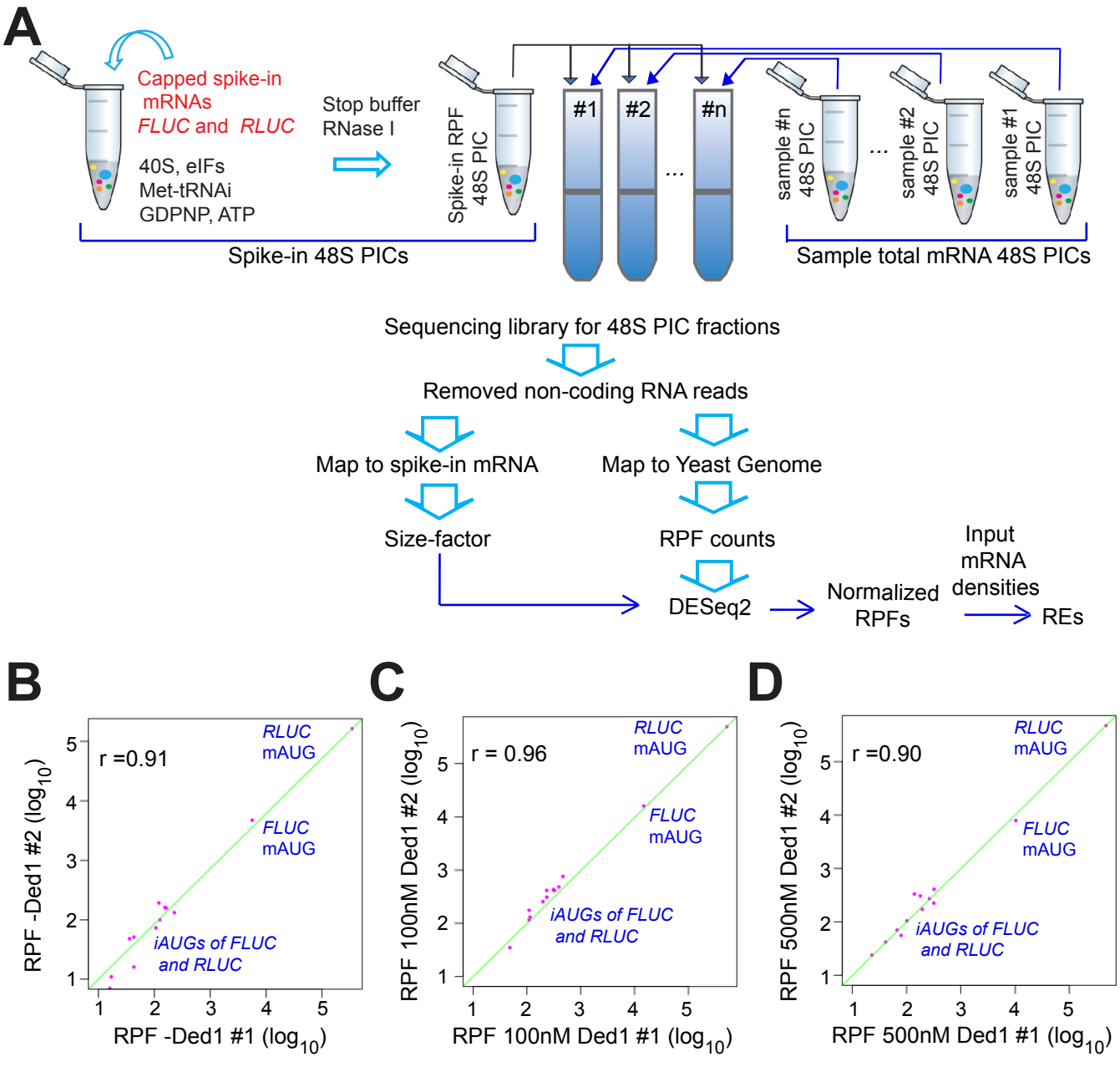
A
Capped spike-in mRNAs
FLUC and RLUC
40S, eIFs
Met-tRNAi
GDPNP, ATP
Stop buffer
RNase I
Spike-in RPF 48S PIC
#1
#2
#n
sample #n 48S PIC
sample #2 48S PIC
sample #1 48S PIC
Spike-in 48S PICs
Sample total mRNA 48S PICs
Sequencing library for 48S PIC fractions
Removed non-coding RNA reads
Map to spike-in mRNA
Map to Yeast Genome
Size-factor
RPF counts
DESeq2
Normalized RPFs
Input mRNA densities
REs
B
r =0.91
RLUC mAUG
FLUC mAUG
iAUGs of FLUC and RLUC
RPF -Ded1 #2 (log10)
RPF -Ded1 #1 (log10)
C
r = 0.96
RLUC mAUG
FLUC mAUG
iAUGs of FLUC and RLUC
RPF 100nM Ded1 #2 (log10)
RPF 100nM Ded1 #1 (log10)
D
r =0.90
RLUC mAUG
FLUC mAUG
iAUGs of FLUC and RLUC
RPF 500nM Ded1 #2 (log10)
RPF 500nM Ded1 #1 (log10)

**Figure 1-S2. Internal spike-in normalization controls using preformed 48S PICs on non-native mRNAs**. **(A)** Steps in applying 48S-PIC spike-in controls for data normalization. Firefly and Renilla luciferase mRNAs (*FLUC* and *RLUC)* were in vitro transcribed from PCR-amplified gene templates containing T7 promoters and enzymatically capped using previously described protocols (Acker et al. 2007). The 48S PICs formed on the spike-in mRNAs were prepared separately from the testing samples in a recruitment reaction followed by RNase I treatment to digest unprotected mRNA. A constant amount of spike-in 48S PICs were resolved by sedimentation through the same sucrose gradients containing the experimental samples. The RPFs from these spike-in PICs served as internal controls for losses occurring during library construction and allowed data normalization across experimental samples. For deep sequencing data processing, non-coding RNA reads were removed and the remaining RPFs were aligned to spike-in mRNA sequences for calculating sample size factors and also aligned to the yeast genome to produce RPF counts on all yeast mRNAs. The RPF counts for all mRNAs in the genome were applied to DESeq2 using sample size factors calculated from the geometric means of spike-in mRNA RPFs mapped to *FLUC*/*RLUC* main AUGs and a number of internal AUGs. Recruitment efficiency (RE) values were calculated by normalizing the size-factor corrected RPFs to input mRNA densities. **(B-D)** Scatterplots of *FLUC* and *RLUC* RPF reads at the main and internal AUGs, in the first two of three replicate samples for each condition. The green diagonal line is for 1:1 ratio and the Spearman correlation coefficients (r) were calculated using "cor.test" function in R using option "method = spearman."

# Figure 1-S3

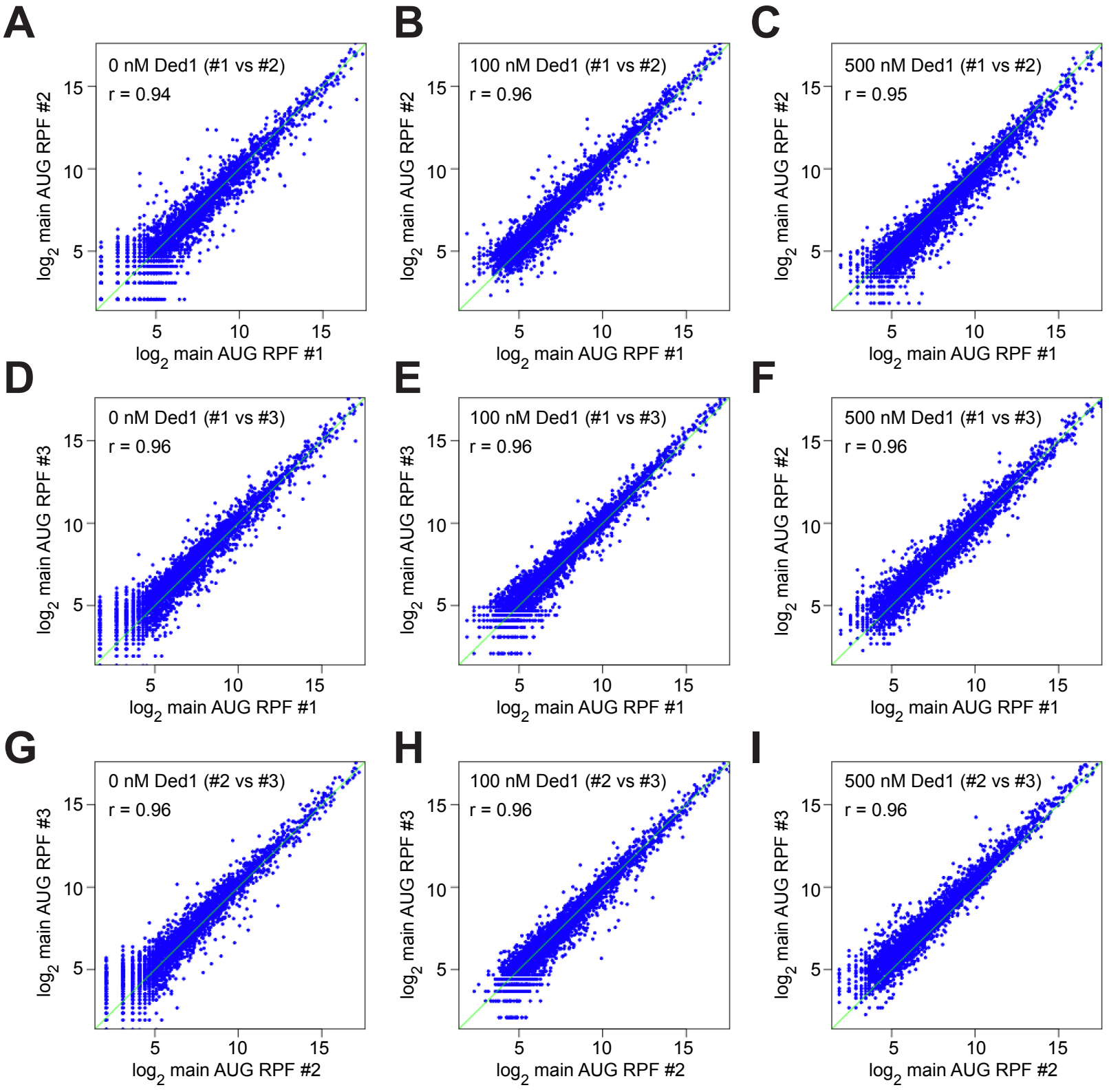
A
0 nM Ded1 (#1 vs #2)
r = 0.94
log2 main AUG RPF #2
log2 main AUG RPF #1
B
100 nM Ded1 (#1 vs #2)
r = 0.96
log2 main AUG RPF #2
log2 main AUG RPF #1
C
500 nM Ded1 (#1 vs #2)
r = 0.95
log2 main AUG RPF #2
log2 main AUG RPF #1
D
0 nM Ded1 (#1 vs #3)
r = 0.96
log2 main AUG RPF #3
log2 main AUG RPF #1
E
100 nM Ded1 (#1 vs #3)
r = 0.96
log2 main AUG RPF #3
log2 main AUG RPF #1
F
500 nM Ded1 (#1 vs #3)
r = 0.96
log2 main AUG RPF #2
log2 main AUG RPF #1
G
0 nM Ded1 (#2 vs #3)
r = 0.96
log2 main AUG RPF #3
log2 main AUG RPF #2
H
100 nM Ded1 (#2 vs #3)
r = 0.96
log2 main AUG RPF #3
log2 main AUG RPF #2
I
500 nM Ded1 (#2 vs #3)
r = 0.96
log2 main AUG RPF #3
log2 main AUG RPF #2

**Figure 1-S3. Transcriptome-wide reproducibility of RPFs among replicates**

**(A-I)** Scatterplots of log2 main AUG ribosome occupancies (normalized by the geometric means of RPF reads on *FLUC* and *RLUC* spike-in mRNAs) for comparing each of two of the three replicates in different conditions, 0 nM Ded1 (A, D and G), 100 nM Ded1 (B, E and H) and 500 nM Ded1 (C, F and I) for all mRNAs with ⩾ 90 total RPF reads in the 9 samples combined. Spearman correlation coefficients (r) were calculated as in Fig. 1-S2B-D.

# Figure 1-S4

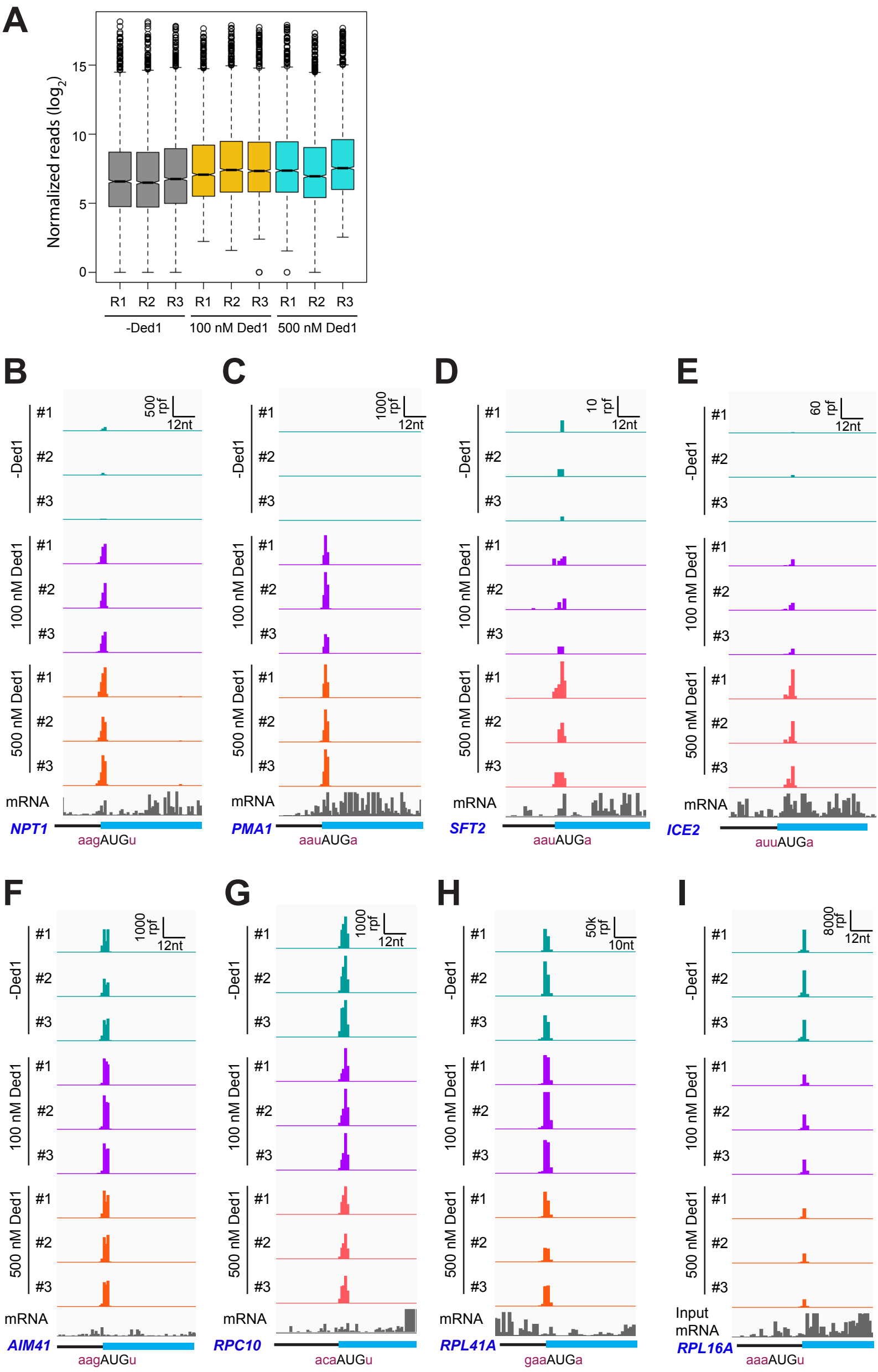
A
Normalized reads (log2)
15
10
5
0
R1 R2 R3 R1 R2 R3 R1 R2 R3
-Ded1
100 nM Ded1
500 nM Ded1
B
C
D
E
F
G
H
I
-Ded1
100 nM Ded1
500 nM Ded1
#1
#2
#3
500 rpf
1000 rpf
10 rpf
60 rpf
1000 rpf
1000 rpf
50k rpf
8000 rpf
12nt
10nt
mRNA
Input mRNA
NPT1
aagAUGu
PMA1
aauAUGa
SFT2
aauAUGa
ICE2
auuAUGa
AIM41
aagAUGu
RPC10
acaAUGu
RPL41A
gaaAUGa
RPL16A
aaaAUGu

**Figure 1-S4. RPFs on main AUGs are consistent among replicates.**
**(A)** Box plot analysis of normalized RPF reads for 3052 mRNAs with > 90 total reads in 9 samples (each of 3 replicates for 0, 100 and 500 nM Ded1). **(B-I)** 48S PIC-protected fragments (RPFs) and input mRNA reads for 3 replicates of each of the 3 conditions (0, 100 and 500 nM Ded1) on 8 example mRNAs across 3' portions of the 5'UTR and 5' portions of the CDS regions flanking the main AUGs. RPF and nt scales are shown in the top right corner of each panel. The position of the main CDS and the −3 to −1 and +4 context nucleotides surrounding the main AUG are labeled as in Fig. 1E-F. mRNAs shown are (B) *NPT1*; (C) *PMA1*; (D) *SFT2*; (E) *ICE2*; (F) *AIM41*; (G) *RCP10*; (H) *RPL41A;* and (I) *RPL16A*.

# Figure 3-S1

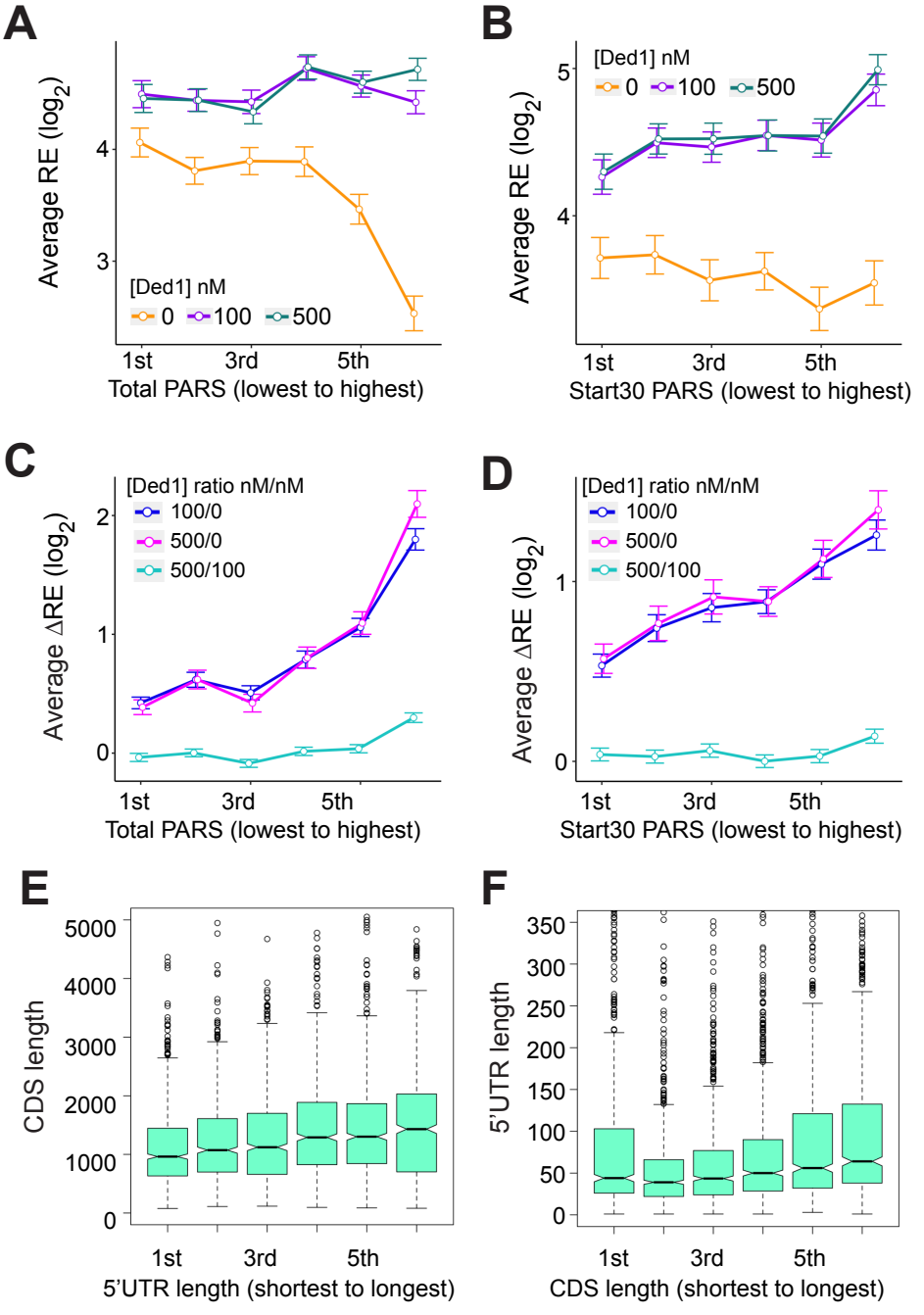
A
Average RE (log2)
[Ded1] nM
0
100
500
1st
3rd
5th
Total PARS (lowest to highest)
B
Average RE (log2)
[Ded1] nM
0
100
500
1st
3rd
5th
Start30 PARS (lowest to highest)
C
Average ΔRE (log2)
[Ded1] ratio nM/nM
100/0
500/0
500/100
1st
3rd
5th
Total PARS (lowest to highest)
D
Average ΔRE (log2)
[Ded1] ratio nM/nM
100/0
500/0
500/100
1st
3rd
5th
Start30 PARS (lowest to highest)
E
CDS length
1st
3rd
5th
5'UTR length (shortest to longest)
F
5'UTR length
1st
3rd
5th
CDS length (shortest to longest)

**Figure 3-S1. Ded1 preferentially stimulates 48S PIC formation on structured mRNAs. (A, B)** Line plot analysis of log2 average REs at 0, 100 and 500 nM Ded1for mRNAs binned according to total PARS scores (A) or the sum of PARS scores of the 30 nucleotides surrounding the start codon (for mRNAs with a 5'UTR of ⩾15 nt) (Start30 PARS, B). **(C, D)** Line plot analysis of log2 average ΔREs for 100/0 nM, 500/0 nM and 500/100 nM Ded1 for the 2035 mRNAs observed in RecSeq that have annotated PARS scores binned according to Total PARS (C) or Start30 PARS (D) scores from the lowest to highest. **(E-F)** Box plots comparing 5'UTR or CDS lengths for the 4694 yeast mRNAs that have annotated 5'UTRs (Pelechano et al. 2013) for CDS lengths plotted for mRNAs binned by 5'UTR length from the shortest to the longest (E), or 5'UTR lengths plotted for mRNAs binned by CDS lengths from shortest to longest (F). All bins contain equal numbers of mRNAs.

# Figure 3-S2

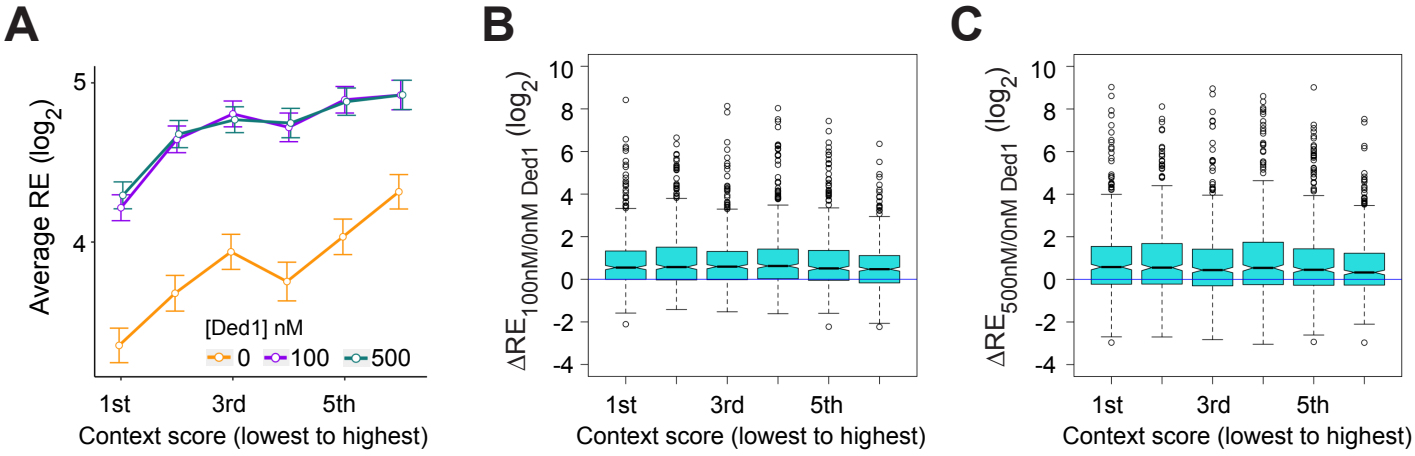
A
Average RE (log2)
5
4
[Ded1] nM
0
100
500
1st
3rd
5th
Context score (lowest to highest)
B
ΔRE100nM/0nM Ded1 (log2)
10
8
6
4
2
0
-2
-4
1st
3rd
5th
Context score (lowest to highest)
C
ΔRE500nM/0nM Ded1 (log2)
10
8
6
4
2
0
-2
-4
1st
3rd
5th
Context score (lowest to highest)

**Figure 3-S2. Ded1 has little effect on discriminating main AUG context scores. (A)** Line plot analysis of average REs for the 2768 observed in RecSeq that have annotated 5'UTR lengths >5 nt, divided into six equal-sized bins according to context scores from lowest to the highest at 0, 100 and 500 nM Ded1. **(B-C)** Box-plot analyses of $\Delta RE_{100/0nM\ Ded1}$ (B) and $\Delta RE_{500/0nM\ Ded1}$ (C) values for the same mRNA bins as in (A).

# Figure 5-S1

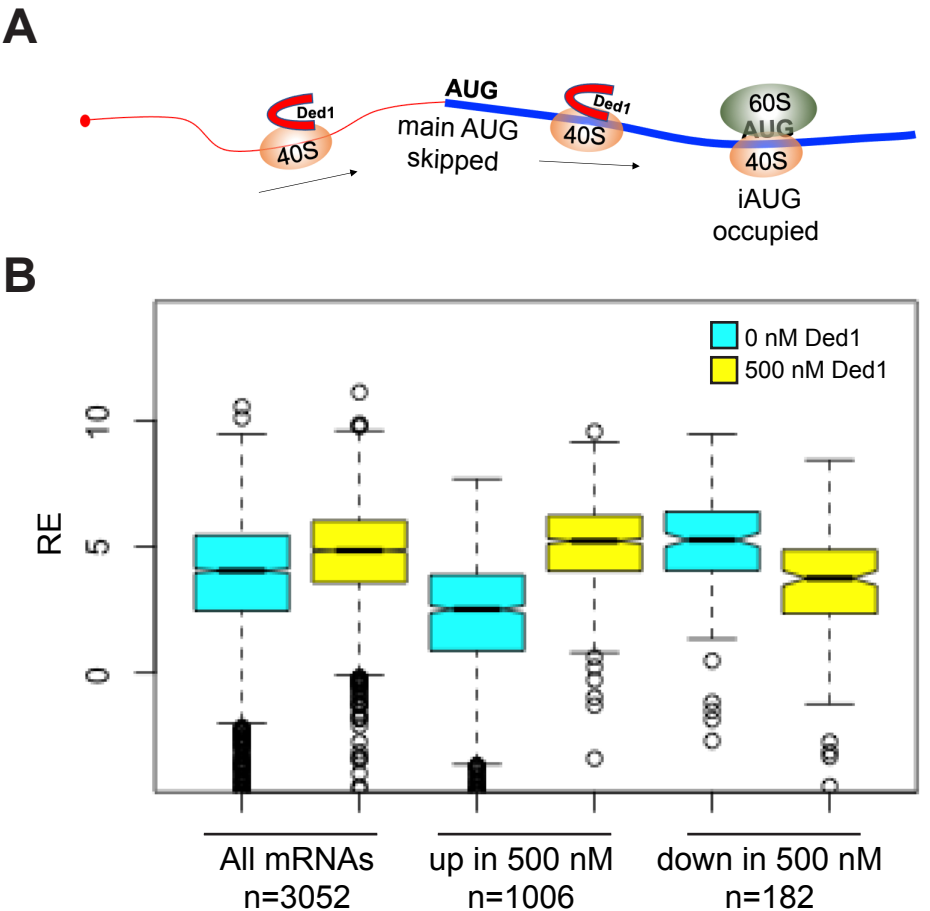
A
Ded1
40S
AUG
main AUG
skipped
Ded1
40S
60S
AUG
40S
iAUG
occupied
B
0 nM Ded1
500 nM Ded1
RE
0
5
10
All mRNAs
n=3052
up in 500 nM
n=1006
down in 500 nM
n=182

**Figure 5-S1. Supporting evidence that Ded1 promotes leaky scanning of the main start codon. (A)** Schematic of a 43S PIC leaky scanning through the main AUG and assembling at an internal AUG in the presence of Ded1. **(B)** Evidence that mRNAs whose recruitment is inhibited by 500 nM Ded1 in Rec-Seq assays generally assemble 48S PICs very efficiently without Ded1. Boxplot analysis of REs of groups of mRNAs at 0 nM (cyan) or 500 nM (yellow) Ded1 for all 3052 mRNAs observed in Rec-Seq, the 1006 mRNAs with significantly increased mRPFs at 500 nM Ded1 versus no Ded1 (Fig. 2B, red dots); and the 182 mRNAs with significantly decreased mRPFs with 500 nM Ded1 versus no Ded1 (Fig. 2B, blue dots).

# Figure 5-S2

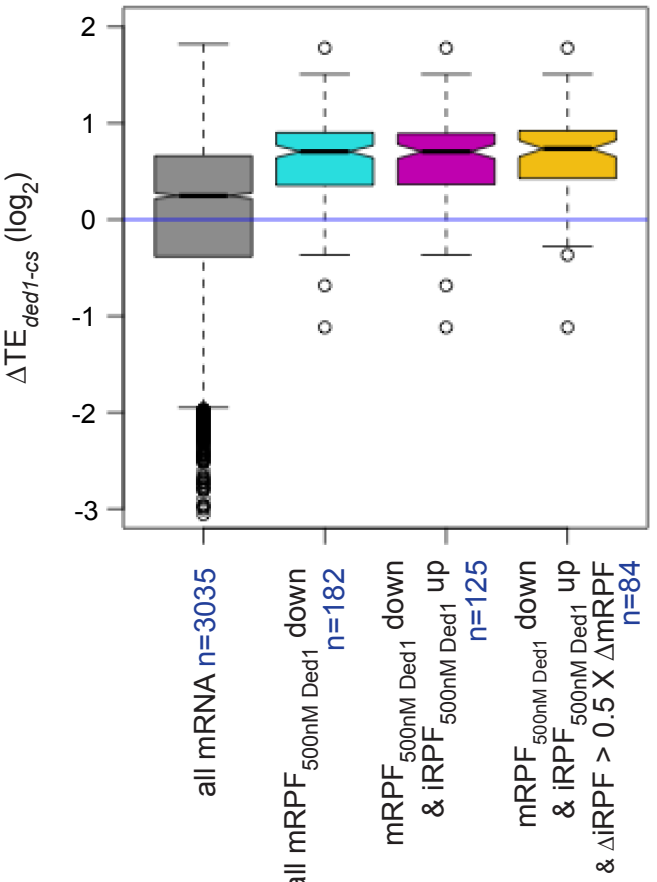
ΔTE$_{ded1\text{-}cs}$ (log$_2$)
2
1
0
-1
-2
-3
all mRNA n=3035
all mRPF$_{500nM\ Ded1}$ down n=182
mRPF$_{500nM\ Ded1}$ down & iRPF$_{500nM\ Ded1}$ up n=125
mRPF$_{500nM\ Ded1}$ down & iRPF$_{500nM\ Ded1}$ up & ΔiRPF > 0.5 X ΔmRPF n=84

**Figure 5-S2. mRNAs with reduced RE at 500 nM Ded1 versus no Ded1 in Rec-Seq assays tend to show increased relative TE in the *ded1-cs* mutant versus WT in ribosome profiling experiments.** Boxplot analysis of $\Delta TE_{ded1\text{-}cs}$ for the groups of mRNAs described in Figure 5L-M: The 182 mRNAs with mRPFs significantly reduced at 500 nM Ded1 versus no Ded1 (cyan); the 125 mRNAs with significantly decreased mRPFs and increased iRPFs with 500 nM Ded1 versus no Ded1 (magenta); the 84 mRNAs from the previous set that had an increase in iRPFs that was at least 50% the of the decrease in mRPFs (yellow circles in Fig. 5M; orange).

# Figure 6-S1

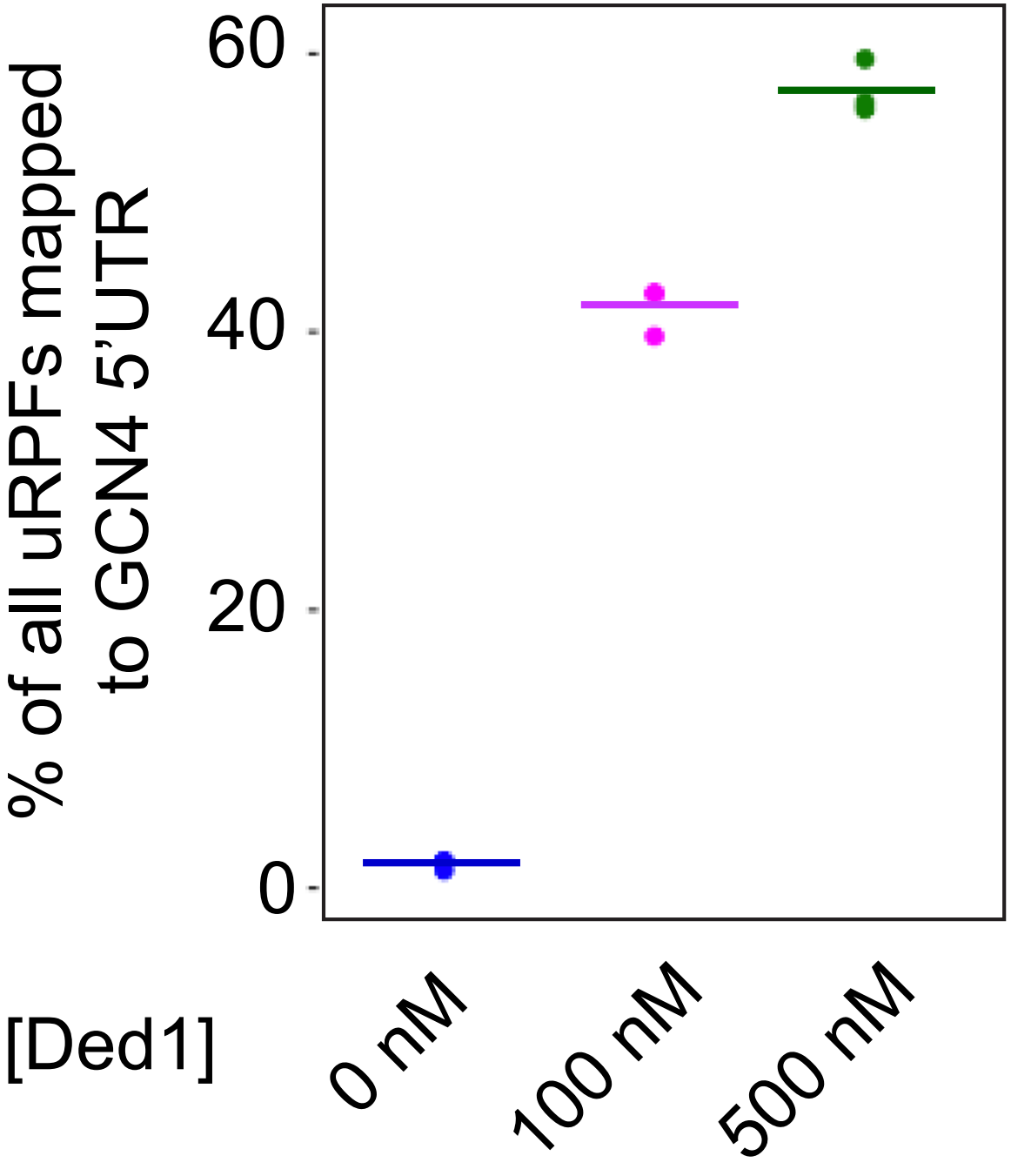
% of all uRPFs mapped to GCN4 5'UTR
60
40
20
0
[Ded1]
0 nM
100 nM
500 nM

**Figure 6-S1. Approximately half of all uRPFs map to the *GCN4* 5'UTR.** Percentages of all uRPFs mapped to the *GCN4* 5'UTR for each of the three replicates with 0 (blue), 100 (magenta), or 500 (green) nM Ded1 concentrations. Colored bars indicate the means of the replicates.